# UNIVERSITAT POLITÈCNICA DE CATALUNYA

## Programa de Doctorat:
## AUTOMATIC CONTROL, ROBOTICS AND COMPUTER VISION

### Tesi Doctoral:

# FAULT DETECTION AND

# FAULT TOLERANT CONTROL IN

# WIND TURBINES

## Christian Tutivén Gálvez

### Directores:
### Dr. José Rodellar
### Dra. Yolanda Vidal

### Mayo de 2018

UNIVERSITAT POLITÈCNICA DE CATALUNYA

Department of Mathematics

Title:

FAULT DETECTION AND
FAULT TOLERANT CONTROL IN
WIND TURBINES

UNIVERSITAT POLITÈCNICA DE CATALUNYA - Campus Diagonal
Besós

Av. d'Eduard Maristany, 10-14, 08930 Barcelona.

Advisors:

Dr. José Rodellar

Dra. Yolanda Vidal

*To Luciana*

# ABSTRACT

Renewable energy is an important sustainable energy in the world. Up to now, as an essential part of low emissions energy in a lot of countries, renewable energy has been important to the national energy security, and played a significant role in reducing carbon emissions. It comes from natural resources, such as wind, solar, rain, tides, biomass, and geothermal heat. Among them, wind energy is rapidly emerging as a low carbon, resource efficient, costeffective sustainable technology in the world. Due to the demand of higher power production installations with less environmental impacts, the continuous increase in size of wind turbines and the recently developed offshore (floating) technologies have led to new challenges in the wind turbine systems.

Wind turbines (WTs) are complex systems with large flexible structures that work under very turbulent and unpredictable environmental conditions for a variable electrical grid. The maximization of wind energy conversion systems, load reduction strategies, mechanical fatigue minimization problems, costs per kilowatt hour reduction strategies, reliability matters, stability problems, and availability (sustainability) aspects demand the use of advanced (multivariable and multiobjective) cooperative control systems to regulate variables such as pitch, torque, power, rotor speed, power factors of every wind turbine, etc. Meanwhile, with increasing demands for efficiency and product quality and progressing integration of automatic control systems in high-cost and safety-critical processes, the fields of fault detection and isolation (FDI) and fault tolerant control (FTC) play an important role.

This thesis covers the theoretical development and also the implementation of different FDI and FTC techniques in WTs. The purpose of wind turbine FDI systems is to detect and locate degradations and failures in the operation of WT components as early as possible, so that maintenance operations can be performed in due time (e.g., during time periods with low wind speed). Therefore, the number of costly corrective maintenance actions can be reduced and consequently the loss of wind power production due to maintenance operations is minimized.

The objective of FTC is to design appropriate controllers such that the resulting closed-loop system can tolerate abnormal operations of specific control components and retain overall system stability with acceptable system performance.

Different FDI and FTC contributions are presented in this thesis and published in different JCR-indexed (3 papers) journals and international conference proceedings (9 papers). These contributions embrace a wide range of realistic WTs faults (both, actuator and sensor faults) as well as different WTs types (onshore, fixed offshore, and floating). In the first main contribution, the normalized gradient method is used to estimate the pitch actuator parameters to be able to detect faults in it. In this case, an onshore WT is used for the simulations. Second contribution involves not only to detect faults but also to isolate them in the pitch actuator system. To achieve this, a discrete-time domain disturbance compensator with a controller to detect and isolate pitch actuator faults is designed. Third main contribution designs a super-twisting controller by using feedback of the *fore-aft* and *side-to-side* acceleration signals of the WT tower to provide fault tolerance capabilities to the WT and improve the overall performance of the system. In this instance, a fixed-jacket offshore WT is used. Throughout the aforementioned research, it was observed that some faults induce to saturation of the control signal leading to system instability. To preclude that problem, the fourth contribution of this thesis designs a dynamic reference trajectory based on hysteresis. Finally, the fifth and last contribution is related to floating WTs and the challenges that this type of WTs face. So finally, a FTC is designed taking into account the platform pitch motion of a floating-barge WT. The performance of the proposed contributions are tested in simulations with the aero-elastic code FAST.

**Keywords:** fault detection, isolation, fault tolerant control, wind turbines.

# ACKNOWLEDGEMENT

First of all, I want to thank God for giving me health, wisdom and strength to finish this stage of my life. To my parents, for being my personal growth example and teaching me that limits do not exist. And with them, to my whole family for all the unconditional support over these years. I want to thank José, Yolanda, my tutor and co-tutor, as well as Leonardo and the CoDAlab (Control, Dynamics and Applications) research group for helping me and receiving me as a member of their family from the first day I arrived. Thank you for inviting me to be part of this great team. This thesis is not only mine, it is a job of the whole CoDAlab team...

*Christian Tutivén*
Barcelona, 2018

# CONTENTS

# LIST OF TABLES

# LIST OF FIGURES

xvi

xvii

# CHAPTER 1

# INTRODUCTION

This chapter outlines the main lines of inquiry on which this thesis research is engaged. It takes the reader from an introduction of the research field to the thesis's contents, through the hypothesis statements and the exposition of the specific objectives.

## 1.1  Motivation

The use of wind energy is not a new technology but draws on the rediscovery of a long tradition of wind power technology. Today, energy production based on the burning of coal and oil or on the splitting of the uranium atom is meeting with increasing resistance, regardless of various reasons. Following the oil crisis of 1973, governments realized that it was necessary to explore and implement other forms of energy such as wind and solar. Getting the energy from the wind turbines (WTs) is synonymous of not producing harmful gases like carbon dioxide. In 1997, the Kyoto Protocol was signed, which has as principal purpose to reduce $CO_2$ emissions. One way to achieve this is by using renewable sources [1]. That was when the wind power became one of the protagonists in renewable energy, and consequently has experienced an exponential growth.

In 2015, increase in wind generation was equal to almost half of global electricity growth [2]. This was due to different factors: industrial restructuring, improved energy efficiency and the substantial growth of renewables. Actually the global wind power installed capacity increased from approximately 59GW at the end of 2005 to 433GW at the end of 2015 [2], see Figure 1.1.

This fast expansion of the wind power market has also come with some problems. WTs are unmanned and remote power plants, they are exposed to highly variable and harsh weather
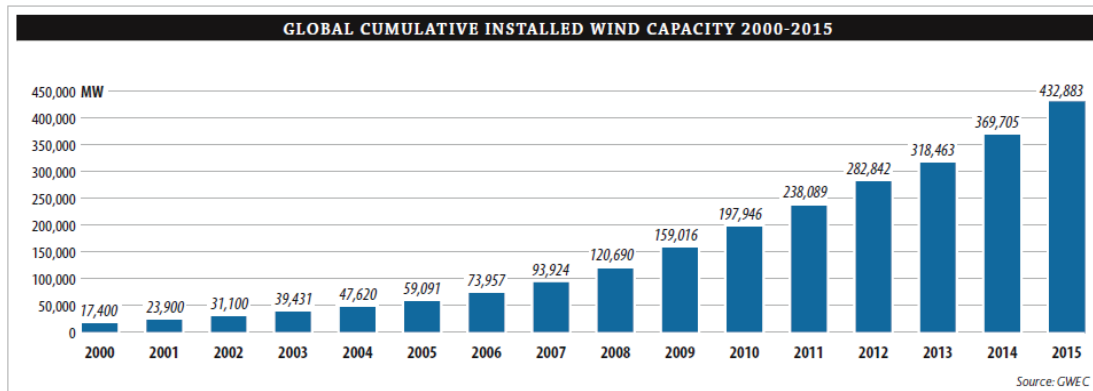
Figure 1.1. Global cumulative installed wind capacity 2000-2015.

Source:( [2])

conditions, including calm to severe winds, tropical heat, lightning, arctic cold, hail, and snow. Due to these external variations, WTs undergo constantly changing loads, which result in highly variable operational conditions that lead to intense mechanical stress [3, 4]. Consequently, the operational unavailability of WTs reaches 3% of the lifetime of a WT. Moreover, operation and maintenance costs can account for 10% -20% of the total cost of energy for a wind project, and this percentage can reach 35% for a WT at the end of life [4]. Thus, research into methods of fault detection and isolation (FDI), as well as fault tolerant control (FTC) techniques that allow WTs to continue operating in the presence of faults (at least during a reasonable time to take a corrective action if the fault is severe and correctly detected) are the crux of the matter, as they will extend operating periods and, thus, minimize downtime and maximize the productivity of WTs [5, 6]. The past few years have seen a rapid growth in interest in wind turbine FDI and FTC. For instance, [7] and [8] provide overviews of the recent status and practical aspects of these two research fields applied to WTs.

## 1.2 Objectives

The overall aim of this thesis is to propose and develop fault detection and isolation systems, as well as fault tolerant control systems for different types of wind turbines, which are an interesting class of large-scale systems.

A proper fault detection and isolation system should ensure that its objective is achieved in a short time so as not to cause damage to the wind turbine and to plan the respective maintenance.

The objective behind FTC is that the WT system can tolerate abnormal operations of specific control components and retain an acceptable performance.

The specific objectives of this thesis are the following:

- To explore the wind turbine state of the art: types, aerodynamics, operations regions, baseline model, baseline controllers, components faults and WT software simulation;

- To review the different FDI and FTC existing techniques and discuss their applicability in WTs;

- To implement a pitch actuator fault detection technique in an onshore WT;

- To design a fault detection and isolation strategy combined with a FTC for onshore WTs;

- To propose and design a control that takes into account the accelerations that occur in the WT tower due to the different faults and apply this technique to an shore WT;

- To implement a FTC using a hysteresis based approach to avoid saturation in controlled WTs;

- To design a FTC control which additionally reduces the platform pitch motion (a significant problem for floating structures) in floating barge offshore WTs;

- To test, over a simulation environment, the designed FDI and FTC techniques and compare the results with the existing baseline controllers.

The contributions of this thesis show my evolution in the consolidation of knowledge in the area of WTs. It is noteworthy the natural process of the proposed contributions starting from a land-based WT, then with a fixed offshore 5MW WT, and finally with a floating offshore type WT.

## 1.3   Layout of the thesis

In particular, the specific objectives have been achieved and organized in the following way:

- Chapter 2 provides a brief review of WTs systems. The baseline model and the different controllers used in WTs are presented to introduce the main concepts of the system under study. Also WTs faults and the software used for the simulations are presented.

- Chapter 3 introduces the main ideas of fault diagnosis and fault-tolerant control. First, a revision of FDI theory and model-based techniques are presented; next a brief introduction to FTC techniques is exposed.

- Chapter 4 develops a fault detection method for the most common pitch actuator faults using the normalized gradient method to estimate the parameters of the pitch actuator. The publication derived from this chapter is:

  **Conference**: **C. Tutivén**, Y. Vidal, L. Acho, and J. Rodellar, *"A fault detection method for pitch actuators faults in wind turbines"*, International Conference on Renewable Energies and Power Quality. La Coruña, Spain (2015).

- Chapter 5 designs a FDI and FTC for pitch actuator faults by combining a discrete disturbance compensator with a discrete controller. The publications derived from this chapter are:

  **Journal**: Y. Vidal, **C. Tutivén**, J.Rodellar, and L. Acho, *"Fault diagnosis and fault-tolerant control of wind turbines via a discrete time controller with a disturbance compensator"*, Energies, Vol. 8, No. 5, pp. 4300–4316 (2015). Journal factor impact: 2.077 (Q2).

  **Conference**: Y. Vidal, J. Rodellar, L. Acho, and **C. Tutivén**, *"Active fault tolerant control for pitch actuators failures tested in a hardware-in-the-loop simulation for wind turbine controllers"*, Mediterranean Conference on Control and Automation. Torremolinos, Spain (2015).

  **Conference**: J. Rodellar, L. Acho, **C. Tutivén**, and Y. Vidal, *"Fault tolerant control for wind turbine pitch actuators"*, Thematic Conference on Smart Structures and Materials. Ponta Delgada, Portugal (2015).

- Chapter 6 designs a passive acceleration-based fault-tolerant control techniques to provide robustness to the WT system against disturbance and uncertainties. The publications derived from this chapter are:

  **Journal**: **C. Tutivén**, Y. Vidal, J. Rodellar, and L. Acho, *"Acceleration-based fault-tolerant control design of offshore fixed wind turbines"*, Structural Control and Health Monitoring, Vol. 24, No. 5 (2016). Journal factor impact: 2.355 (Q2).

**Conference**: **C. Tutivén**, Y. Vidal, L. Acho, and J. Rodellar, *"Super-twisting controllers for wind turbines"*, International Conference on Renewable Energies and Power Quality. Madrid, Spain (2016).

**Conference**: Y. Vidal, L. Acho, J. Rodellar, and **C. Tutivén**, *"Wind turbines controllers design based on the super-twisting algorithm"*, European Control Conference. Aalborg, Denmark (2016).

**Conference**: J. Rodellar, **C. Tutivén**, L. Acho, and Y. Vidal, *"Fault tolerant control design of floating offshore wind turbines"*, European Conference on Structural Control. Sheffield, England (2016).

**Conference**: J. Rodellar, **C. Tutivén**, Y. Vidal, and L. Acho, *"Adapting fault-tolerant control to integration"*, Smart and Multifunctional Materials, Structures and Systems. Perugia, Italy (2016).

- Chapter 7 designs a dynamic reference trajectory strategy to avoid saturation in controlled WTs. The publications derived from this chapter are:

  **Journal**: **C. Tutivén**, Y. Vidal, L. Acho and J.Rodellar, *"Hysteresis-based design of dynamic reference trajectories to avoid saturation in controlled wind turbines"*, Asian Journal of Control, Vol. 19, No. 2, pp. 1–12 (2016). Journal factor impact: 1.421 (Q3).

  **Conference**: **C. Tutivén**, Y. Vidal, L. Acho and J. Rodellar, *"Variable structure strategy to avoid torque control saturation of a wind turbine in the presence of faults"*, International Conference on Renewable Energies and Power Quality. Madrid, Spain, (2016).

  **Conference**: L. Acho, J. Rodellar, **C. Tutivén**, and Y. Vidal, *"Passive fault tolerant control strategy in controlled wind turbines"*, International Conference on Control and Fault-Tolerant Systems. Barcelona, Spain, (2016).

- Chapter 8 develops a passive FTC controller for offshore floating WTs.

- Chapter 9, provides the conclusions of the thesis and a proposal of future work to continue the research in the subject.

# CHAPTER 2

# BACKGROUND ON WIND TURBINES

In this chapter the background on WTs is reviewed in order to introduce the main concepts and the used notation. First a revision of the WT system and its different types are presented; then, the WTs aerodynamics are exposed. The WTs operating regions are presented next. Afterwards the WTs baseline model is given and the WTs faults are presented. A brief introduction to FAST and Turbsim simulators are exposed and the used reference WTs are presented. Then WTs baseline controllers are given. Finally, the performance indices used in the thesis are introduced.

## 2.1 Wind turbines classification

WTs can be classified firstly in accordance with their aerodynamic function and, secondly, according to their constructional design. The aerodynamic tip-speed ratio is used to characterise wind rotors between low-speed and high-speed ones. Apart from the American WT, almost all other WTs designs are of the high-speed type [9]. Classification according to constructional design aspects is more common. They can be classified by the shape of its structure, the different sizes, their generated electric power, as well as the number of blades and the place where they are installed.

### 2.1.1 Structural classification

Wind turbines can be classified in accordance to its axis of rotation: there are vertical axis WT (VAWT) and horizontal axis WT (HAWT), as shown in Figure 2.1.

7

Figure 2.1. Horizontal axis wind turbine (left) and vertical axis wind turbine (right).

Source:( [10, 11])

HAWTs have an advantage over VAWTs as the entire rotor can be placed atop a tall tower, where it can take advantage of larger wind speeds higher above the ground. Some of the other advantages of HAWTs over VAWTs, for utility-scale turbines, include pitchable blades, improved power capture and structural performance, and no need for guy wires (which are tensioned cables used to add structural stability) [12].

The generating capacity of modern commercially-available turbines ranges from less than 1 kilowatt (kW) to several MW.

In this thesis, HAWTs with a 3 blade configuration are used, as they are the most commonly produced [12]. Moreover, this thesis deals with the mega-watt WTs as there are many research challenges related to these large size WTs.

**Horizontal axis wind turbine**

A HAWT can be considered to be an airscrew that extracts kinetic energy from the driving air and converts it into mechanical energy. The similarity of a HAWT to a propeller (which puts energy into the air) enables the same theoretical development used for the propeller to be followed for the HAWT [9].

The HAWTs represent 99% of the total turbines currently installed [11], and are subdivided into:

- Upwind WT, with the rotor on the front of the unit (see Figure 2.2 left) .

- Downwind WT, with the rotor on the back side of the turbine (see Figure 2.2 right).
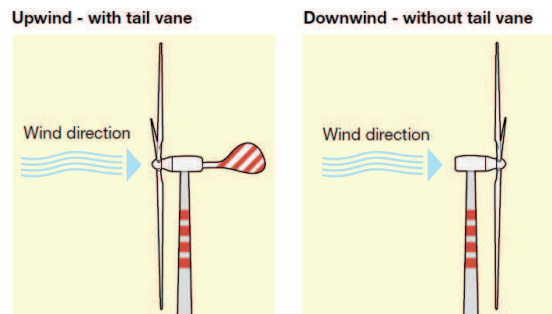


Figure 2.2. Upwind HAWT (left) and downwind HAWT (right).

Source:( [11])

The choice of upwind versus downwind configuration affects the choice of yaw controller and the turbine dynamics, and thus the structural design [12].

HAWTs may also be variable pitch or fixed pitch, meaning that the blades may or may not be able to rotate along their longitudinal axes. The fixed-pitch WTs are less expensive initially, but the reduced ability to control loads and to change the aerodynamic torque are making them less common [12]. Variable-pitch turbines may control all or part of their blades to rotate along the pitch axis.

As indicated in [13], the main subsystems of the HAWTs are the rotor, the transmission mechanism, the nacelle and the tower. Next subsections include a review of the two subsystems that are important for the developed research work: rotor subsystem and transmission mechanism.

**Rotor subsystem**

The rotor main components are the blades that are mounted on the hub. When the rotor rotates, the blades generate an imaginary surface which is called sweeping area. The blades are responsible for capturing the wind energy of the wind and transforming it into a kinetic energy.

As noted above, the HAWTs can be classified into downwind turbines and upwind turbines denoting the location of the rotor relative to the tower. The choice of the turbine configuration affects the choice of the orientation controller (Yaw) and the dynamics of the turbine, therefore also to the structural design. The orientation motor is the one that allows turning the WT to align with the wind and is almost always included in the large turbines. However, because gyroscopic forces are dangerous, a rotation of the turbine at high speed is generally not desirable. Most large turbines spin at speeds of less than 1 %/s. Therefore, the investigation of advanced controllers for orientation control is not as much of an interest as the advanced controllers for other actuators [14].

Wind turbines can be variable pitch or fixed pitch, meaning that their blades may or may not be able to rotate along their longitudinal axes using actuators and control systems, thus achieving change the attack angle (pitch angle) of the wind on the blades. The pitch mechanism provides a control of aerodynamic loads.

**Transmission mechanism subsystem**

The WT transmission mechanism is the subsystem consisting of the mechanical and electrical elements that convert the mechanical energy into electric power. The transmission mechanism is located at the top, so is important that it design is to operates with low maintenance.

Its main parts are the turbine shaft assembly (also called low speed or primary shaft), the gearbox, the generator drive shaft (also called high speed or secondary shaft), a rotor brake and a generator, in addition to auxiliary equipment for control, lubrication and cooling functions. Figure 2.3 shows the main parts of a WT, between which are the elements of the drive-train (low speed shaft, gears, high speed shaft).
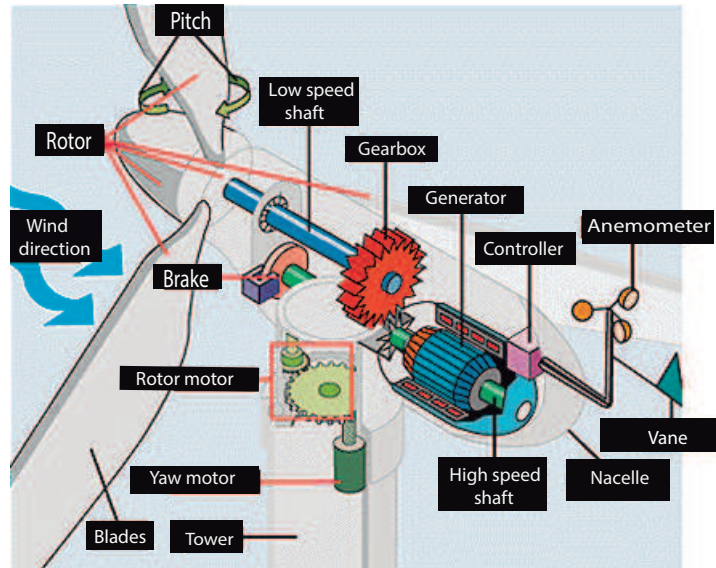
Figure 2.3. General WT transmission mechanism.

Source:( [12])

The turbine shaft assembly is one of the most critical components in a HAWT, because it has structural and mechanical functions. Rotor weight, thrust, torque and lateral forces cause fatigue to this component. The main shaft is formed by bearings, couplings and lubrication, it also includes a rotor control and safety system (such as the sensor and a brake rotor ), hydraulic rotation coupling, collector rings (for power and data transfer) and connects the electrical equipment and mechanically with the necessary cables and pipes.

If the HAWT has a rotor brake, its disc may be mounted on this shaft instead of on the turbine shaft for braking power multiplication. If there is a pitch angle control as a mechanism for braking the rotor, the rotor brake is generally used only for emergencies, stops and maintenance.

In addition, WTs can be fixed speed or variable speed. Variable speed tend to operate near their highest aerodynamic efficiency in a greater percentage of time than fixed speed, but they have to process the energy which is generated in such a way that it can be supplied to the electrical network at the appropriate frequency. With a wide variety of types of generators used in WTs, variable speed WTs are becoming more and more popular, thanks to improvements in

generator technology and in the power electronics the costs decrease.

## 2.1.2 Placement classification

The WTs can be classified by the place where they are installed and the main difference is the foundation. As can be seen in Figure 2.4, in this case, WTs can be classified in:

- Onshore WTs (they stand on a concrete foundation).

- Fixed offshore WTs (they have the foundation on the sea bed).

- Floating offshore WTs (they have the foundation in the water).
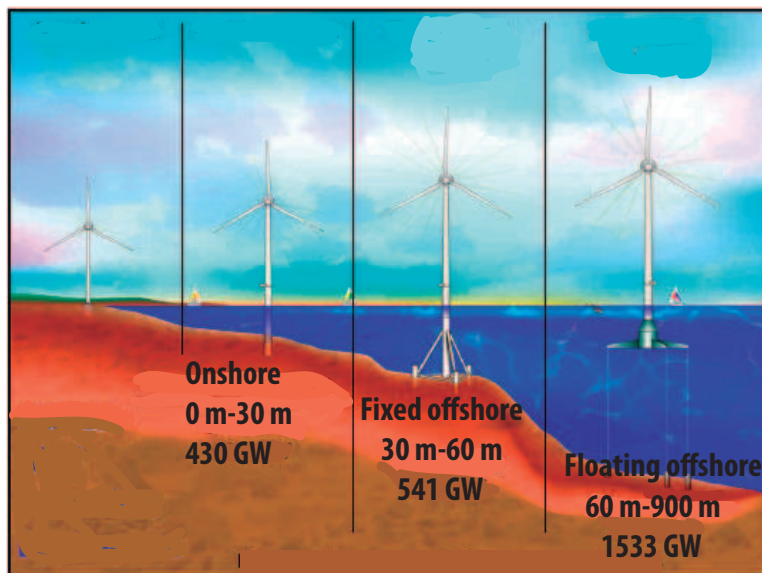


Figure 2.4. Classification of WTs by installation place.

Source:( [15])

Land-based wind power has been the worlds fastest growing energy source on a percentage basis for more than a decade [16]. Onshore wind is cheaper while requiring less infrastructure and less advanced and specialized technology. The biggest hurdle to the optimization of onshore WTs is the variability of wind speeds over land [17]. Wind turbines are optimized for a specific wind speed, and undergo a rather drastic loss in efficiency when the wind speed varies from this ideal speed. In fact, because onshore turbines are optimized for the low-speed winds that are

most common on land, when high-energy wind gusts blow through these wind farms, they are often so inefficient that it is more cost effective to shut them down to reduce wear and tear and minimize risk of damage. Additionally, wind direction is rather variable over land. Horizontal axis turbines (by far the most common variety) must be pointed into the wind to collect energy from the wind, so if the wind changes direction they are also either very inefficient or simply shut down. New turbines can rotate slightly or gently change the pitch of their blades to adapt to changing wind direction and speed. WTs are being placed further offshore because of the better wind resource, scarcity of land available for development, reduced visual impact and like a solution for the wind problems mentioned before.

The advantages of installing wind energy offshore include the following [18, 19]:

- The wind tends to blow more strongly and consistently, with less turbulence intensity and smaller shear at sea than on land.

- The size of an offshore WT is not limited by road or rail logistical constraints if it can be manufactured near the coastline.

- The visual and noise annoyances of WTs can be avoided if the turbines are installed a sufficient distance from shore.

- Vast expanses of uninterrupted open sea are available and the installations will not occupy land, interfering with other land uses.

These advantages are offset by several disadvantages of placing WTs offshore [18, 19]:

- A higher capital investment is required for offshore WTs because of the costs associated with marinization of the turbine and the added complications of the foundation, support structure, installation, and decommissioning.

- Offshore installations are less accessible than onshore installations, which raises the operations and maintenance costs and possibly increases the downtime of the machines.

- Not only do offshore WTs experience environmental loading from the wind, but they must also withstand other conditions, such as hydrodynamic loading from waves and sea currents. As a result, the complexity of the design increases.

Different offshore locations require different support structure designs [15]. In shallow water, where the water depth is less than 30 meters (m), monopiles and gravity-based substructures

that extend to the seabed may be used. At transitional water depths of 30 to 60 m, fixed-bottom, multimember support structures such as jackets and tripods may be used. For water depth that is greater than 60 m, floating platforms may be required.

More than 70% of the world's offshore wind resource is located in deep water around the world [20]. Thus, floating foundations are likely to represent the long-term future for the off-shore wind industry, as they will be the most economical in depths greater than 60m [21]. Several floating structures have been studied in the literature, including barge, spar-buoy, and tension leg platforms [22], [23], [24]. Figure 2.5 shows these floating structures, which are clas-sified in terms of how the designs achieve static stability. In [15] is presented this classification:

- The spar-buoy concept, which can be moored by catenary or taut lines, achieves stability by using ballast to lower the center of mass below the center of buoyancy.

- The tension leg platform (TLP) achieves stability through the use of mooring-line tension brought about by excess buoyancy in the tank.

- The barge is generally moored by catenary lines and achieves stability through its water-plane area.
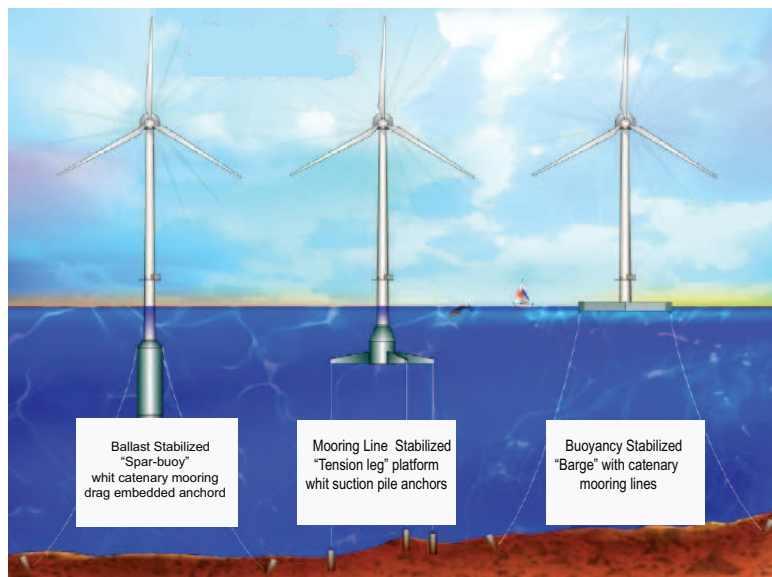


Figure 2.5. Floating WTs classification.

Source:( [22])

This thesis considers onshore, fixed offshore (jacket structure) and floating offshore WTs, and their characteristics will be shown in Section 2.8.

## 2.2 Aerodynamics of wind turbines

The energy production of a WT depends on interaction between the WT rotor and the wind. The first aerodynamic analyses of WTs were carried out by Betz [25] and Glauert [26] in 1926 and 1935 respectively. The wind power is given by

$$P_{wind} = \frac{1}{2}\rho A_b V_{wind}^3, \tag{2.1}$$

where $\rho$ is the air density, $A_b$ is the swept area by blades, and $V_{wind}$ is the wind speed. For calculations $V_{wind}$ is considered uniform in all the swept area by blades, but in reality it is different at each point within area.

The wind relationship between the wind power and the WT extracted power is called aerodynamic efficiency $(C_p)$. Betz proved that the maximum power extractable by an ideal turbine rotor with infinite blades from wind under ideal conditions is 59.26% of the power available in the wind. This limit is known as the Betz limit [27]. In practice, wind turbines are limited to two or three blades due to a combination of structural and economic considerations, and hence, the amount of power they can extract is closer to about 50% of the available power [28].

The aerodynamic efficiency is the relationship between turbine power and wind power and is called turbine power coefficient, $C_p$, which can be described by

$$C_p = \frac{P_t}{P_{wind}}, \tag{2.2}$$

where $P_t$ is the power captured by the turbine and $P_{wind}$ is the power available in the wind for a turbine of that size.

A simplified model of the rotor is used in [14, 29–32], which assumes an algebraic relationship between the wind speed and the extracted mechanical power, which is described by

$$P_m(u) = 0.5C_p(\beta, \lambda)\rho\pi R_{rot}^2 V_{wind}^3, \tag{2.3}$$

where $R_{rot}$ is the rotor radius, $\beta$ is the pitch angle and $\lambda$ is the tip speed, which is described by

$$\lambda = \frac{R_{rot}\omega_r}{V_{wind}}, \tag{2.4}$$

where $\omega_r$ is the angular rotor speed. As shown in [33], changes in wind speed or rotor speed produce variation in the power coefficient, so the generated power changes. There is a relationship between the aerodynamic torque coefficient and the power coefficient, which is described as

$$P_m = \omega_r T_a, \tag{2.5}$$

where the expression of the aerodynamic torque is given by

$$T_a = 0.5C_q(\beta, \lambda)\rho\pi R_{rot}^3 V_{wind}^2, \tag{2.6}$$

and

$$C_q(\beta, \lambda) = \frac{C_p(\beta, \lambda)}{\lambda}. \tag{2.7}$$

For a perfectly rigid low velocity shaft, a simple single mass model for a WT can be considered [14, 29, 33–35] as

$$J_t\dot{\omega}_g = T_a - K_t\omega_g - T_g, \tag{2.8}$$

where $J_t$ is the WT total inertia (Kg m$^2$), $K_t$ is WT total external damping (Nm rad$^{-1}$s), $T_a$ is the aerodynamic torque (Nm) and $T_g$ is the generator torque (Nm). The scheme of a one mass model can be seen in Figure 2.6.
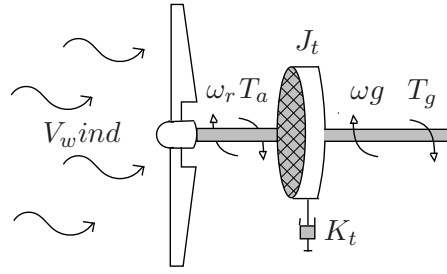
Figure 2.6. Turbine one mass model.

Source:(Author)

If the rotor acceleration $\dot{\omega}_r$ is isolated from the Equation (2.8) the following, is obtained

$$\dot{\omega}_g = \frac{T_a - K_t\omega_g - T_g}{J_t},\qquad(2.9)$$

where it is considered that the generator torque is the system control signal, so from now will be called control torque $T_c$ and will be a signal helping to achieve the desired goals.

## 2.3 Operating regions

The wind has a power that can be captured by the WT, which depends on the wind speed. The variable-pitch variable-speed WT operates typically in two different regions, the full load region and the partial region, see Figure 2.7. In the full load region, the wind has enough energy to run the turbine at its rated rotor speed, and the main task of the controller is to adapt the aerodynamic efficiency of the rotor by pitching the blades into or out of the wind in order to keep the rotor speed at its rated value. On the contrary, the maximum aerodynamic efficiency is maintained in the partial load region, and the controller task is to follow the maximum power production by changing the rotor speed and consequently the generator torque [6]. Blade pitching is activated only in the full load region, while in the partial load region the blades are kept at zero pitch angle in order to maintain the maximum aerodynamic efficiency of the rotor.

This work is concentrated in the full load region of operation, thus only the baseline controllers in this region will be recalled (see Section 2.9.1).

17
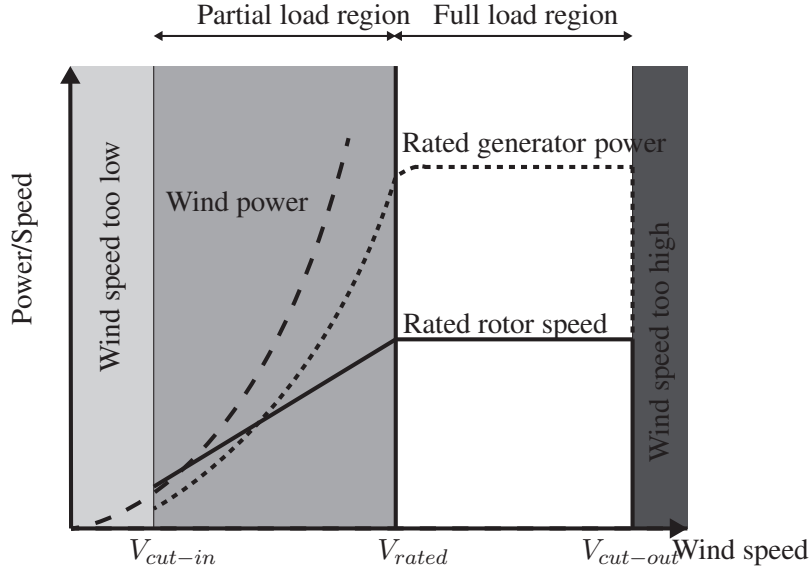
Figure 2.7. Wind turbine operating regions.

Source:(Author)

## 2.4 Wind turbines baseline model

This section describes the development of a generic dynamic model for a 5MW three-bladed upwind variable-speed variable pitch-controlled turbine. The WT consists of a rotor assembly, gear-box, and generator. A complete description of the WT model can be found in [36]. Hereafter, only the generator-converter actuator model and the pitch actuator model are recalled in order to introduce the notation and the concepts employed in following sections.

### 2.4.1 Generator-converter model

The generator-converter system can be modeled by a first-order differential equation, see [37, 38], which is given by

$$\dot{\tau}_g(t) + \alpha_{g,c}\tau_g(t) = \alpha_{g,c}\hat{\tau}_c(t), \tag{2.10}$$

where $\tau_g$ is the generator torque, $\hat{\tau}_c$ is the saturated reference torque to the generator (given by the controller) and $\alpha_{g,c}$ is the generator and converter model parameter (in the simulations $\alpha_{g,c} = 50s^{-1}$ [36]. The electrical power produced by the generator can be modeled by

18

$$P_e(t) = \eta_g \omega_g(t) \tau_g(t), \tag{2.11}$$

where $\eta_g$ is the generator efficiency (in the simulations $\eta_g = 0.98$) and $\omega_g$ is the generator speed measurement, see Figure 2.8.

### 2.4.2 Pitch actuator model

The hydraulic pitch system can be modelled by a second order system, see [5], with the filtered reference angle $\hat{\beta}_c$ and the actual pitch angle $\beta_i$ as

$$\ddot{\beta}_i(t) + 2\zeta\omega_n\dot{\beta}_i(t) + \omega_n^2\beta_i(t) = \omega_n^2\hat{\beta}_c(t), \tag{2.12}$$

where $\zeta$ is the damping factor and $\omega_n$ is the natural frequency. This diferential equation is associated to the pitch control system of every blade ($i = 1, 2, 3$). For the healthy case, the parameters $\zeta = 0.6$ and $\omega_n = 11.11$rad/s are used [5].
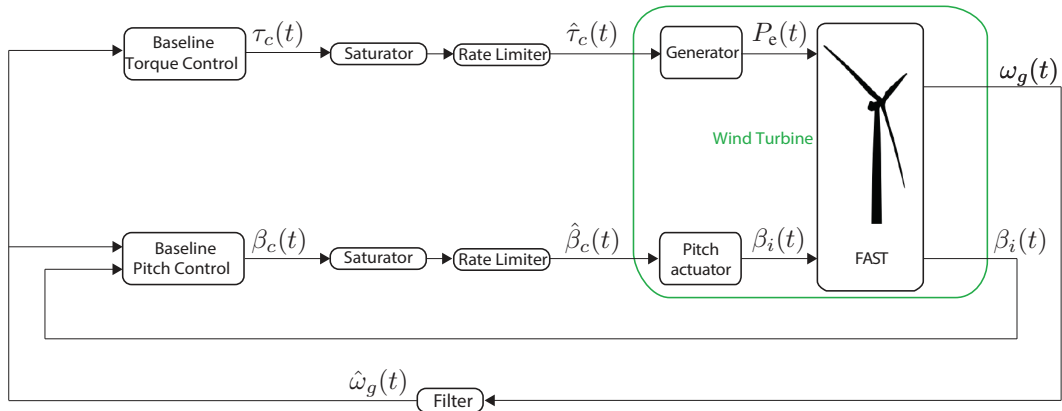


Figure 2.8. Block diagram of the baseline WT closed loop system.

Source:(Author)

## 2.5 Wind turbines faults

A fault is any change in the behavior of any of the components of the system (non-allowed deviation of some of its properties or parameters characteristics) so that it can no longer satisfy

the function for which it has been designed [39, 40]. Automatic control systems are susceptible to faults and can be amplified by the control loop, causing malfunction, e.g. reducing the WT electrical power production. In addition, the control loops can hide the faults avoiding being observed until reaching a degree such that they produce an irreparable fault that forces to stop the system or process [40].

Faults in general could be categorized according to their temporal profile as incipient or abrupt [6]. Incipient faults are slow to happen and progress slowly with time and system dynamics are gradually changed, on the contrary, abrupt faults are sudden and unexpected. Abrupt faults are generally more easier to detect than the incipient faults; however, they might have severe consequences on the system.

According to WTs reliability analysis [6], the most common faults occur in the pitch system, power electronics, generator assembly and in turbine sensors [41]. Actually, one of the recent studies is the Reliawind project survey that studied WT subassembly reliability information from of 35,000 down events obtained from 350 onshore WTs operating for varying length of time [41]. The Reliawind survey shares the well-known failure rates to the public domain, where the pitch system failure rate dominates by more than 20% failures/turbine/year.

Very recently, the research community started to draw attention of this topic, aiming to analyze the dynamic response of WTs during different fault scenarios, and comparing their structural loading to the loading created during normal operation or extreme events in order to estimated the severity of each fault on the turbine structure [6]. Due to the great interest in fault tolerant control in WTs coming from the industry and academia, a first benchmark model about fault tolerant control of WTs was presented in [42]. In this paper, Odgaard presented different kinds of possible faults in WTs. After that he presented others benchmark and competition papers including more fault scenarios. Also, the fault scenarios were updated and additional information detailing their relevance was provided. These faults cover sensor, actuator, and process faults in different parts of the WT.

Only the studied WT faults will be recalled in this section and are described in Table 2.1.

### 2.5.1 Pitch actuator dynamics faults

The hydraulic pitch system consists of the main pump that provides the hydraulic pressure to the system, a set of valves that have different tasks such as the servo valves that control the position of the actuators and the blade pitch motion is achieved through an actuator. The system is also

Table 2.1. Faults considered in this thesis.

| Fault | Type |
|---|---|
| Pitch actuator fault | Changed dynamics (see Table 2.2) |
| Pitch actuator fault | Stuck/unstuck pitch actuator |
| Pitch position sensor | Fixed pitch angle measurement |

Source:( [37])

provided with a controller that accepts the error signal between the measured blade pitch angle and the set reference one and issues the appropriate command to the servo valves. The reference pitch angle is set by the baseline GSPI controller (see Section 2.9.1).

A fault may change the dynamics of the pitch system by varying the damping ratio and natural frequencies from their nominal values to their faulty values in Equation (2.12). The parameters for the pitch system under different conditions are given in Table 2.2. The normal air content in the hydraulic oil is $7\%$. The high air content in the oil (F1) is an incipient reversible process, which means that the air content in the oil may disappear without any necessary repair to the system. The high air content in oil correspond to $15\%$.

On the contrary to high air content in oil, pump wear (F2) is an irreversible slow process over the years that results in low pump pressure and represents the situation of $75\%$ pressure in the pitch system. As this wear is irreversible, the only possibility to fix it is to replace the pump which will happen after pump wear reaches certain level. Hydraulic leakage is another irreversible incipient fault, but is introduced considerably faster than the pump wear. The parameters stated for hydraulic leakage correspond to a pressure of only $50\%$. When this fault reaches a certain level, system repair is necessary, and if the leakage is too fast, it will lead to a pressure drop and the preventive procedure is deployed to shut down the turbine before the blade is stuck in undesired position. These faults are introduced only in the pitch actuator model of blade 3 (other blades are healthy) and are used in Sections 4, 5, 6 and 8.

Table 2.2. Parameters for the hydraulic pitch system under different conditions.

| Condition | $\omega_n$(rad/s) | $\zeta$ |
|---|---|---|
| Fault-free (FF) | 11.11 | 0.6 |
| High air content in the oil (F1) | 5.73 | 0.45 |
| Pump wear (F2) | 7.27 | 0.75 |
| Hydraulic leakage (F3) | 3.42 | 0.9 |

Source:( [43, 44])

### 2.5.2   Stuck/unstuck pitch fault

In [45] a stuck/unstuck fault (F4) of the pitch actuator is studied. In particular, the actuator is stuck to 0 degrees at the beginning of the computation, then after 50 s it gets unstuck and then each period of 75s is switched between being stuck/unstuck. This fault is modeled using the following ordinary differential equation:

$$\dot{\beta}_i = p(-\beta_3 - \beta_1), \tag{2.13}$$

where $p$ is a pulse generator of amplitude 10, period 150 s, pulse width (% of period) 50, and a phase delay of 50s. When $p$ equals 0 the actuator is stuck and when $p$ equals 10 then $\beta_i$ follows again the pitch control. Initially, the actuator is stuck to 0%. This fault is introduced only in the pitch actuator of blade 3 (other blades are healthy) and is used in Sections 6 and 8.

### 2.5.3   Fixed pitch angle measurement fault

The origin of a possible fixed pitch angle measurement fault (F5) can be either electrical or mechanical [37]. Moreover, noise can be present in measurements. Thus, in the numerical simulations, random noise is added to the pitch measurements as proposed in [5]. This noise represents measurement noise either due to the measuring process or due to electrical noise in the system. In Section 7 this fault is introduced only to the third pitch angle measurement, $\beta_3$, which holds a constant fault value of 1 deg. (see [5]).

## 2.6   FAST simulator

The FAST code [46] is an aerolastic simulator capable of predicting both the extreme and fatigue loads of two and three bladed HAWTs. This simulator was developed by the National Renewable Energy Laboratory (NREL) and has been accepted by the scientific community and is used by many researchers in the development of new control systems for WTs. We select this simulator for validation due to the fact that in 2005 the Germanischer Lloyd WindEnergie evaluated FAST and found it suitable for the calculation of onshore WT loads for design and certification [47].

22

An interface has also been developed between FAST and *Simulink*® with *MATLAB*®, enabling users to implement advanced turbine controls in Simulink's convenient block diagram form.

FAST has two different forms of operation or analysis modes [46]. The first analysis mode is time-marching of the nonlinear equation of motion, that is simulation. During simulation, WT aerodynamic and structural response to wind-inflow conditions is determined in time. Active controls for determining many aspects of the turbine operation may be implemented during simulation analyses. Outputs of simulations include time-series data on the aerodynamic loads as well as loads and deflections of the structural members of the WT. These outputs can be used, for example, to predict both the extreme and fatigue loads of HAWTs. The aerocoustic signature of an operating turbine is another output that can be obtained from simulation.

The second form of analysis provided in FAST is linearization [46]. FAST has the capability of extracting linearized representations of the complete nonlinear aeroelastic WT modeled in FAST. This analysis capability is useful for developing state matrices of a WT plant to aid in controls design and analysis. It is also useful for determining the full system modes of an operating or stationary HAWT through the use of a simple eigenanalysis.

Another feature available in FAST is the ADAMS preprocessor [46]. The ADAMS preprocessor feature is separate from the two analysis modes available in FAST. It is not considered an analysis mode of FAST, because it does not make use of the aeroelastic wind WT model available in FAST. Instead, the ADAMS preprocessor uses the input parameters available in the FAST input files to construct an ADAMS dataset of a complete aeroelastic WT. ADAMS then becomes the code in which different WT analyses (simulation or linearization) are performed.

Several FAST models of real and composite WTs of varying sizes are available in the public domain. In this work, onshore, fixed-offshore (jacket structure) and floating offshore (barge) versions of a large WTs that are representative of real utility-scale multi-megawatt turbines described by [36] are used. These WTs are conventional three-bladed upwind variable-speed variable pitch-controlled turbines. In fact, are fictitious 5-MW machines with their properties based on a collection of existing WTs of similar rating, since not all turbines properties are published by manufacturers. The main properties of these turbines are listed in Section 2.8.

## 2.7 Wind modeling and its simulator

In fluid dynamics, turbulence is a flow regime characterized by chaotic property changes [48]. This includes low momentum diffusion, high momentum convection, and rapid variation of pressure and velocity in space and time [49]. In the simulations, new wind data sets are generated in order to capture a more realistic turbulent wind simulation and, thus, to test the turbine controllers in a more realistic scenario. The turbulent-wind simulator TurbSim [50], developed by NREL, is used and a full TurbSim wind field is employed in the simulations.

TurbSim is a stochastic, full-field, turbulent-wind simulator. It uses a statistical model (as opposed to a physics-based model) to numerically simulate time series of three-component wind-speed vectors at points in a two-dimensional vertical rectangular grid that is fixed in space [51]. TurbSim output can be used as input into AeroDyn-based [52] codes such as FAST [46] or MSC.ADAMS [53]. AeroDyn's InflowWind module uses Taylor's frozen turbulence hypothesis to obtain local wind speeds, interpolating the TurbSim-generated fields in both time and space. Spectra of velocity components and spatial coherence are defined in the frequency domain, and an inverse Fourier transform produces time series. The basic simulation method is summarized in Figure 2.7.
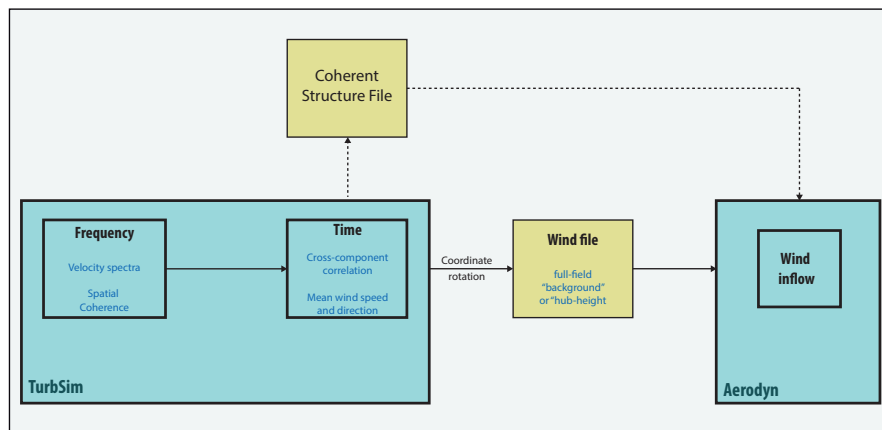


Figure 2.9. TurbSim simulation method: a transformation from the frequency domain to time domain producing wind output compatible with AeroDyn; optional coherent structures are written to a separate file and superimposed in AeroDyn (they require a full-field background wind file).

Source:( [51])

The generated wind data has the following characteristics:

- Grid settings and position matched with the rotor diameter, and the center of the grid positioned at hub height. This represents a grid size of $130 \times 130$m centered at $19.55$m.

- The Kaimal turbulence model is selected.

- The turbulence intensity is set to $10\%$.

- Normal wind type is chosen with a logarithmic profile.

- Reference height is set to $90.25$m. This is the height where the mean wind speed is simulated.

- Mean (total) wind speed is set to $18.2$m/s.

- The roughness factor is set to $0.01$m which corresponds to a terrain type of open country without significant buildings and vegetation.
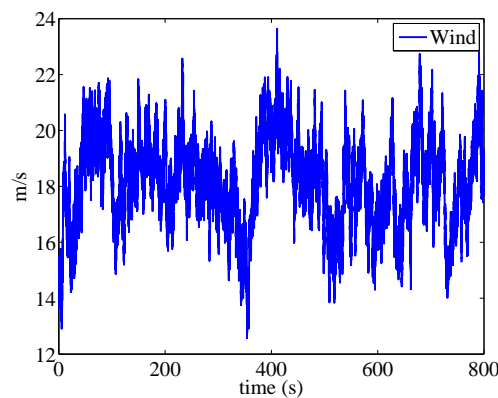


Figure 2.10. Hub-height wind speed for simulation tests. It is noteworthy the simulated wind gust is from 350s to 400s (approximately) where wind speed moves from 12.91m/s up to the maximum of 22.57m/s, followed by an abrupt decrease in the next 100s.

Source:(Author)

It can be seen from Figure 2.10 that the wind speed covers the full load region (also called region 3) as its values range from 12.91m/s up to the maximum of 22.57m/s.

## 2.8   Reference wind turbines

Several FAST models of real and composite WTs of varying sizes are available in the public domain. In this thesis, onshore, fixed offshore (jacket structure) and floating offshore (barge)

25

versions of a large WT, that are representative of the real utility-scale land- and sea-based multi-megawatt turbines described by [36], are used. These are horizontal axis, three-bladed, upwind, variable-speed, variable pitch-controlled WTs. Next subsections recall the characteristics of these WTs.

### 2.8.1 Onshore wind turbine

The onshore version of a large WT that is representative of real utility-scale land- and sea-based multi-megawatt turbine described by [36] is used in Sections 4, 5 and 7. The main properties of the onshore WT are listed in Table 2.3.

Table 2.3. Main properties of wind turbines.

| Reference wind turbine | |
| --- | --- |
| Rated power | 5MW |
| Number of blades | 3 |
| Rotor/Hub diameter | 126m, 3m |
| Hub height | 90m |
| Cut-In, Rated, Cut-Out Wind Speed | 3m/s, 11.4m/s, 25m/s |
| Nominal generator speed | 1173.7rpm |
| Gearbox ratio | 97 |

Source:( [36])

### 2.8.2 Fixed-jacket offshore wind turbine

As reference, the jacket support structure (see Figure 2.11) by the UpWind project is used [54]. The definition of the jacket support structure consists of a jacket substructure, a transition piece and a tower. Four legs of the jacket are supported by piles, which are modeled as being clamped at the seabed. The legs are inclined from the vertical position and stiffened by four levels of X-braces. Additionally, mud braces are placed just above the mud line to minimize the bending moment at the foundation piles. The jacket and the tower are connected through a rigid transition piece. The elevation of the entire support structure is 88.15m, whereas the hub height is 90.55m. This WT is analyzed for a site of 50m water depth.

A complete description of this WT model can be found in [36] and a detailed descripton of the jacket model is given in [54]. The main properties of the fixed-jacket offshore WT used in
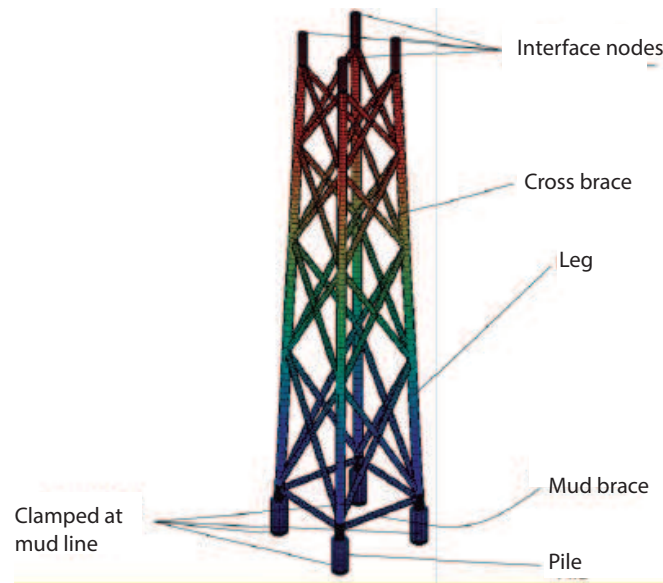
Figure 2.11. Jacket structure.

Source:( [55])

Section 6 are listed in Table 2.3.

### 2.8.3 Floating-barge offshore wind turbine

WTs on barge platforms are subjected to completely different and soft foundation properties, than seen for onshore WTs and they must also withstand the offshore wind and wave environment. This leads to an increase in the platform motion and can also cause instability. Also six degrees of freedom (DOFs) are introduced to characterize the motion of the support platform. For floating systems, it is crucial that all six rigid-body modes of motion of the support platform are included in the development [15]. These include translational surge, sway, and heave displacement DOFs, along with rotational roll, pitch, and yaw displacement DOFs, as shown in Figure 2.12. These added DOFs, if not taken into account actively or passively, can negatively affect the power production and turbine structural loading [56]. The analysis of offshore WTs must also account for the dynamic coupling between the motion of the support platform and the WTs, and for the dynamic characterization of the mooring system for compliant floating platforms. The load comparison between land-based and floating turbines shows a dramatic increase in the loading of the floating structure, basically, in the tower base *fore-aft* and *side-side* bending moments, blade flapwise and edgewise bending moments, and drive-train torsional loading [22].
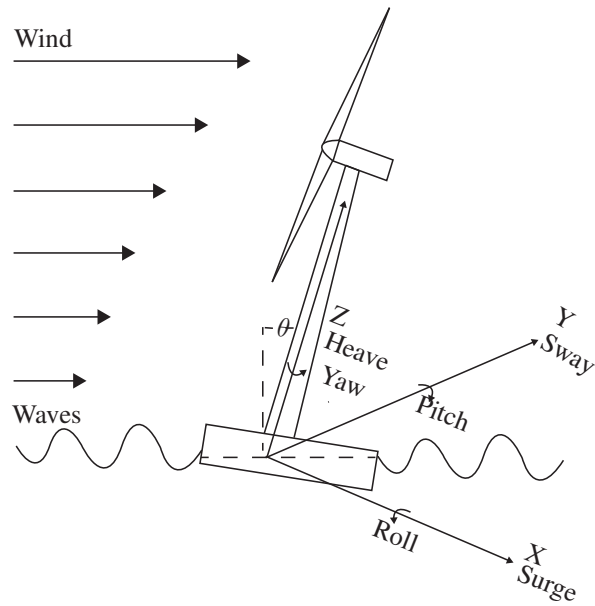
Figure 2.12. Offshore floating WT and its marine platform.

Source:(Author)

A potential problem in offshore floating wind turbines (OFWTs), is that excessive loads occur due to the large platform pitch motion in above rated conditions [22, 23, 57–60]. These large motion and load are a result of a poorly damped mode in the platform pitch direction, which is increased by the coupling between the blade pitch control system (for power regulation) and the platform dynamics. Reference [57] shows a physical explanation for this poorly damped mode that can be summarized as follows, "as the platform pitches upwind in the above rated conditions, the relative wind speed seen by the rotor increases." To maintain a constant rotor speed and constant power output, the WT control system increases the collective pitch angle of the blades. This results into reduced rotor thrust, and so exacerbates the motion of the platform in the upwind direction. A similar effect occurs when the platform pitches downwind; because the rotor thrust decreases with increasing relative wind speed in the above rated conditions, it results in a negative damping contribution to the platform pitch motion.

The main properties of this turbine and the barge platform are listed in Table 2.3 and Table 2.4. This OFWT is used in Section 8.

The full nonlinear models of the NREL 5MW WTs [15, 36] are simulated using FAST, while the controllers are implemented in Matlab/Simulink.

28

Table 2.4. Properties of the floating-barge offshore WT.

| Reference wind turbine | |
| --- | --- |
| Barge platform length | 40m |
| Barge platform width | 40m |
| Barge platform height | 10m |
| Barge platform draft | 4m |
| Barge platform mass | 5,452,330kg |
| Water depth | 150m |

## 2.9   Wind turbines baseline controllers

### 2.9.1   Wind turbines baseline control strategy in full load region

The three-bladed 5MW reference WT given by FAST contains torque and pitch controllers for the full load region, see [36]. This section recall these controllers and refer to them as the baseline torque and pitch controllers, as their performances will be used for comparison with the proposed technique stated in this thesis. Also the baseline controllers are used in the literature for comparison purposes, e.g. [6, 14, 34, 61, 62].

In the full load region, the torque controller maintains regulated the generated power, thus the generator torque is proposed inversely proportional to the filtered generator speed [46], or,

$$\tau_c(t) = \frac{P_{\text{ref}}}{\hat{\omega}_g(t)}, \tag{2.14}$$

where $P_{\text{ref}}$ is the reference power (normally the nominal value is used), and $\hat{\omega}_g$ is the filtered generator speed. This controller will be referred as the baseline torque controller. As the generator may not be able to supply the desired electromechanic torque depending on the operating conditions, and in the case of overshooting, the torque controller is saturated to a maximum of 47402.9 Nm, rate limited to a maximum of 15000 Nm/s [36], and finally called $\hat{\tau}_c$. It is important that the control design takes into account these actuator limits. Otherwise, undesirable effects can appear, such as transient response, degradation of the closed-loop performance, and even closed-loop instability [63]. Obviously, all these degradation performance effects arrive from the saturation core, among other harmful events. Furthermore, saturation can induce the appearance of cycles.

To assist the torque control with regulating the WT electrical power output, while avoiding significant loads and maintaining the rotor speed within acceptable limits, a collective pitch controller is added to the generator speed tracking error. The collective blade pitch Gain Scheduling PI-controller (GSPI) is one of the first well-documented controllers and it is used in the literature as a baseline controller to compare the obtained results. This GSPI control is a collective pitch controller that compensates the nonlinearities in the turbine by changing the controller gains according to a scheduling parameter. This controller was originally developed by Jonkman for the standard land-based 5MW turbine, see [36]. The GSPI control has the filtered generator speed as input and the pitch servo set-point, $\beta_c$, as output. That is,

$$\beta_c(t) = K_p(\gamma)(\hat{\omega}_g(t) - \omega_{g,r}(t)) + K_i(\gamma)\int_0^t (\hat{\omega}_g(t) - \omega_{g,r}(t))d\tau,$$  (2.15)

$$i = 1, 2, 3,$$

where $\omega_{g,r}$ is the reference generator speed (usually the nominal value is used) and the scheduling parameter $\gamma$ is obtained by averaging the measurements of all pitch angles as

$$\gamma = \frac{\sum_{i=1}^{3} \beta_i(t)}{3}.$$  (2.16)

The scheduled gains are calculated following [36]. Finally, to not exceed the mechanical limitations of the pitch actuator, the input signal $\beta_c$ is saturated to a maximum of 90° and a rate limit of 8°/s [36], and finally called $\hat{\beta}_c$.

The torque and pitch controllers use the generator speed measurement as a feedback input. To mitigate high-frequency excitation of the control system, is filtered the generator speed measurement, using a recursive, single-pole low-pass filter with exponential smoothing as proposed by [36, 64].

### 2.9.2   Modified baseline control strategy in full load region

Controls are already used in operating onshore turbines to damp undesirable structural resonances and reduce the dynamic response to turbulence in the wind. Therefore, in floating platforms it is conceivable that controls could be used to limit the response of the entire turbine/platform system to stochastic wave loading, for example, reduce platform motion,

have a good regulating power output performance, and reduce structural loading to name a few objectives. The control of OFWTs is a relatively new area of research. Several control strategies, such as feeding back the tower-top acceleration in an additional control loop, pitching to stall, and detuning the pitch controller gains, have been reported in [65] to increase the damping of the barge platform pitch motion. For the first strategy, the results did not show a major improvement in the damping of the pitch motion, but it did show a massive increase in the generator power and rotor speed behavior. Secondly, by pitching the blade to stall (instead of feather), a good regulation of the generator power and rotor speed are obtained, but at the same time the platform pitch damping is actually worse than the baseline case. This seemingly contradictory result can be explained by examining the damping ratios. Detuning the gains for the collective pitch controller improved the power and speed regulation and reduced the platform pitch motion. However, one of Jonkman's recommendations is to use the potentials of the multi-input multi-output (MIMO) state-space-based control systems, which are not yet extended to floating WTs.

In this section, the usual baseline control strategy described in [36] is not used, it is replaced by its modification described in [66], with the objective of eliminating the potential for negative damping of the platform-pitch mode and improving the floating turbine system's response.

The first modification was a change in the generator-torque control strategy when operating at rated power (that is, control Region 3). That is, the new control law in Region 3 is set to a constant generator-torque signal (rated toque):

$$\tau_c(t) = 43093.55 \text{Nm}. \tag{2.17}$$

With this change, the generator-torque controller does not introduce negative damping in the rotor-speed response (which must be compensated by the blade-pitch controller), and so, reduces the rotor-speed excursions that are exaggerated by the reduction in gains in the blade-pitch controller. This improvement, though, comes at the expense of some overloading of the generator, as power increases with the above rated rotor-speed excursions. Larson and Hanson [23] have demonstrated the effectiveness of this modification.

The second modification was a reduction of gains in the blade-pitch-to-feather control system. Larsen and Hanson [23] found that the smallest controller-response natural frequency must be lower than the smallest critical support-structure natural frequency to ensure that the

support-structure motion of an OFWT with active pitch-to-feather control remain positively damped. The new reduced proportional gain at minimum blade-pitch setting is 0.006275604s and the reduced integral gain at minimum blade-pitch setting is 0.0008965149 [66]. The gain-correction factor in the gain-scheduling law of the blade-pitch controller is unaffected by this change. Finally, to not exceed the mechanical limitations of the pitch actuator, the input signal $\beta_c$ is saturated to a maximum of 90° and a rate limit of 8°/s [36], and finally called $\hat{\beta}_c$. It is important that the control design takes into account these actuator limits. Otherwise, undesirable effects, such as transient response, degradation of the closed-loop performance, and even closed-loop instability, can appear [63].

## 2.10   Performance indices

In order to compare the performance of the different strategies, four performance indices that measure the accumulated tower acceleration in *fore-aft* and *side-to-side* directions, the platform pitching motion, the error in the generator speed in addition to the generated power error are considered. As the main interest is to reduce tower top and platform pitching motions while keeping minimum power fluctuations, smaller values of the defined performance indices represent the better controller behavior. The response of the generator velocity, electrical power, and the acceleration are analyzed through the following performance indices:

$$J_{P_1}(t) = \int_0^t |P_e(\tau) - P_{\text{ref}}| \, d\tau, \, [J].$$

$$J_{P_2}(t) = \frac{1}{t} \int_0^t |P_e(\tau) - P_{\text{ref}}| \, d\tau.$$

$$J_{\omega_1}(t) = \int_0^t |\omega_g(\tau) - \omega_{g,r}| \, d\tau, \, [J]$$

$$J_{\omega_2}(t) = \frac{1}{t} \int_0^t |\omega_g(\tau) - \omega_{g,r}| \, d\tau.$$

$$J_{xi}(t) = \frac{1}{t} \int_0^t |a_{x,i}(\tau)| \, d\tau, \quad i = 1, 2, 3.$$

$$J_{yi}(t) = \frac{1}{t} \int_0^t |a_{y,i}(\tau)| \, d\tau, \quad i = 1, 2, 3.$$

$$J_1(t) = \int_0^t |a_{fa}(\tau)| \, d\tau, \, [m/s]$$

$$J_2(t) = \int_0^t |a_{ss}(\tau)| \, d\tau, \, [m/s]$$

$$J_3(t) = \int_0^t |\vartheta(\tau)| \, d\tau, \, [m/s]$$

where $J_{P_1}(t)$ is the accumulated generated power error, $J_{P_2}(t)$ is the normalized integral absolute generated power error, $J_{\omega_1}$ is the accumulated generator speed error and $J_{\omega_2}$ is the normalized integral absolute generator speed error. Note that $a_{xi}(t)$ are the *fore-aft* and $a_{yi}(t)$ the *side-to-side* acceleration at nodes located at the tower bottom ($i = 1$), at mid-tower height ($i = 2$), and at the tower top ($i = 3$). Also $J_1$ and $J_2$ are the accumulated *fore-aft* acceleration ($a_{fa}(t)$) and *side-to-side* acceleration ($a_{ss}(t)$), respectively, at the tower top. Finally $J_3(t)$ is the accumulated platform pitch position ($\vartheta$) performance index.

# CHAPTER 3

# STATE OF THE ART IN FDI AND FTC IN WIND TURBINES

Systems are vulnerable to faults. Actuator faults and erroneous sensor measurements reduce the performance of control systems and lead to operating points far from the optimal ones. In technological systems, where many highly automated components interact in a complex way, a fault in a single component may cause the malfunction of the whole system, and may even cause a complete breakdown. In many situations, the system has to be stopped to avoid damage machinery and humans. Thus, research into methods of FDI, as well as FTC techniques play an increasing role in modern technology. Due to the simultaneously increasing economic demands and the numerous ecological and safety requirements to be met, high dependability of technological systems has become a dominant goal in industry.

This chapter introduces the main ideas of fault diagnosis and fault-tolerant control. First, a revision of FDI theory and model-based technique are presented; next a brief introduction to FTC techniques is exposed.

## 3.1   Fault detection and isolation

To recognize the terminology in the field of fault diagnosis and understand the goals of the particular contributions and to compare the different approaches, the IFAC Technical Committee: SAFEPROCESS (Fault Detection, Supervision and Safety for Technical Processes) has started an initiative to define common terminology [67].

A fault is an unexpected change of system function, although it may not represent physical failure or breakdown [67]. Such a fault or malfunction hampers or disturbs the normal operation of an automatic system, thus causing an unacceptable deterioration of the performance of the system or even leading to dangerous situations. The difference between fault and failure is that the first one indicates that a malfunction may be tolerable at its present stage and the second denotes a complete breakdown of a system component or function [67]. A fault must be diagnosed as early as possible even it is tolerable at its early stage, to prevent any serious consequences.

A monitoring system which is used to detect faults and also to determine the type, size and location of the most possible fault, as well its time of detection, is called a fault diagnosis system. Fault diagnosis is very often considered as fault detection and isolation, abbreviated as FDI, in the literature. Such a FDI system normally consists of the following tasks [67]:

- **Fault detection:** to make a binary decision - either that something has gone wrong or that everything is fine.

- **Fault isolation:** to determine the location of the fault, e.g., which sensor or actuator has become faulty.

- **Fault identification:** to estimate the size and type or nature of the fault.

Faults are detected by setting fixed or variable thresholds on residual signals generated from the difference between actual measurements and their estimates obtained by using the process model. A number of residuals can be designed with each having sensitivity to individual faults occurring in different locations of the system. The analysis of each residual, once the threshold is exceeded, then leads to fault isolation.

Recently, there has been much interest in FDI in WTs. For example, observer-based schemes are provided in [68]. Support vector machine-based schemes are used in [69]. An automated fault detection and isolation scheme design method is presented in [70]. The work in [71] is based on parity equations. Data-driven methods are used in [72]. Finally, [73] is based on a generalized likelihood ratio method.

FDI techniques can be classified into three categories [74]:

- signal processing based

- techniques based on knowledge (data-based)

- model based

### 3.1.1 Signal processing based FDI techniques

Many measured signals show oscillations that are either of harmonic or stochastic nature, or both. If changes of these signals are related to faults in the actuator, the process and sensors, signal processing based FDI techniques can be applied.

By assuming special mathematical models for the measured signal, suitable features are calculated as, for example, amplitude, phases, spectrum frequencies and correlation functions for certain frequency band width of the signal. A comparison with the observed features for normal behavior provide changes of the features which then are considered as analytical symptoms [75].

The signal models can be classified in [75]:

- **Non-parametric models:** like frequency spectra, correlation functions or parametric models.

- **Parametric models:** like amplitudes for distinct frequencies or ARMA type models.

And some signal analysis methods for harmonic oscillations and stochastic signals are:

- **Analysis of periodic signals:** bandpass filtering, fourier analysis, correlation functions, fourier transform, fast fourier transformation (FFT), maximum entropy spectral estimation and cepstrum analysis.

- **Analysis of non-stationary periodic signals:** short-time fourier transform and wavelet transform.

- **Analysis of stochastic signals:** correlation analysis, spectrum analysis and signal parameter estimation with ARMA-model.

- **Vibration analysis of machines:** vibration of rotating machines,vibration signal models, vibration analysis methods and speed signal of combustion engines.

In the literature we can find several articles for FDI in wind turbines using signal processing based techniques. For example, [76] takes advantage of the information on vibrations from the mechanical WT in a wide range of load and speed conditions to detects faults (unbalance

and misalignment). A new noise-controlled second-order enhanced stochastic resonance (SR) method based on the Morlet wavelet transform is proposed to extract fault feature for wind turbine vibration signals in [77]. In [78] is presented the application of the spectral kurtosis technique for detection of a tooth crack in the planetary gear of a wind turbine and [79] proposes a method of using generator stator currents for imbalance fault detection of direct-drive wind turbines generators.

### 3.1.2 Data-based FDI techniques

In a process data-based model, both inputs and outputs are known and measured. The main objective of a data-based model is to mathematically relate measured inputs to measured outputs. There are a number of ways the input/output data can be transformed and used as a priori knowledge in a diagnostic system. This process of transformation is also known as feature extraction or parameter extraction. When the model features or parameters have not physical significance, these models are referred to as black-box models [80]. Some examples of black-box modeling techniques include:

- Linear regression (LR)

- Multiple linear regression (MLR)

- Artificial neural networks (ANNs)

- Fuzzy logic (FZ)

Model parameters of an empirical model that is carefully crafted based on first principles often have physical significance; these models are referred to as gray-box or mechanistic models. Gray-box models often use linear or multiple linear regressions to estimate model parameters (e.g., coefficients) from measured inputs and outputs, while preserving the physical significance of terms appearing in the models [80].

These techniques are using in wind turbines FDI research. For example, a data-driven fault detection scheme is proposed with robust residual generators directly constructed from available process data in [72]. In [81] is used a classical back propagation neural network to studied and to diagnose four kinds of typical patterns of wind turbine gearbox faults. A automated SCADA data analysis is used to detect wind turbines faults in [82] and a support Vector Machines (SVM) are used for fault detection and isolation in a variable speed horizontal-axis WT, in [83].

### 3.1.3 Model-based FDI techniques

In this case, which is the approach used in this thesis, FDI makes use of mathematical models (mainly differential equations) of the system to represents the relations between measured input signals and output signals to extract information on possible changes caused by faults. These relations are mostly relations in the form of process model equations but can also be causalities, e.g. in the form of if-then rules.

Model-based fault detection methods extract special features (like parameters, state variables or residuals) and use a priori information on the process avaliable in terms of a mathematical model to compare the observed features with their nominal values [84]. Faults are thus detected by setting fixed or variable thresholds on residual signals generated from the difference between actual measurements and their estimates obtained by using the process model [85].

Figure 3.1 shows the general and logic block diagram of model-based FDI system. It comprises two main stages: residual generation and residual evaluation. This structure was first suggested by Chow and Willsky in [86] and now is widely accepted by the fault diagnosis community. The two blocks are described as follows:

- **Residual generation:** Its purpose is to use the available input and output signals to generate a fault indicating signal - residual. This auxiliary signal is designed to reflect the onset of a possible fault in the analyzed system [67]. The residual should be normally zero or close to zero when no fault is present, but it is distinguishably different from zero when a fault occurs [87]. This means that the residual is characteristically independent of system inputs and outputs, in ideal conditions [85]. The algorithm (or processor) used to generate residuals is called a residual generator. Residual generation is thus a procedure for extracting fault symptoms from the system, with the fault symptom represented by the residual signal. The residual should ideally carry only fault information. To ensure reliable FDI, the loss of fault information in residual generation should be as small as possible. A number of residuals can be designed with each having sensitivity to individual faults occurring in different locations of the system. The analysis of each residual, once the threshold is exceeded, then leads to fault isolation [85].

- **Residual evaluation:** This block examines residuals for the likelihood of faults and a decision rule is then applied to determine if any faults have occurred. The residual evaluation block, shown in Figure 3.1, may perform a simple threshold test (geometrical methods) on the instantaneous values or moving averages of the residuals. On the other hand, it

may consist of statistical methods, e.g., generalised likelihood ratio testing or sequential probability ratio testing [88–91].
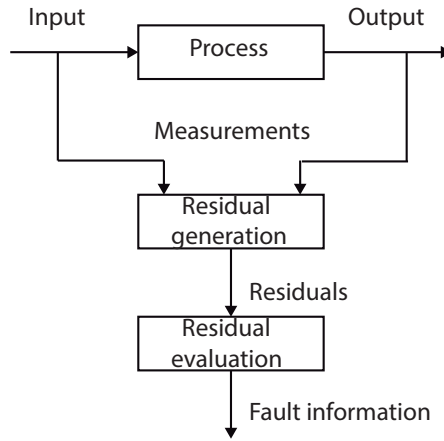


Figure 3.1. Structure of model-based FDI system.

Residual generators based on different methods, such as state and output observers, parity relations and parameter estimations, are just special cases in this general framework. The basic idea behind the observer techniques is to estimate the outputs of the system from the measurements by using either Luenberger observers in a deterministic setting or KaIman filters in a noisy environment. The output estimation error (or its weighted value) is therefore used as residual [85]. The basic idea of the parity relations approach is to provide a proper check of the parity (consistency) of the measurements acquired from the monitored system [85]. And finally, the parameter estimation approach is based on the assumption that the faults are reflected in the physical system parameters and the basic idea is that the parameters of the actual process are estimated on-line using well-known parameter estimations methods. The results are thus compared with the parameters of the reference model obtained initially under fault-free assumptions. Any discrepancy can indicate that a fault may have occurred [85].

**FDI via parameter estimation**

In most practical cases, the process parameters are not known at all, or they are not known exactly enough. Then, they can be determined with parameter estimation methods, by measuring input, $u(t)$, and output signals, $y(t)$, if the basic structure of the model is known [88, 91].

This approach is based on the assumption that the faults are reflected in the physical system parameters such as friction, mass, viscosity, resistance, inductance, capacitance, etc. The basic idea of the detection method is that the parameters of the actual process are repeatedly estimated on-line using well known parameter estimation methods and the results are compared to the parameters of the reference model (obtained under the faulty-free condition) [67]. Any substantial discrepancy indicates a fault. This technique normally uses the input-output mathematical model of a system in the following form:

$$y(t) = f(M, u(t)), \tag{3.1}$$

where $M$ is the model coefficient vector, which is directly related to the system physical parameters.

The basic procedure for carrying out FDI using parameter estimation is [67]:

- Establish the process model using physical relations.

- Determine the relationship between model coefficients and process physical parameters.

- Estimate the normal model coefficients.

- Calculate the normal process physical parameters.

- Determine the parameter changes which occur for the various fault cases.

During the system operation, the model system coefficients are periodically identified from the measurable inputs and outputs. The results are thus compared with the parameters of the reference model which is obtained a priori under fault-free assumptions.

This approach generates residuals using an on-line parameter identification algorithm. The residual can be defined in either of the following ways:

$$\begin{cases} r(k) = \hat{M}_k - M_0 \\ r(k) = y(k) - f(\hat{M}_{k-1}, u(k)) \end{cases} \tag{3.2}$$

where $M_0$ is the normal model coefficient.

The identification techniques can be classified in:

- Identification with correlation functions

- Parameter estimation for linear processes

- Identification of nonlinear processes

**FDI via state observers**

As state observer use an output error between a measured process output and an adjustable model output. State observers adjust the state variables according to initial conditions and to the course of the measured input and output signal [75].

Several approaches have been proposed for FDI which are based on Kalman filter, classical Luenberger state observer and the so-called output observer.

A linear time-invariant system with faults is considered which can be described by the state-space model [92]

$$\dot{x}(t) = Ax(t) + Bu(t) + R_1 f(t), \tag{3.3}$$

$$y(t) = Cx(t) + Du(t) + R_2 f(t), \tag{3.4}$$

Here a fault can be detected by comparing the residual evaluation function $J(r(t))$ with a threshold function $T(t)$ according to the test given below:

$$J((r(t)) \leq T(t) \text{ for } f(t) = 0$$
$$J((r(t)) \geq T(t) \text{ for } f(t) \neq 0$$

If the threshhold is exceeded by the residual evaluation function, a fault is likely.

With the assumption that the structure and the parameter of the model are known, a state observer is used to reconstruct the unmeasured state variable based on measured inputs and outputs

$$\dot{\hat{x}}(t) = A\hat{x}(t) + Bu(t) + Le(t), \tag{3.5}$$

$$e(t) = y(t) - C\hat{x}(t), \tag{3.6}$$

where $e(t)$ is an output error which acts through the observer matrix $L$ on the reconstructed state derivatives $\hat{x}$(t). Substituting (3.5) in (3.6) yields the implementation of the state observer

$$\dot{\hat{x}}(t) = (A - LC)\hat{x}(t) + Bu(t) + Ly(t) \tag{3.7}$$

where it is assumed that the system is observable.

Define the state error

$$\dot{e}_x(t) = \dot{x}(t) - \dot{\hat{x}}(t), \tag{3.8}$$

between the real process states and the observed states. Under the assumption that the process and model parameters are identical and by substituting (3.3) in (3.7), this error becomes

$$\dot{e}_x(t) = (A - LC)e_x(t). \tag{3.9}$$

Hence, the state error vanishes asymptotically,

$$\lim_{t \to \infty} e_x(t) = 0, \tag{3.10}$$

for any initial state deviation $[x(0) - \hat{x}(0)]$ if the observer is stable, which can be reached by proper design of the observer feedback matrix $L$, e.g. by pole placement.

Some examples can be found of FDI of wind turbines. An observer based scheme is proposed in [93] to detect sensor faults in wind turbines. In [68], interval observers and unknown but bounded description of the noise and modeling errors are used to detect the faults and analyzing the observed fault signatures on-line and matching them with the theoretical ones obtained using structural analysis and a row-reasoning scheme it can be isolate. Finally, in [94] an unknown input observer is presented to estimate faults in the converter and isolate them either to be an actuator fault or a sensor fault.

**Sliding modes for FDI**

In the Luenberger observer, the output estimation error is fed back linearly into the observer. However, in the presence of unknown signals, the Luenberger observer is usually unable to force the output estimation error to zero and the observer states will also not converge to the system states. A sliding mode observer [95, 96] provides an attractive solution to this problem. It feeds back the output estimation error via a nonlinear switching term. Provided a bound on the magnitude of the disturbances is known, the sliding mode observer can force the output estimation error to converge to zero in finite time (as opposed to the linear observer which only converges asymptotically), while the observer states converge asymptotically to the system states. During the sliding motion, the equivalent output error injection (the analogue to the equivalent control) contains information about the unknown signals, and by suitably scaling the equivalent output error injection, an accurate estimate of the unknown signals can be obtained. The first sliding mode observer in the literature appeared in [96]. Walcott and Zak [97] improved on this design by including a linear feedback term such that the sliding patch can be enlarged. Edwards and Spurgeon [95] modified the sliding surface of the WalcottZak observer and presented a systematic numerical design method for the observer. In addition, the work in [95] identified necessary and sufficient conditions for the existence of the observer in terms of the original system matrices, and hence the class of systems for which the observer is feasible, is known.

Sliding mode observers can be used to reconstruct faults and thus detect and isolate them. Some sliding observer techniques are:

- Utkin observer

- Edwards-Spurgeon observer for fault reconstruction

- Using linear matrix inequalities (LMI)

- Robust sliding observer

This thesis uses the model-based approach, as in recent years these techniques seem to have received more attention in academia and industry. For example in [98], a counter based thresholding can detect smaller faults with higher probability and lower false alarms. Sanchez et al. [99] propose use analytical redundancy relations (ARRs) and interval observers for wind turbines and its application to a realistic wind turbine FD benchmark. In [100] a multi-physics

graphical model-based fault detection and isolation method is developed for Doubly-Fed Induction Generator based wind turbines. Finally, [101] is based on a Takagi-Sugeno model based fault estimation with application to wind turbines.

### 3.1.4 Model uncertainty and robust model-based FDI

A perfectly accurate mathematical model of a physical system is never available. Usually, the parameters of the system may vary with time and the characteristics of the disturbances and noises are unknown so that they cannot be modeled accurately. Hence, there is always a mismatch between the actual process and its mathematical model even if there are no process faults. These discrepancies cause difficulties in FDI applications, such false alarms and missed alarms. The effect of modeling uncertainties is therefore one of the most crucial points in the model-based FDI concept, and the solution to this problem is the key for its practical applicability [92, 102, 103].

To overcome these difficulties, a model-based FDI system has to be robust to modelling uncertainty. Sometimes, the reduction in sensitivity to model uncertainty does not meliorate the problem, because such a sensitivity reduction may be associated to a reduction to fault sensitivity. A more meaningful formulation of the robust FDI problem is to increase the robustness to uncertainty modeling, whilst without losing (or even with an increase of) fault sensitivity. An FDI scheme designed to provide satisfactory sensitivity to faults, associated with the necessary robustness with respect to modeling uncertainty, is called a robust FDI scheme [92, 102, 103].

In the context of automatic control, the term robustness is used to describe the insensitivity or invariance of the performance of control systems with respect to disturbances, model-plant mismatches or parameter variations. Fault diagnosis schemes, on the other hand, must of course also be robust to the mentioned disturbances, but, in contrast to automatic control systems, they must not be robust to actual faults. On the contrary, while generating robustness to disturbances, the designer must maintain or even enhance the sensitivity of fault diagnosis schemes to faults. Furthermore, the robustness as well as the sensitivity properties must be independent of the particular fault and disturbance mode. Generally, the problem of robust FDI can be divided into the tasks of robust residual generation followed by robust residual evaluation.

The importance of robustness in model-based FDI has been widely recognized by both academia and industry. The development of robust model-based FDI methods has been a key research topic during the last 20 years. A number of methods have been proposed to tackle this

problem, for example, the unknown input observer, eigenstructure assignment, optimally robust parity relation methods. However, this is still an active research area under development for practical applicable methods.

We can find some examples. In [72] a robust data-driven fault detection approach is proposed with application to a wind turbine benchmark. Simani et al. [104] use fuzzy models in the form of Takagi-Sugeno prototypes to represent the residual generators used for robust fault detection and isolation; Shadi, et al. [105] use a mixed unknown input-proportional integral observer method and the parameter estimation method for a robust fault diagnosis to detect various critical and common sensor faults, actuator faults and components faults. Finally, [106] designed an unknown input observer-based robust fault estimation for systems corrupted by partially decoupled disturbances.

## 3.2    Fault tolerant control

In control systems, robustness and fault tolerance capabilities are also important properties, which should be considered in the design process, calling for a generic and powerful tool to manage parameter variations and model uncertainties [107]. The objective of FTC is to design appropriate controllers such that the resulting closed-loop system can tolerate abnormal operations of specific control components and retain overall system stability with acceptable system performance [108]. Ideally, the closed loop system should be capable of maintaining its pre-specified performance in terms of quality, safety, and stability despite the presence of faults [109].

A standard control problem aims to design a control law to sastify a number of prescribed objectives under a restriction set. A mathematical model is used to describe the system dynamics. The restriction set is determined by the mathematical model structure and its parameters [74].

Actually, hardly a mathematical model represents adequately the system behavior due to perturbations problems, measurement noise, non-modeled dynamics, time-varying and uncertain parameters. The solution to the control problem to achieve the objectives, in the presence of uncertainty in the model, can be solved assuming a fixed structure for it, but with unknown parameters belonging to a parameter set, applying robust control techniques [74].

The occurrence of faults in the system can cause changes in the restrictions and also changes

in the parameters, causing the problem to be unsovable when calculating the control law unless the set of objectives is modified [74].

In general, the FTC approaches can be classified into two types: the passive approach and the active approach. In active schemes, the controller is reconfigured whenever a fault is detected [110]. In [74], active FTC is defined as a technique based on the system state (normal or fault) starting from the estimation of the system constraints and the system parameters. In passive FTC schemes, the controller's structure is fixed [111] and is based on the design of a unique control law able to achieve its objectives both in normal and fault situations [74]. Hence, when the fault occurs, the controller is able to maintain the stability of the system with an acceptable degradation of its performance, and requires neither fault detection (FD) and diagnosis systems nor a controller reconfiguration. In contrast, for active FTC it is indispensable to use a FD algorithm in order to react to the system failures actively by reconfiguring the controllers or accomodating to the fault so that the stability and acceptable performance of the entire system can be maintained [74, 112]. The difference between reconfiguration and accommodation to the fault is that the first one changes the inputs and outputs of the controller as well as readjusts the control law, while the second one consists in solving the problem maintaining the structure of the controller and modifying only the parameters. The accommodation strategy can be off-line (precalculated controller) and on-line (on-line estimated controller). The use of one or the other will depend on the proposed control objectives and on the type of faults present in the system.

Some off-line accomodation techniques are [74]:

- **LTI models:** techniques applied on an invariant time linear model plant, such as model matching, model following, optimal LQR and EA (eigenstructure assignment).

- **LTI family models:** techniques applied to a plant whose mathematical model is non-linear and has been decomposed into several models, which correspond to linearizations around certain predefined points in such a way that the area of interest in the state space is covered, such as multimodels, gain-scheduling and LPV (linear parameter varying).

- **Non-lineal models:** control techniques that are applied to systems whose model is directly non-linear. In this case, soft-computing techniques are used to implement the controllers. Techniques as diffused, neuronal and neuro-diffused controls, belong to this group.

The on-line accomodation obtains a control law from the actual restrictions after the fault appears. To estimate the fault effect on the restrictions, there are two alternatives [74]:

- **Off-line estimation:** the effect of the faults on the restrictions has been studied previously, parametrizing them according to the fault. When the fault is diagnosed, the restrictions will be changed according to the fault, which will also affect the controller since it is also calculated online from them. Some examples are model predictive control (MPC) and feedback static linearization.

- **On-line estimation:** the effect of the fault on the restrictions is estimated online so that the controller, which is also calculated online from them, will adapt to the changes that occur. This group includes techniques such as adaptive control, feedback dynamic linearization and dual predictive control.

Finally, the fault tolerant control system design stages are [74]:

- System analysis

- Diagnosis system design

- Tolerant mechanism design

- Supervisor system design

- Enforcement and test

Due to the great interest in fault tolerant control in WTs coming from the industry and academia, a first benchmark paper and competition about fault detection and isolation of WTs was presented in [37]. This benchmark, provides a model on which researchers working in the field of fault diagnosis and fault-tolerant control can compare different methods in their field applied to a WT. The benchmark also presented different types of faults and test sets. These faults cover sensor, actuator, and process faults in different parts of the WT. After the announcement of results of the 1rst benchmark, a second challenge was presented in [5]. In this work the WT is modeled in the FAST simulator [50]. This means that a higher-fidelity, more detailed, aerodynamic, structural and realistic WT model was used and likely making the results of greater applicability to the wind industry. Also, the fault scenarios were updated and additional information detailing their relevance was provided. While still being a relatively new research topic, recent years have seen a growing number of publications in wind turbine FTC. For example, a set value-based observer method is proposed in [113], and [114] proposes a control allocation method for FTC of the pitch actuators. A virtual sensor/actuator scheme is applied in [115]. Takagi-Sugeno fuzzy-based methods for FTC for operation below rated

wind speed are presented in [116]. The work in [117] presents an active FTC scheme based on adaptive methods, and a model predictive control scheme is used for FTC in [118]. The design of a dynamic reference trajectory based on hysteresis to avoid saturation in controlled WT is presented in [119]. A compensation technique for input constraints avoidance to the pitch control of a WT is proposed in [120], and [121] proposes a new indirect adaptive fault-tolerant controller design method via state feedback for actuator fault compensation. The recent survey paper [122] reviews the concepts and the state of the art in the field of FTC. Existing literature on wind turbine FTC is still scarce [123].

This thesis presents both types of schemes applied to WT since the application of active and passive FTC is important for the power industry.

# A FAULT DETECTION METHOD FOR PITCH ACTUATOR FAULTS IN WIND TURBINES

This chapter presents a model-based fault detection method for pitch actuators faults using the normalized gradient method to estimate the parameters of the pitch actuator. One major difficulty is that the input signal to the parametric estimation method must be a persistent excitation. To circumvent this, a chattering term is added to the pitch control law and the usual low-pass filters are not used for the parametrization in the normalized gradient method (thus acceleration information is used). In order to verify the proposed method, simulations are conducted within a Hardware in the Loop (HiL) platform using the WT simulation software FAST (Fatigue, Aerodynamics, Structures, and Turbulence).

## 4.1 Fault detection method

This section describes the proposed method to estimate the pitch actuator parameters given in (2.12) as well as the design of two residual signals for fault detection (FD) purposes.

Recall the pitch actuator model described in Chapter 2, Equation (2.12)

$$\ddot{\beta}_i(t) + 2\zeta\omega_n\dot{\beta}_i(t) + \omega_n^2\beta_i(t) = \omega_n^2\hat{\beta}_c(t).$$

Its transfer function is

$$\frac{Y(s)}{U(s)} = \frac{\omega_n^2}{s^2 + 2\zeta\omega_n s + \omega_n^2},\qquad(4.1)$$

where $Y(s)$ is the actual angle $\beta_i(s)$, and $U(s)$ is the reference angle $\hat{\beta}_c(s)$. In time domain

$$\omega_n^2 u = \ddot{y} + 2\zeta\omega_n \dot{y} + \omega_n^2 y,\qquad(4.2)$$

and isolating the acceleration

$$\ddot{y} = \omega_n^2 u - 2\zeta\omega_n \dot{y} - \omega_n^2 y,\qquad(4.3)$$

that can be rewritten as

$$\ddot{y} = (\omega_n^2, -2\zeta\omega_n, -\omega_n^2)\ \begin{pmatrix} u \\ \dot{y} \\ y \end{pmatrix} = \theta^T \phi\,,$$

where $\theta^T$ is the vector of parameters and $\phi$ is the regression vector.

Using the normalized gradient method [124], we obtain the following estimation

$$\hat{\ddot{y}} = (\hat{\theta}_1,\ \hat{\theta}_2,\ \hat{\theta}_3)\ \begin{pmatrix} u \\ \dot{y} \\ y \end{pmatrix} = \hat{\theta}^T \phi\,,$$

where

$$\dot{\hat{\theta}} = \frac{-\varrho e \phi}{1 + g\phi^T \phi};\qquad g > 0,\qquad(4.4)$$

where $\varrho$ is a positive number called the estimator gain, $g$ is a design parameter (for the simulation $\varrho = 20$ and $g = 100$) and $e$ is the error defined by

$$e = \hat{\ddot{y}} - \ddot{y}.\qquad(4.5)$$

Note that $\hat{\theta}_1$, $\hat{\theta}_2$ and $\hat{\theta}_3$ are the estimations of $\omega_n^2$, $-2\zeta\omega_n$ and $-\omega_n^2$, respectively, and $\ddot{y}$ is the acceleration signal.

*Remark:* Note that the usual low-pass filters are not utilized in the parametrization and therefore acceleration information is employed. Different parameter estimation methods were tested with and without the usual low-pass filters and the results showed that the estimated values approached much faster the real values when the filters were not used.

We propose the following residual signals $r_1$ and $r_2$:

$$r_1 = \hat{\ddot{y}} - \ddot{y}_h, \tag{4.6}$$

$$r_2 = || \hat{\theta} - \theta_h ||, \tag{4.7}$$

where $\theta_h = (\omega_n^2, \; -2\zeta\omega_n, \; -\omega_n^2)^T = (123, \; -13, \; -123)^T$ are the healthy parameter values and $\ddot{y}_h$ is the healthy pitch actuator acceleration, which is numerically obtained using

$$\ddot{y}_h = \omega_n^2 u - 2\zeta\omega_n \dot{y}_h - \omega_n^2 y_h,$$

with the healthy parameter values.

*Remark:* The measurement noise is not taking into taking account and the noise can affect the stimation quality. However, a proper filtering of the noise can allow have a good parameter estimation even if the system is affected by noise [125], [126].

## 4.2   Experimental setup

### 4.2.1   Hardware in the loop

In this section, the experimental setup used for the simulations is explained. The dynamics of the WT are simulated in FAST, which emulates all the input signals needed by the controllers. The torque controller is implemented in the open source Arduino microcontroller, which will be connected via USB to a computer where the turbine is simulated. Fig. 4.1 shows the experimental configuration of the HiL, for more details see [45].
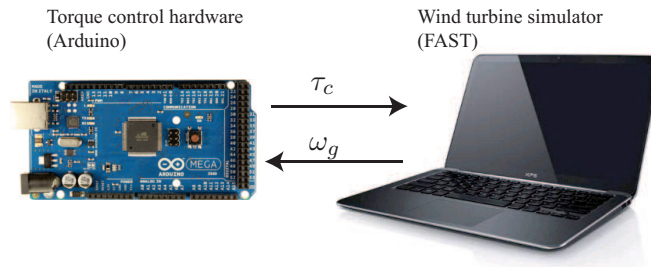
Figure 4.1. Diagram of the experimental configuration of the HiL.

Source:( [127])

The proposed HiL platform allows to test the performance of the torque controller when running in real-time and a fault exists in the pitch actuator. Note that testing these cases experimentally can seriously damage the WT, thus a HiL approach is preferable.

## 4.3   Simulation results

The onshore WT described in Section 2.8.1 is used in the simulations along with the baseline torque and pitch controllers described in Section 2.9.1. The block diagram system is shown in Figure 4.3.
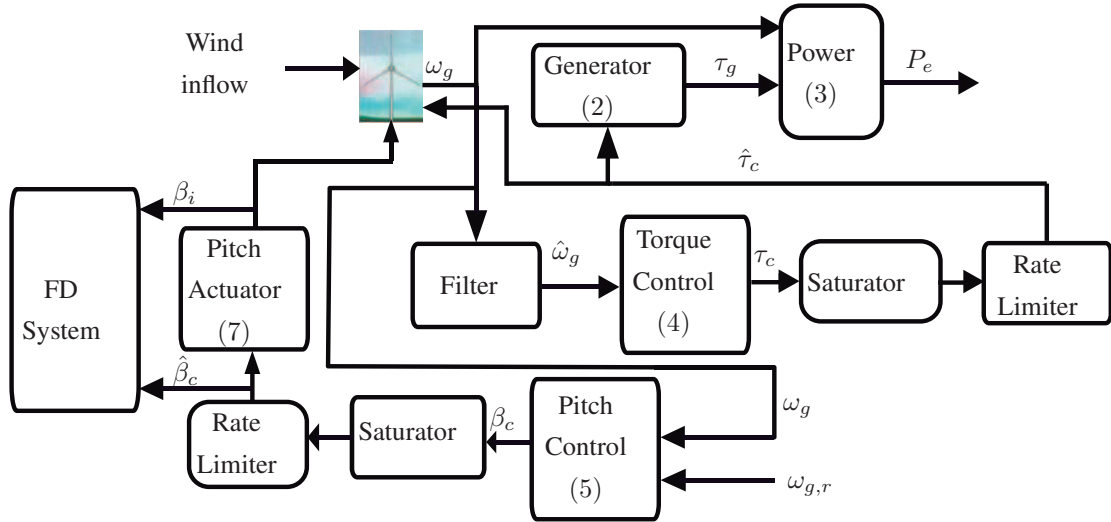
Figure 4.2. Block diagram of the pitch actuator fault detection method along with the baseline controllers. Note that the torque control is allocated in a controller hardware.

Source:( [127])

Here is considered the Fault 1 (High air content in the air) described in Section 2.5.1, Table 2.2. The fault is linearly introduced from 300s to 320s and is fully active from 320s to 600s (see [5]).

To finally setup the FD method, a threshold is prescribed for the residual signals using their maximum values (in absolute value) in the healthy case. For $r_1$ the prescribed threshold is $0.4$ and for $r_2$ is $0.85$. Fig. 4.3 (left) shows that with signal $r_1$ the fault is detected at around 308s, while Fig. 4.3 (right) shows that with signal $r_2$ the fault is detected at around 302s. In both cases the fault is detected before it is fully active, i.e. during its linear introduction.

In Figures 4.4, 4.5 and 4.6 it can be seen that, when a fault appears, the estimated parameters $\hat{\theta}_1$, $\hat{\theta}_2$ and $\hat{\theta}_3$, in a very short time, differ from the healthy reference values as they start the (slow) convergence to the faulty reference values. Recall that the main contribution of the work presented in this chapter is a FD method, and this is accomplished even with a slow parameter convergence.
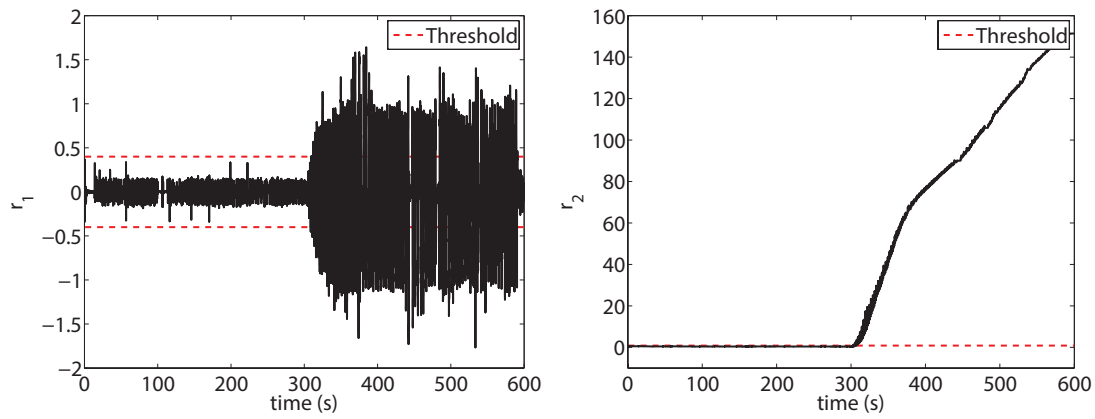
Figure 4.3. Residual signal $r_1$ (left) and residual signal $r_2$ (right).
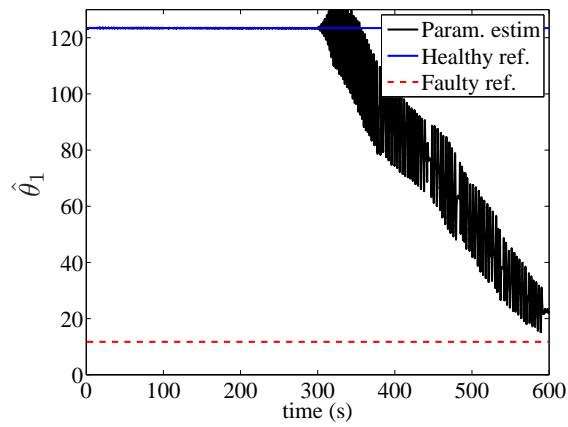


Figure 4.4. Estimation of $\theta_1$.
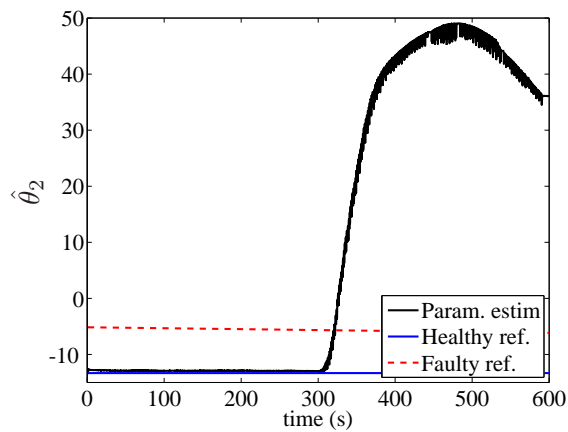


Figure 4.5. Estimation of $\theta_2$.
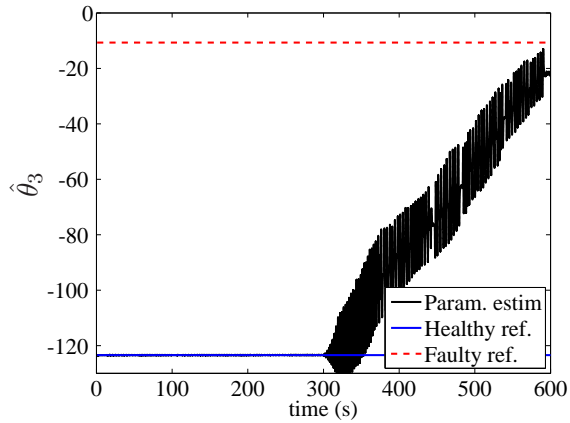
Figure 4.6. Estimation of $\hat{\theta}_3$.

The following results will show that the proposed closed-loop is robust against the studied fault.

Figure 4.7 (left) shows that the torque controller has an acceptable performance, maintaining the generated power closed to the desired value (5 MW) despite the appearance of a fault at time 300s. From Fig. 4.7 (right), the torque action of the proposed controller achieves reasonable values.
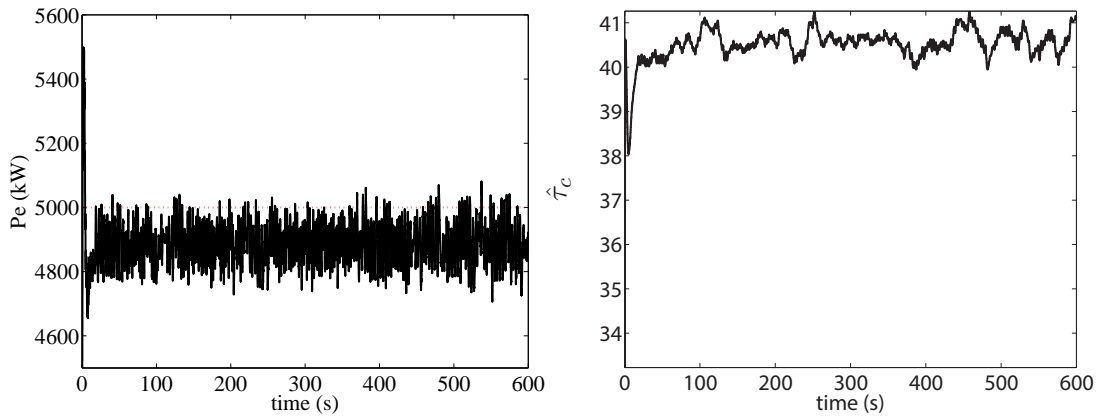


Figure 4.7. Generated electrical power (left) and torque control (right).

The generator speed, as shown in Fig. 4.8 (left) is near its nominal value due to the controllers action. Figures 4.8 (right) and 4.9 show that the pitch control signal is regulated within the allowed variation domain. This means that none of the variations exceed the mechanical limitations of the pitch actuator. Note also that, when all the pitch actuators are in healthy

condition, all blades have the same behavior, however when a fault exists in one of them a difference between the variation of the pitch angle 1 (healthy) and the pitch angle 3 (faulty) can be observed.
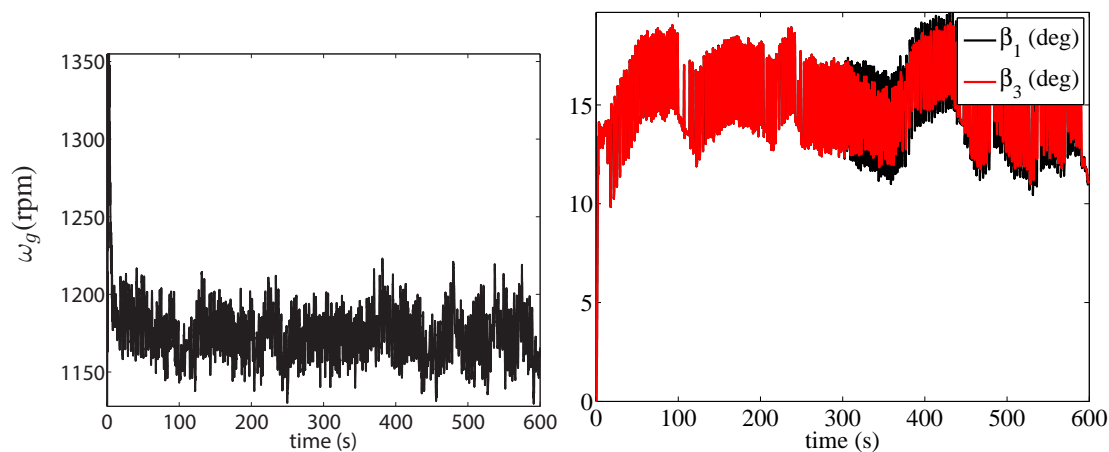


Figure 4.8. Generator speed (left) and pitch control (right).
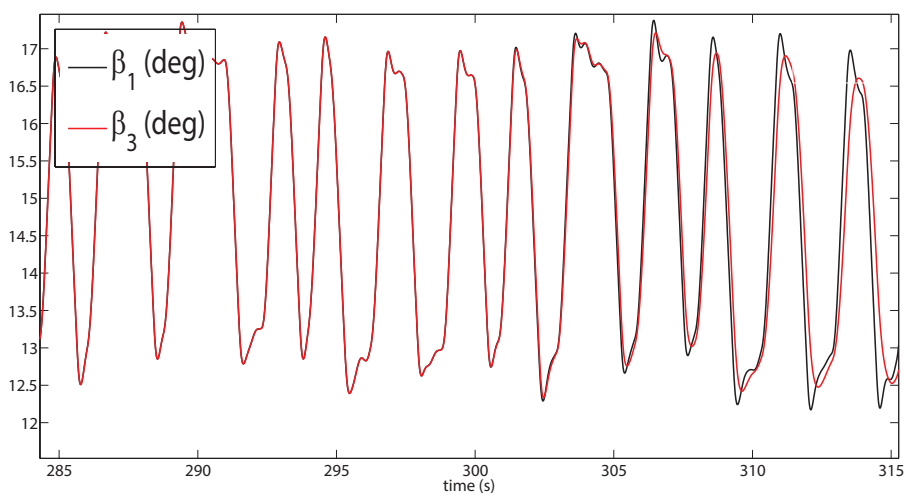


Figure 4.9. Zoom of the pitch control signal.

It can be seen in Figures 4.10 and 4.11 that the *fore-aft* and the *side-to-side* acceleration at different tower heights is of the same magnitude than for the case presented in [36] (where a gain-scheduling PI is used for the pitch controller). Thus, the addition of the chattering term helps to the FD method without much variation in the tower acceleration.

58
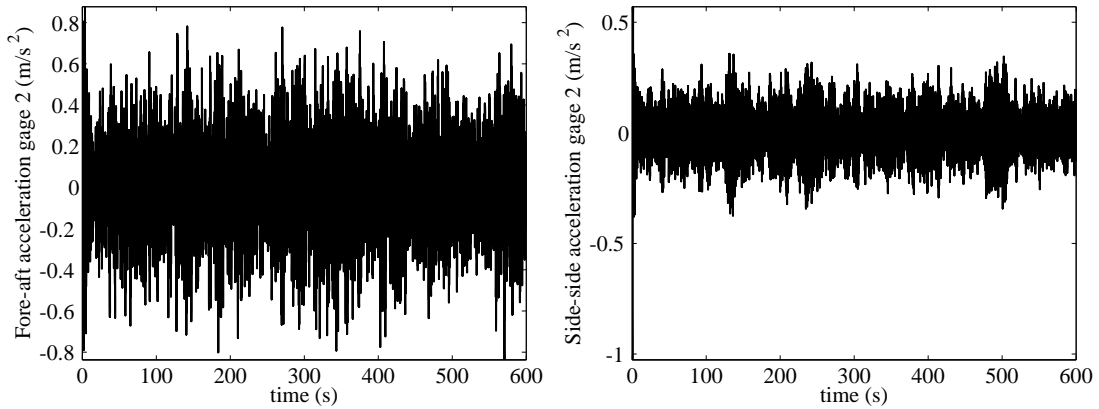
Figure 4.10. *Fore-aft* acceleration at mid tower (left) and *side-to-side* acceleration at mid tower (right).
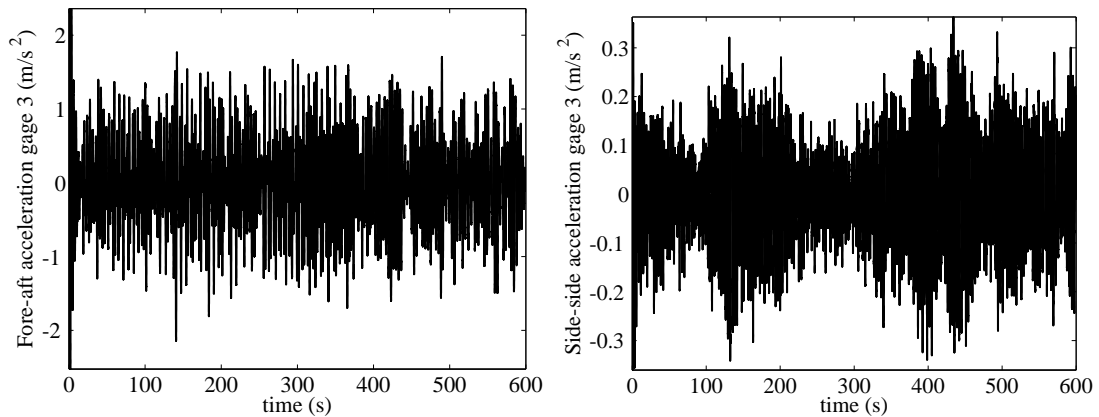


Figure 4.11. *Fore-aft* acceleration at tower top (left) and *side-to-side* acceleration at tower top (right).

## 4.4   Conclusions

A WT fault detection method for pitch actuator faults is studied in this chapter. Although only one type of fault is presented in the simulations, any fault that implies a change in the dynamics of the pitch actuator will be detected using this method. Note that, even if the approximation of the estimated parameters to the fault values is slow, the two proposed residual signals detect in short notice the appearance of the fault. In this work, measurement noise was not taken into account and it can greatly affect the quality of the estimated parameters. However, a proper noise filtering should solve this drawback. This is left as future work. Moreover, according to

the experiments, the overall closed-loop system is robust against the studied faults. Finally, the numerical simulations in HiL platform have demonstrated the performance of the proposed fault detection method.

CHAPTER 5

# FAULT DIAGNOSIS AND FAULT-TOLERANT CONTROL OF WIND TURBINES VIA A DISCRETE TIME CONTROLLER WITH A DISTURBANCE COMPENSATOR

This chapter develops a fault diagnosis and FTC for pitch actuators in WTs. This is accomplished by combining a disturbance compensator with a controller, both of which are formulated in the discrete-time domain. The disturbance compensator has a dual purpose: to estimate the actuator fault (which is used by the FDI algorithm) and to design the discrete-time controller to obtain a FTC. That is, the pitch actuator faults are estimated and then the pitch control laws are appropriately modified to achieve a FTC with a comparable behavior to the fault-free case. The performance of the FD and FTC schemes are tested in simulations with the aero-elastic code FAST.

## 5.1 Fault tolerant control

This section details the design of the FTC strategy based on a control plus disturbance estimator in the discrete-time domain. The control objective is the tracking of the reference signal $\beta_c(t)$

given by the baseline pitch controller, which is described in Section 2.9.1, Equation 2.15) and its corresponding velocity even in the case of pitch actuator fault. The model is recalled here to ease the reading:

$$\beta_c(t) = K_p(\gamma)(\hat{\omega}_g(t) - \omega_{g,r}(t)) + K_i(\gamma)\int_0^t (\hat{\omega}_g(t) - \omega_{g,r}(t))d\tau,$$

$$i = 1, 2, 3,$$

The block diagram in Figure 5.1 shows the connections between the WT (simulated using FAST), the FTC system, the pitch actuator and the torque and pitch controllers. To discretize continuous signals, a conventional sampler is used. As can be seen in the block diagram in Figure 5.1, a switch closes to admit an input signal every sampling period $T_s$. The sampler converts the continuous-time signal into a train of pulses occurring at the sampling instants $kT_s$ for $k = 0, 1, 2, ....$. Traditionally, a discrete-time signal is considered to be undefined at points in time between the sample times. In this work, discrete-time signals remain defined between sample times by holding on the value at the previous sample time. That is, when the value of a discrete signal is measured between sample times, the value of the signal at the previous sample time is observed. This is known as a *zero-order hold* or staircase generator as the output of a zero-order hold is a staircase function. In this chapter, the notation $[k]$ is used for these discrete-time signals.
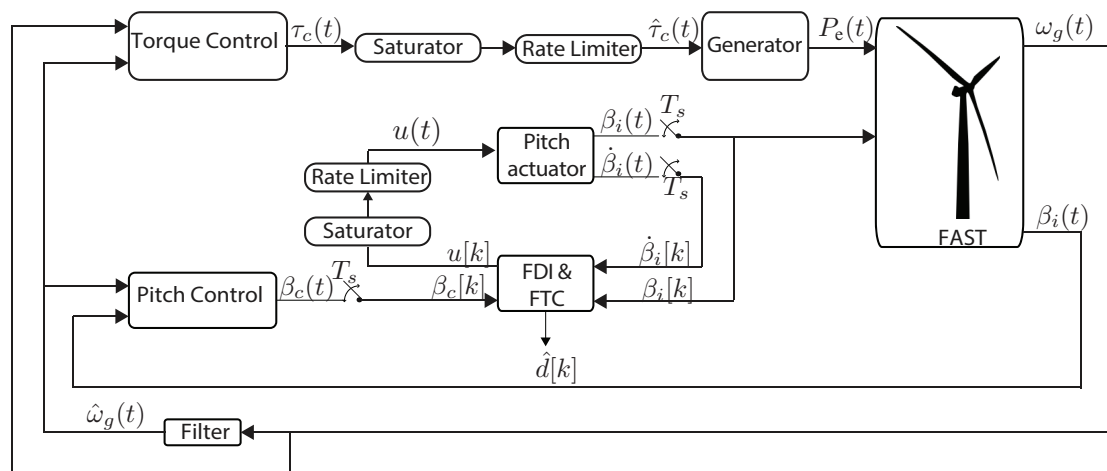


Figure 5.1. Block diagram of the closed loop system. Note that the torque control and the pitch control already include their respective saturator and rate limiter blocks.

Source:( [38])

62

Taking the pitch actuator system given in Equation (2.12), the state space representation in discrete-time, using Euler approximation [1], leads to

$$x[k + 1] = (A + \Delta A)x[k] + bu[k]) = Ax[k] + \Delta Ax[k] + bu[k] \qquad (5.1)$$

where

$$x[k+1] = \begin{pmatrix} \beta_i[k+1] \\ \dot\beta_i[k+1] \end{pmatrix}, \quad A = \begin{pmatrix} 1 & T_s \\ -\omega_n^2 T_s & 1 - 2\zeta\omega_n T_s \end{pmatrix}, \quad x[k] = \begin{pmatrix} \beta_i[k] \\ \dot\beta i[k] \end{pmatrix},$$
$$b = \begin{pmatrix} 0 \\ T_s\omega_n^2 \end{pmatrix} \qquad (5.2)$$

where $\Delta A$ accounts for a fault in the system, and thus $\Delta Ax[k]$ is a disturbance term that will be estimated.

In order to design the control law $u[k]$, the control objective is that, even in a faulty case, the real pitch angle $\beta_i$ follows the commanded reference pitch angle $\beta_c$ (given by the pitch controller), as well as the velocity $\dot\beta_i$ follows the commanded reference $\dot\beta_c$. That is, the objective is to ensure the asymptotic convergence of the tracking error vector to zero. The error vector is defined as
$$e[k] = (e_1[k], e_2[k])^T = (\beta_i[k] - \beta_c[k], \dot\beta_i[k] - \dot\beta_c[k])^T.$$

Following the results in [129], the switching function is defined with the error vector and a column vector $c$ as follows:
$$s[k] = c^T e[k], \qquad (5.3)$$

and then, for system (5.2), the sliding surface (5.3) gives the asymptotic convergence of tracking error vector to zero designing vector $c$ such that the matrix

$$\left[ I - b\left(c^T b\right)^{-1} c^T \right] A \qquad (5.4)$$

is contractive (eigenvalues inside the unit circle). When using a sample time $T_s = 0.0125$ (see [36]) and the fault-free values for the parameters $\omega_n$ and $\zeta$, it is found that vector

$$c = (1,\, 0.25)^T$$

ensures that matrix (5.4) is contractive (with one eigenvalue equal to zero and the other assigned

---

[1]For the ordinary differential equation $\dot z = f(z)$, the Euler discretization is defined as $\frac{z_{k+1} - z_k}{T_s} = f(z_k)$, such that $z_{k+1} = z_k + T_s f(z_k)$ where $T_s$ is the sampling time [128].

arbitrarely as in the application example given by [129]). Finally, to achieve the sliding mode, a new control law with a disturbance estimation law is proposed [129] as follows:

$$u[k] = -\hat{d}[k] + \left(c^T b\right)^{-1} \left[ c^T \begin{pmatrix} \beta_c[k] \\ \dot{\beta}_c[k] \end{pmatrix} - c^T Ax[k] + qs[k] - \eta\mathrm{sign}(s[k]) \right], \qquad (5.5)$$

$$\hat{d}[k] = \hat{d}[k-1] + (c^T b)^{-1} g\left[ s[k] - qs[k-1] + \eta\mathrm{sign}(s[k-1]) \right], \qquad (5.6)$$

where $0 \leq q \leq 1$, $0 < g < 1$, and $\eta > 0$ and $\hat{d}[k]$ is the fault estimator or also called the disturbance estimator. In the numerical simulations: $q = g = 1/2$ and $\eta = 100$. As can be seen in Equation (5.5), the proposed discrete controller for active FTC is dependent on a fault estimate, $\hat{d}[k]$, provided by the fault diagnosis system. Note that [129] contributes a disturbance compensator and controller for regulation or tracking purposes only. The novelty of the present work is to extend the work in [129] by its inclusion in a new fault tolerant control scheme and fault detection system (see the block diagram in Figure 5.1). The design of a continuous residual signal capable of isolating the type of fault (among the studied faults high air content in the oil (F1), pump wear (F2), and hydraulic leakage (F3)) is also a contribution of this chapter (see Figure 5.2 and 5.3).

The pitch controller used by the FTC strategy is the baseline GSPI controller, see Section 2.9.1. On the other hand, the used torque controller is the chattering control proposed in [14], which is recalled here to be

$$\dot{\tau}_c(t) = \frac{-1}{\hat{\omega}_g(t)} \left[ \tau_c(t)(a\hat{\omega}_g(t) + \dot{\hat{\omega}}_g(t)) - aP_{\mathrm{ref}} + K_\alpha\mathrm{sign}(P_{\mathrm{e}}(t) - P_{\mathrm{ref}}) \right], \qquad (5.7)$$

where $P_{\mathrm{ref}}$ is the reference power and $P_{\mathrm{e}}$ is the electrical power considered here (only for the control design) to be described as [130]

$$P_{\mathrm{e}}(t) = \tau_c(t)\hat{\omega}_g(t), \qquad (5.8)$$

where $\tau_c(t)$ is the torque control and $\hat{\omega}_g(t)$ is the filtered generator speed. This chattering controller, Equation (5.7), has several advantages (see [14]):

- Ensures that the closed-loop system has finite-time stability of the equilibrium point $(P_{\mathrm{e}}(t) - P_{\mathrm{ref}})$ and the settling-time can be chosen by properly defining the values of the parameters $a$ and $K_\alpha$.

- Does not require information from the turbine total external damping or the turbine total inertia. It only requires the filtered generator speed and reference power of the WT.

In the numerical simulations, the values $a = 1$ and $K_\alpha = 1.5 \cdot 10^5$ are used and a first order approximation of $\dot{\hat{\omega}}_g(t)$ is computed.

This torque controller is saturated to a maximum of 47402.91Nm and a maximum generator torque rate saturation of 15000Nm/s, similarly to the baseline controller.

## 5.2 Simulation results

The characteristics of the WT used in the simulations are described in Chapter 2, Table 2.3.

The results compare the performance of the contributed FTC technique under different faulty scenarios with respect to the fault-free case with the baseline torque controller. When testing the FTC technique, the faults, high air content in oil (F1), pump wear (F2) and hydraulic leakage (F3) are introduced only in the third pitch actuator (thus $\beta_1$ and $\beta_2$ are always fault-free) in the following way:

- From 0s to 100s, it is fault-free.

- From 100s to 200s, a fault F1 is active.

- From 200s to 300s, it is fault-free.

- From 300s to 400s, a fault F2 is active.

- From 400s to 500s, it is fault-free.

- From 500s to 600s, a fault F3 is active.

- From 600s to 700s, it is fault-free.

As can be seen in Figure 5.2 (left), the three types of faults are detected by the disturbance estimator $\hat{d}$ given in Equation (5.6). To finally setup the fault detection and isolation strategy, the proposed residual signal, $r(t)$, is computed as described in Figure 5.3 and its results shown in Figure 5.2 (right). This residual is close to zero when the system is fault-free. On the other hand, when a fault appears it is significantly affected and allows to isolate the type of fault (among the three studied pitch actuator faults). The used thresholds to pinpoint the type of fault are:

- When the signal is smaller than 400 then F2 is detected. This can be seen in the zoom in Figure 5.2 (right)

- When the signal is between 400 and 5000 then F1 is detected.

- When the signal is above 5000 then F3 is detected.
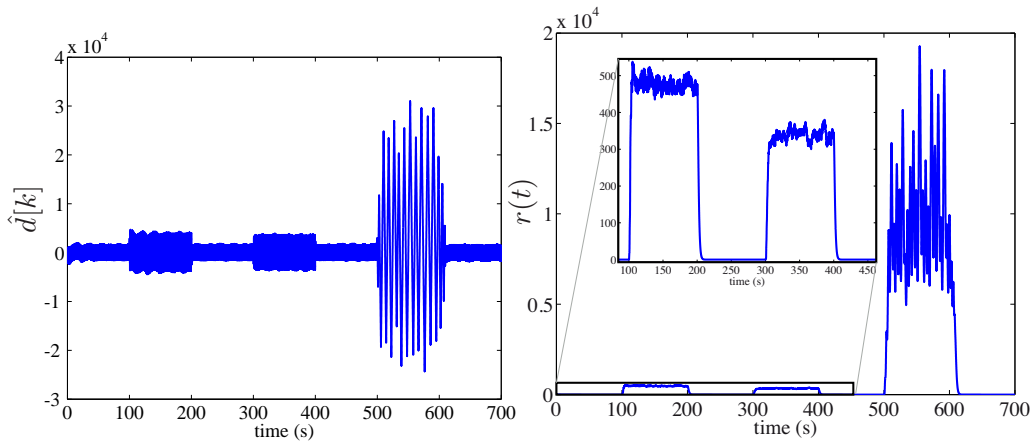


Figure 5.2. Discrete disturbance estimator (left) and the continuous residual signal (right).
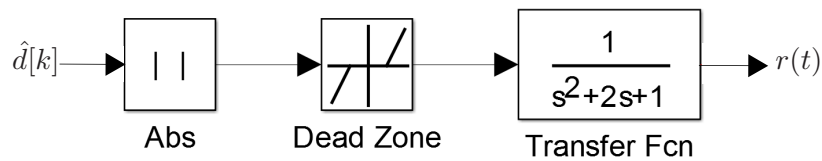


Figure 5.3. Computation of the residual signal, $r(t)$. Note that the Simulink® dead zone block is used (start of dead zone value equal to 0 and end of dead zone value equal to 2000).

Note that the concept of sliding mode surface in discrete-time is in fact a quasi-sliding mode (see, for instance, reference [131]). That is the reason why in Figure 5.4 (left) the typical finite-time convergence, given by continuous slide-mode controllers, is not attained here. In the discrete case, the typical convergence consists in that the values of the trajectory are maintained inside an interval, as can be seen in Figure 5.4 (left).

It can be observed from Figures 5.4 and 5.5 that the system behavior (electrical power and generator speed) with active fault compensation is similar to the behavior of the fault-free case, as the performance indices $J_{P2}(t)$ and $J_{w2}(t)$ values for the fault-free baseline and for the FTC (with faults) are very close. Moreover, the $J_{w2}(t)$ performance index shows that the generator

66

speed is closer to the nominal one during the faults F1 and F2 for the FTC than for the (fault-free) baseline controller. This can be seen in Figure 5.5 (right), as the index values, during the faults F1 and F2, are smaller for the FTC strategy.
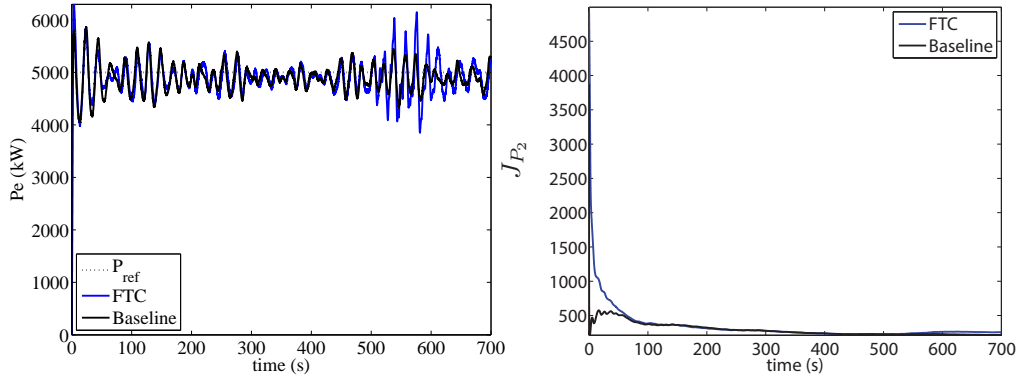


Figure 5.4. Electrical power (left) and $J_{P_2}$ index (right).
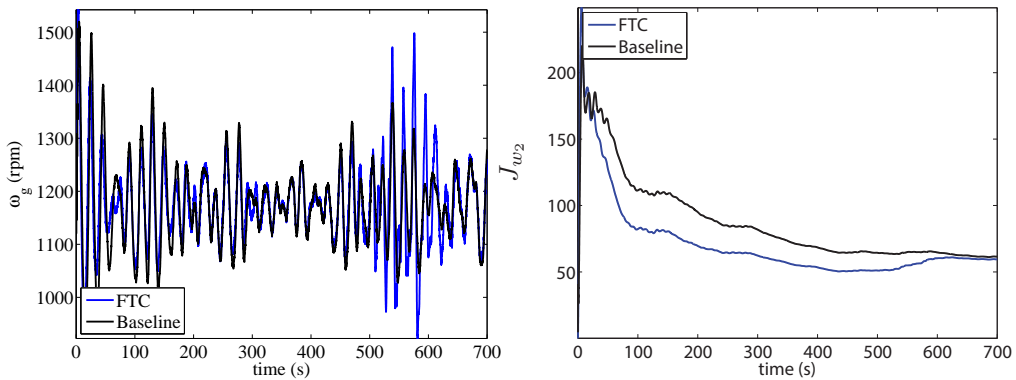


Figure 5.5. Generator speed (left) and $J_{\omega_2}$ index (right).

Figure 5.6 (left) shows that the first pitch angle ($\beta_1$), which is always fault-free, has a slightly different behavior with the FTC than with the baseline control. This is due to the fact that, with the FTC technique, a fault is introduced in the third pitch actuator ($\beta_3$) as can be seen in Figure 5.6 (right). Although higher oscillations are present in the FTC, the pitch control signal is regulated within the allowed variation domain. That is, none of the variations exceed the mechanical limitations of the pitch actuator.

As can be seen in Figure 5.7, the *fore-aft* and *side-to-side* acceleration are similar for the FTC technique (with faults) and for the fault-free baseline control strategy. The performance indices $J_{xi}(t)$ and $J_{yi}(t)$ at different tower heights corroborate this statement, as their values are
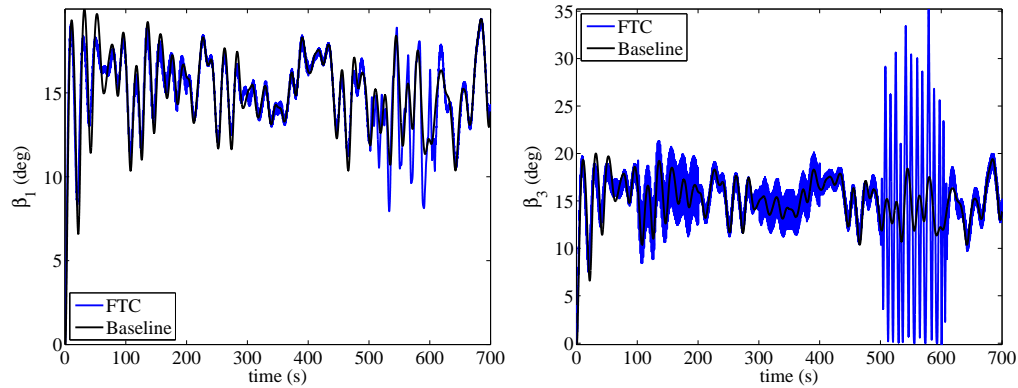
Figure 5.6. First pitch angle (left) and third pitch angle (right).

similar for the FTC and the baseline control strategy.

On the other hand, it is well known that actuator saturation causes stability problems in control systems [132]. This problem might also appear in the proposed FTC technique when torque saturation and/or pitch actuator saturation occur. Note that, although it is out of the scope of this chapter, the problem can be overpassed using, for instance, the well-known anti-windup technique (see [133]).

Finally, note that when a fault appears in a mechanical system, normally this fault will worsen, especially if the system remains in operation. The evolution of the failure can result in a disaster. To be realistic concerning robustness to a mechanical failure, the fault modeling should capture its evolution when the system remains in operation (time-varying parameters, among other nonlinearities). The evolution of the faults is not modeled in this chapter. Thus, the results of this chapter guarantee the controller robustness for a reasonable time in order to take appropriate action and correct the fault.

## 5.3   Conclusions

A WT fault-tolerant control scheme for pitch actuator faults is presented in this chapter based on direct fault estimation by means of a disturbance compensator. With the proposed FTC strategy, the system behavior in FAST simulations with faults is close to the behavior of the baseline controllers in the fault-free case. Meanwhile, the proposed residual signal detects the appearance of the faults in short time. This is in itself a benefit for the development of fault diagnosis schemes for WT. Finally, note that the resulting FTC strategy can also be easily implemented in practice due to the required low data storage and the simple math operations involved at each
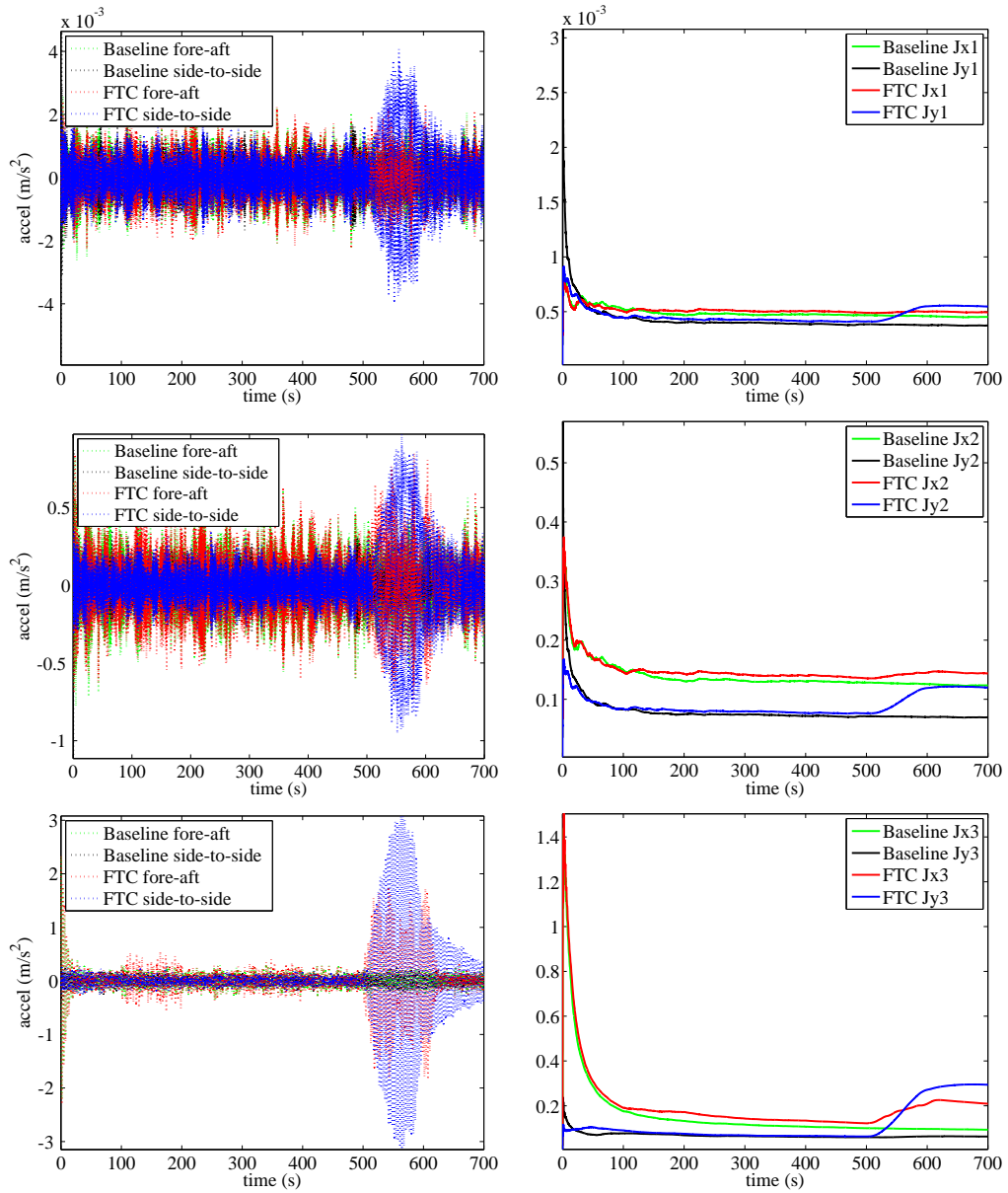
Figure 5.7. *Fore-aft* and *side-to-side* acceleration (left) and related indices (right) at nodes located at the tower top, at mid-tower height, and at the tower bottom.

sampling time (sums and products between scalars).

# CHAPTER 6

# ACCELERATION-BASED FTC DESIGN OF OFFSHORE FIXED WIND TURBINES

Wind turbines are basically controlled by varying the generator load torque (with the so-called torque control) and the blade pitch angles (with the so-called pitch control) based on measurement of the generator shaft speed. These two controllers unitedly work to satisfy the control objectives and it is crucial that they are tolerant to possible faults in the WT system. Passive fault tolerant control comprises the design of robust controllers against disturbances and uncertainties. This enables the controller to counteract the effect of a fault without requiring reconfiguration or fault detection. In this regard, the main contribution of this chapter is to propose new control techniques which not only provide fault tolerance capabilities to the WT system, but also improve the overall performance of the system in both fault free and faulty conditions. Coupled non-linear aero-hydro-servo-elastic simulations of an offshore WT with jacket platform is carried out for several pitch actuator faults. The jacket platform motions and structural loads caused by fault events with the proposed controllers are compared to loads encountered during normal operation and with respect to a well-known baseline controller in the literature. The proposed controllers are based in the super-twisting algorithm (STA) by using feedback of the generator shaft speed as well as the *fore-aft* and *side-to-side* acceleration signals of the WT tower.

## 6.1 Problem statement

To make easier the control system design, most control strategies for WT uncouple the control problem into two different single input single ouput (SISO) control loops: the torque and the pitch controllers (see, for example, [134], [135], [62], [38]). Although the uncoupled assumption (used also in this work), these controllers work collaboratively in the WT overall closed loop system (see, for instance, [135]). In this chapter, scalar STA (see [136] is used to design new torque and pitch controllers. A comprehensive analysis of the STA is conducted, for instance, in [137].

In previous works (see [14], [138], and [139]), it has been proposed the use of classical sliding mode control (SMC) for WT control. Such approaches deal efficiently with the power regulation objective and provide the advantage of robustness against system uncertainties and perturbations, such as measurement noise. Although classical SMC has shown good performance in an uncountable number of applications, its well-known drawback has been the discontinuous behavior of the computed control inputs that may derive into a high-frequency oscillation known as chattering (see [140]). Among great variety of chattering suppression methods, so-called high-order sliding mode control has been intensively studied within the last decade (see, for example, [137]) and has been applied in a wide variety of fields (see, for instance, [141], [142], [143], and [144]). The twisting and super-twisting control algorithms are intended for designing the second-order sliding mode. While the twisting algorithm needs an additional differentiator (preserving the structural requirement for the common first-order sliding mode), the super-twisting algorithm (STA) does not need it. The able properties of the STA are: a) accurate regulation and tracking accomplished with finite-time convergence; b) as the control input is a continuous state function, there is a reduction of mechanical stresses (see [145]) and chattering; c) time derivative of the output is not needed; d) robustness with respect to various internal and external disturbances and model uncertainties; e) relatively simple control laws that can be designed based on nonlinear models. These properties explain high level of research activity related to stability analysis, estimation of the convergence time, and estimation of the admissible range of disturbances (see, among others, [146], [137], [147], and [148]).

The most frequent WT faults induce vibrations in the corresponding WT subsystems [149]. In fact, vibration monitoring has been recently used for fault diagnosis [150], [151]. Thus, by means of vibration mitigation, different faulty conditions can be alleviated leading to a passive FTC strategy. The problem of alleviating vibrations in WT systems is relatively new, being an efficient straightforward method the use of vibration control devices under passive, active or

semi-active schemes (e.g., [152], [153], [154], [155], [156] and [157]). This chapter is concerned with active vibration mitigation but not through the use of specifically tailored devices else by the design of torque and pitch controllers that take care of the vibrational behavior of the WT tower by employing feedback of the *fore-aft* and *side-to-side* acceleration signals at the top of the WT tower. Generally, proposed methods to improve damping through pitch and torque control suffer from increased blade pitch actuator usage [152]. However, in this chapter the blade pitch angle is smoothed leading to a decrease of the pitch actuator usage, among other benefits evidenced through numerical experiments. Therefore, new torque and pitch controllers are proposed based on the STA by introducing the acceleration signals at top tower as a feedback perturbation signal, with the purpose of reducing vibrations. In particular, the torque control objectives are to regulate the electrical power and mitigate vibrations in the *side-to-side* direction and the pitch control objectives are to regulate the generator speed and mitigate vibrations in the *fore-aft* direction. Both controllers work together to obtain an electrical power regulated to the rated electrical power and, at the same time, a generator speed regulated to its nominal value.

Coupled non-linear aero-hydro-servo-elastic simulations of an offshore WT with jacket platform is carried out for several pitch actuator faults. The jacket platform motions and structural loads caused by fault events with the proposed controllers are compared to loads encountered during normal operation and with respect to a well-known baseline controller in the literature.

### 6.1.1 Controllers design

On one hand, we propose the following scalar STA-based torque controller:

$$\tau_c(t) = -\alpha_1 \sqrt{|P_e(t) - P_n|} \text{sign}(P_e(t) - P_n) + y(t), \tag{6.1}$$

$$\dot{y}(t) = -\alpha_2 \text{sign}(P_e(t) - P_n) + \alpha_3 a_{ss}(t),$$

where $\alpha_1, \alpha_2, \alpha_3 > 0$ and $a_{ss}(t)$ is the *side-to-side* acceleration measured at the tower top. Note that we introduce the acceleration as a perturbation signal to give the controller the ability to face with vibrations (and faulty conditions). A stability analysis for this controller is given in the next subsection.

On the other hand, we propose to modify the baseline gain-scheduling pitch controller in the form

$$\beta_c(t) = K_p(\gamma)(\hat{\omega}_g(t) - \omega_{g,n}) + K_i(\gamma)z(t), \tag{6.2}$$

$$\dot{z}(t) = \text{sign}(\hat{\omega}_g(t) - \omega_{g,n}) + \alpha_4 a_{fa}(t),$$

where $\alpha_4 > 0$ and $a_{fa}(t)$ is the *fore-aft* acceleration measured at the tower top. Note that the acceleration is introduced, similarly to the torque controller, as a perturbation signal. For the proposed pitch controller, as it is a gain-scheduling proportional integral control, the controller gains are *heuristically* tuned following the same procedure as in [36].

The block diagram in Figure 6.1 shows the connections between the WT and the proposed torque and pitch controllers.
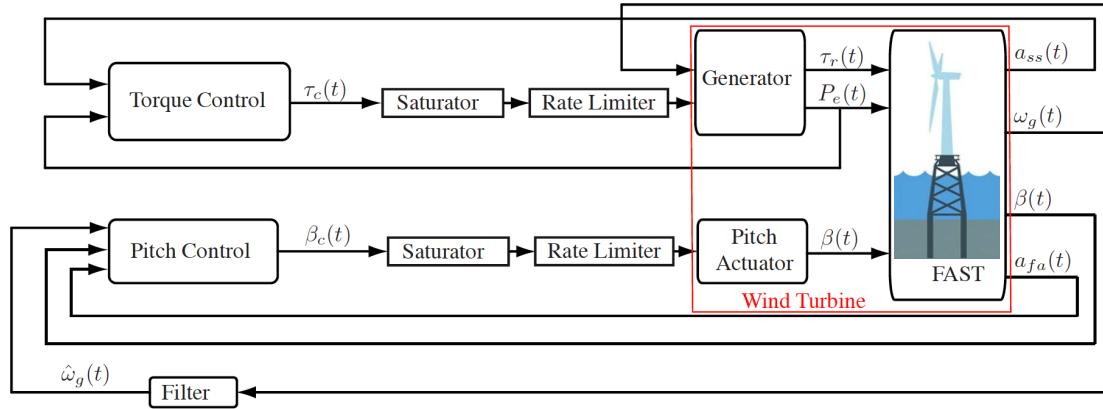


Figure 6.1. Block diagram of the closed loop system.

Source:( [158])

## 6.1.2 Torque control stability analysis

For a perfectly rigid low-speed shaft, a single-mass model for a WT can be considered (see Secton 2.2, ( [33–35, 130]):

$$J_t \dot{\omega}_g(t) = T_a(t) - \tau_c(t), \tag{6.3}$$

where $J_t$ is the turbine total inertia (Kg m$^2$), $\tau_c$ is the generator torque (Nm), and $T_a$ is the aerodynamic torque (Nm) described as

$$T_a(t) = \frac{1}{2} \rho \pi R_{rot}{}^2 \frac{C_p(\lambda, \beta)}{\omega_r(t)} V_{wind}{}^3(t), \tag{6.4}$$

where $\rho$ is the air density (kg/m$^3$), $R_{rot}$ is the rotor radius (m), $\omega_r$ is the rotor speed (rad/s), $V_{wind}$ is the wind speed (m/s), and $C_p(\lambda, \beta)$ is the power coefficient (bounded by the Betz

74

limit). Note that, due to physical constraints, the aerodynamic torque is bounded. Thus, it is realistic to assume that $0 < T_a \leq \gamma$, $\forall t \geq 0$.

The STA-based torque control objective is to regulate the electrical power. Thus, we define the error:

$$e(t) = P_{\mathrm{e}}(t) - P_n,$$

and the control objective is that it converges to zero as time goes on. It is obvious that

$$\dot{e}(t) = \dot{P}_e(t) = \eta_g \left[ \dot{\omega}_g(t)\tau_r(t) + \omega_g(t)\dot{\tau}_r(t) \right].$$

Using (2.10) and (6.3), from the generator-converter model and WT model respectively, the error dynamics can be written as

$$\dot{e}(t) = \eta_g \left[ J_t^{-1} \left( T_a(t) - \tau_c(t) \right) \tau_r(t) + \alpha_{gc}\omega_g(t) \left( \tau_c(t) - \tau_r(t) \right) \right],$$

and, assuming that $\tau_c(t) - \tau_r(t) \approx 0$, it can be simplified to

$$\dot{e}(t) = \eta_g J_t^{-1} T_a(t)\tau_c(t) - \eta_g J_t^{-1} \tau_c^2(t).$$

Finally, linearizing the previous dynamics around $\tau_c(t) = 0$, the error dynamics yields

$$\dot{e}(t) = \eta_g J_t^{-1} T_a(t)\tau_c(t),$$

and, as $\eta_g J_t^{-1} T_a$ is positive and bounded, to prove the local stability of this system is equivalent to study the local stability conditions of the system

$$\dot{e}(t) = \tau_c(t).$$

This system, after substituting (7.1.1) gives the closed loop error dynamics,

$$\dot{e}(t) = -\alpha_1 \sqrt{|e(t)|}\mathrm{sign}(e(t)) + y(t), \tag{6.5}$$

$$\dot{y}(t) = -\alpha_2 \mathrm{sign}(e(t)) + \alpha_3 a_{ss}(t). \tag{6.6}$$

Since we consider that the *side-to-side* acceleration, $a_{ss}(t)$, is a perturbation signal (giving the controller the ability to face with vibrations), system (6.5)-(6.6) is stable as has been proven

in [148]. This finally concludes the stability of the proposed torque control.

## 6.2 Simulation results

The fixed jacket offshore WT described in Section 2.8.2 is considered as a test for the proposed FTC strategy. On the other hand, the aero-hydro-servo-elastic simulation tool FAST v8 [159], is used. The simulations are conducted in the presence of wind turbulence (full load region of operation), waves, and realistic pitch actuator fault scenarios.

In order to compare between different control systems, the described baseline control system in Section 2.9.1 was used as a frame of reference. Simulations were conducted for a realistic wind speed (see Section 2.7), and over 600 s of run time. The waves elevation sequence is illustrated in Figure 6.2 with the waves elevation. The rated and cutout wind speeds are 11.4 m/s and 25 m/s, respectively. Thus, the wind profile lies in the above rated working region.
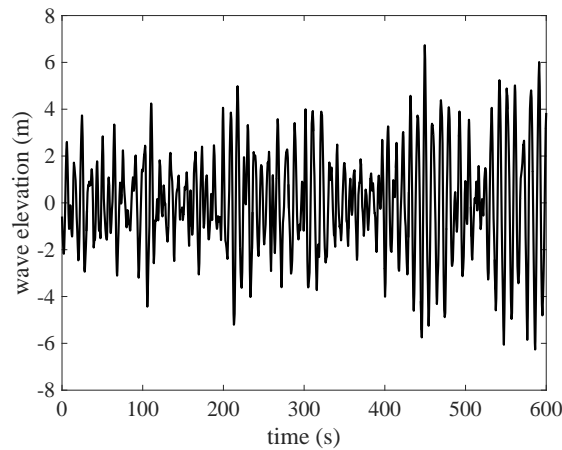


Figure 6.2. Wave elevation (m).

### 6.2.1 Healthy scenario

First, the high performance of the STA controllers is demonstrated in fault-free operation of the WT.

Figure 6.3 presents the electrical power (left) and $J_{P_1}$ index (right) for the proposed STA controllers and compared to the baseline ones. Results show that the proposed controllers improve the power generation quality. Due to the rate-limiter action and the complexity of the WT

model used for simulation (FAST), the finite-time convergence behavior of the STA torque controller is not evidenced in the results, as can be seen in Figure 6.3 (left). The $J_{P_1}$ performance index is improved, that is the error in the regulation of the electrical power is reduced. In a 600 seconds simulation, the accumulated error is almost halved with respect to the baseline strategy as can be seen in Figure 6.3 (right).
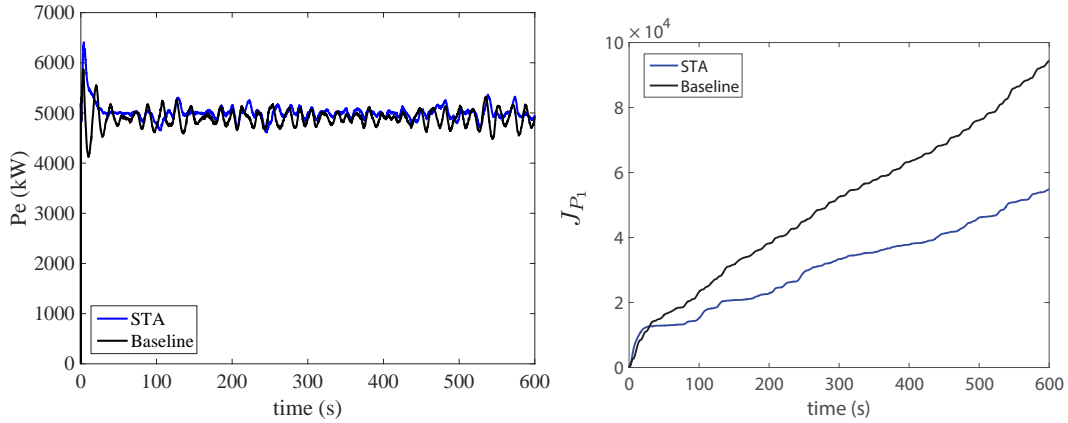


Figure 6.3. Electrical power (left) and $J_{P_1}$ index (right).

Figure 6.4 (left) displays the generator speed. It is observed that higher oscillations are obtained for the baseline controllers. The proposed STA does not induce increased mechanical stress as there are no strong torque variations, as can be seen in Figure 6.4 (right). The torque generator remains smooth and tracks more efficiently the wind fluctuations than in standard control. Indeed, and as expected, this leads to a reduction of the acceleration in the tower, as can be seen in Figure 6.5. It is noteworthy that the acceleration in the *fore-aft* direction has been dramatically improved whereas acceleration in the *side-to-side* direction is comparable to the ones obtained with the baseline control.

The platform rotational and translational data are shown in Figure 6.6. A reduction is obtained in the pitch tilt angle and the horizontal surge displacement with the proposed STA, with comparable results in the roll tilt and yaw angles and the horizontal sway and heave displacements with respect to the baseline controllers.

Recall that, when designing the pitch angle control loop, it is of great importance to avoid a high activity of the pitch, since it could not only damage the pitch actuators but also give rise to unstable modes of operation, see, for instance, [135]. The pitch control, shown in Figure 6.7, is smoothed with the STA-based controllers. This lower pitch activity leads to lower mechanical stress (vibration mitigation) spreading the WT lifetime and also resulting in softer output power.
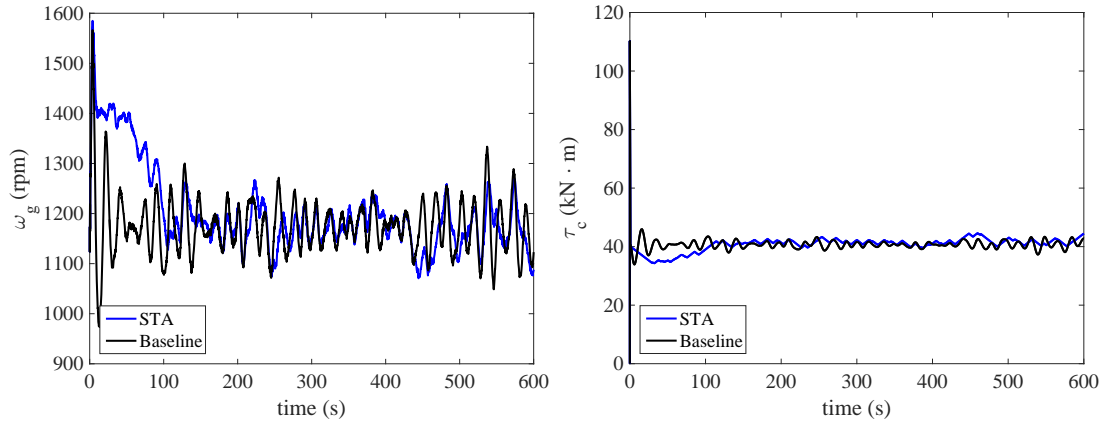
Figure 6.4. Generator speed (left) and torque control (right).
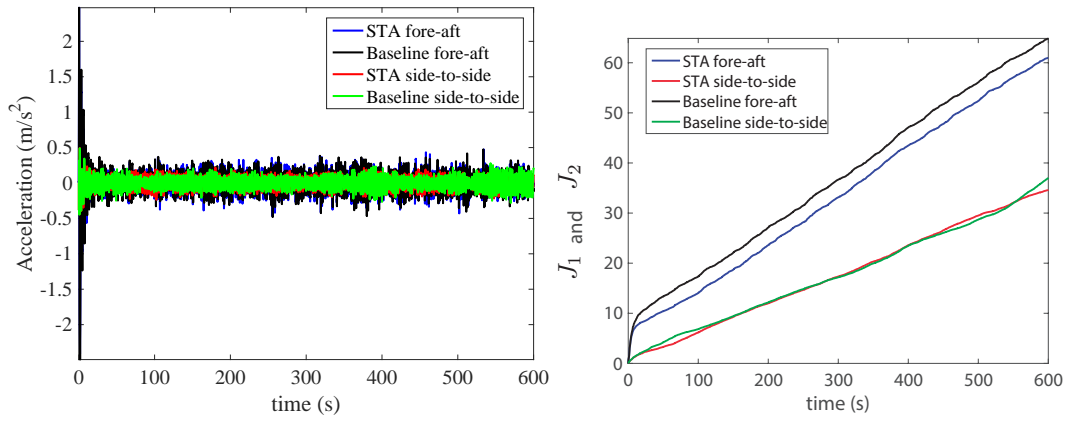


Figure 6.5. *Fore-aft* and *side-to-side* acceleration (left) and related indices (right) at the tower top.



Figure 6.6. Platform rotational data (left) and platform translational data (right).
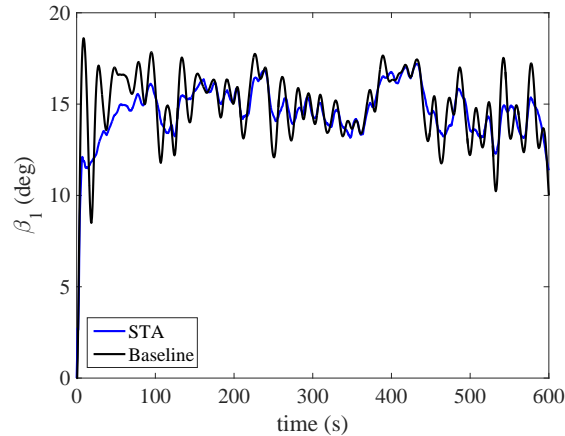
Figure 6.7. Pitch angle.

*Remark 1.* The gains $\alpha_1 = 0.1$, $\alpha_2 = 200$, $\alpha_3 = 1$, and $\alpha_4 = 5$ are used in the simulations. They were selected in order to reduce the *fore-aft* motion. However, other gain values could be used, for example, to obtain also an improvement in the *side-to-side* direction.

## 6.2.2   Stuck pitch actuator

Here the stuck/unstuck fault (see Section 2.5.2) in the picth actuator is modeled and the behavior of the proposed controllers is analyzed in comparison to the baseline ones.

The simulation results for this faulty case are shown in Figures 6.8-6.12. The following observations can be drawn:

- The transient response of the electrical power has a larger oscillation for the baseline controller, as shown in Figure 6.8 (left).

- The generator speed for the baseline controller has larger oscillations, as shown in Figure 6.9 (left).

- The torque action for the baseline controller achieves the saturation limit ($47.40\text{kN·m}$) whereas the proposed controller does not, as shown in Figure 6.9 (right). When achieving the saturation limit vibrations and limit cycles can appear, see [160].

- The acceleration at tower top has been dramatically improved not only in the *fore-aft* but also in the *side-to-side* direction, see Figure 6.10.

- A reduction is obtained in the roll tilt angle and the horizontal sway displacement with the

79

proposed STA, with comparable results in the pitch tilt and yaw angles and the horizontal surge and heave displacements with respect to the baseline controllers, see Figure 6.11.

- The first blade pitch angle remains always within the authorized variation domain, as shown in Figure 6.12 (left), but with higher oscillations for the baseline controller. Thus, our proposed controller induces less vibrations in the structure as the range of movement of the pitch angle is smaller.

- The third blade switches between being stuck/unstuck as can be seen in Figure 6.12 (right).
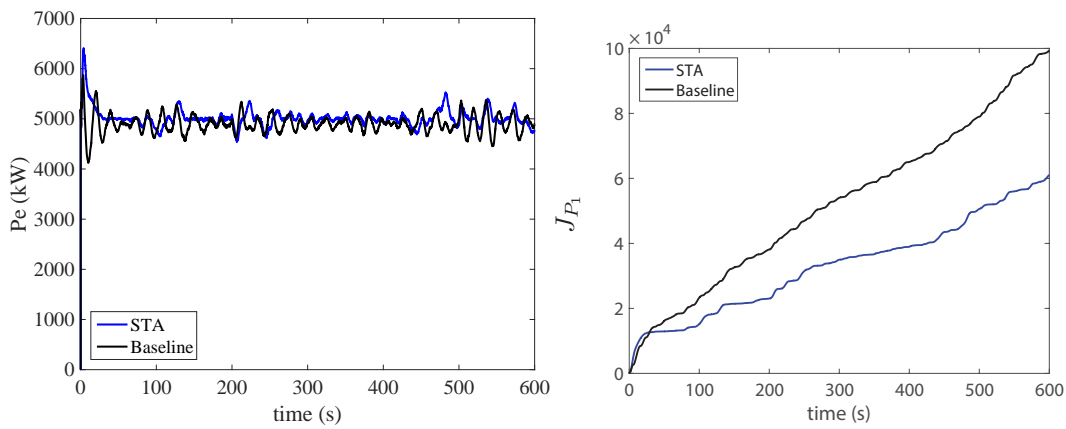


Figure 6.8. Electrical power (left) and $J_{P_1}$ index (right) under stuck/unstuck faulty condition.
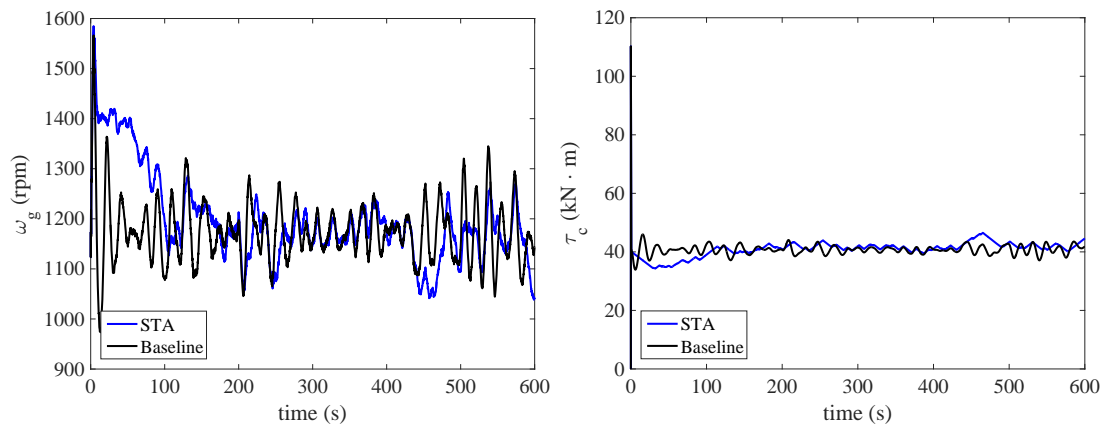


Figure 6.9. Generator speed (left) and torque control (right) under stuck/unstuck faulty condition.
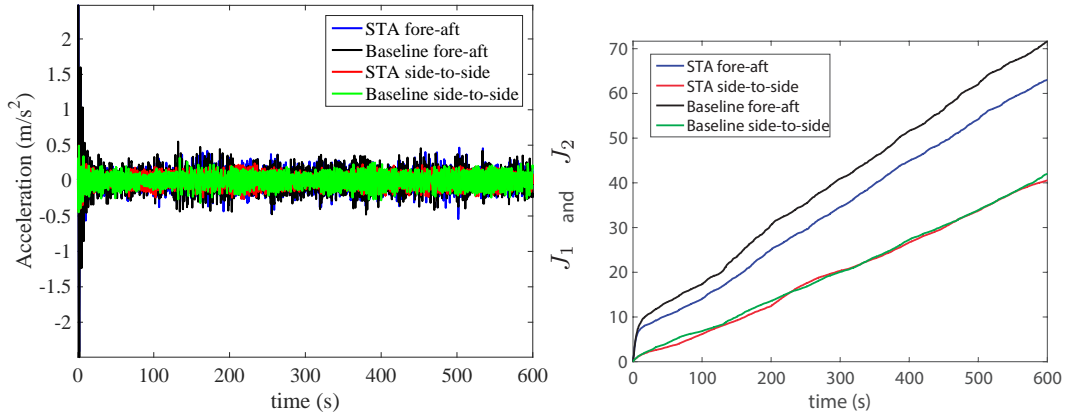
Figure 6.10. *Fore-aft* and *side-to-side* acceleration (left) and related indices (right) at the tower top under stuck/unstuck faulty condition.
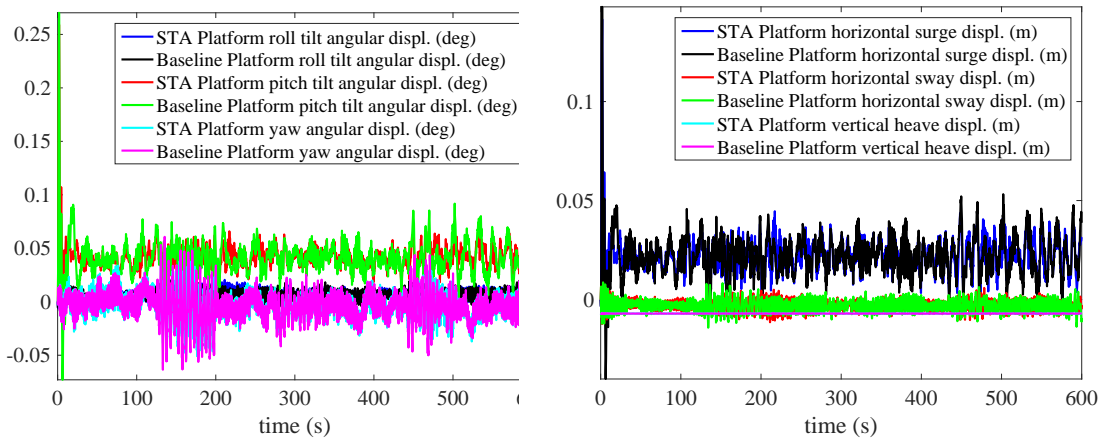


Figure 6.11. Platform rotational data (left) and platform translational data (right) under stuck/unstuck faulty condition.

### 6.2.3 Hydraulic leakage of pitch actuator

This fault changes the dynamics of the pitch actuator. A detailed description can be found in Section 2.5.1, [43], [5], and [161].

The simulation results for this faulty case are shown in Figures 6.13-6.17. The following observations can be made:

- The transient response of the electrical power has a larger oscillation for the baseline controller, as shown in Figure 6.13 (left).

- The generator speed for the baseline controller has larger oscillations, as shown in Figure 6.14 (right).

81
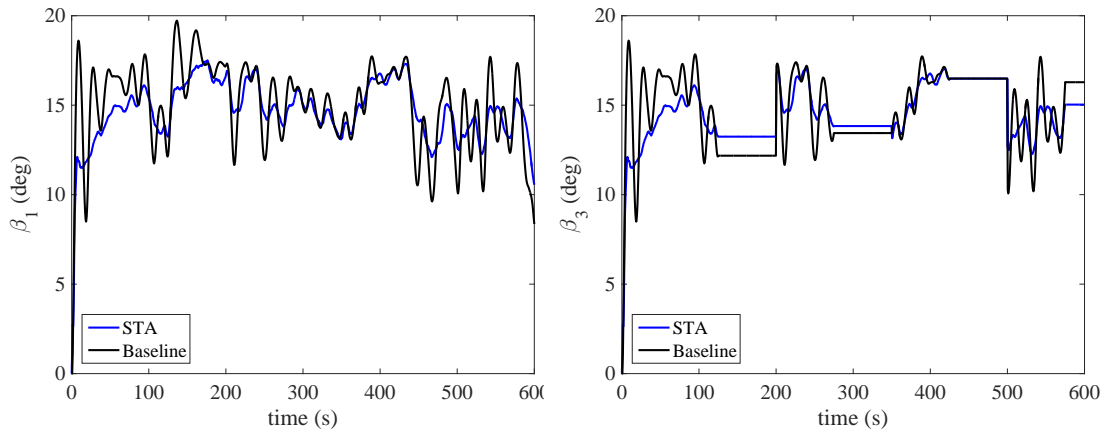
Figure 6.12. Pitch angle under stuck/unstuck faulty condition (only the third pitch actuator is faulty).

- The acceleration at tower top is improved in the *fore-aft* direction and comparable in the *side-to-side* direction, see Figure 6.15.

- Similarly to the healthy case, a reduction is obtained in the pitch tilt angle and the horizontal surge displacement with the proposed STA, with comparable results in the roll tilt and yaw angles and the horizontal sway and heave displacements with respect to the baseline controllers, see Figure 6.16.

- The blade pitch angle remains always within the authorized variation domain, as shown in Figure 6.17, but with higher oscillations for the baseline controller. Thus, our proposed controller induces less vibrations in the structure as the range of movement of the pitch angle is smaller.
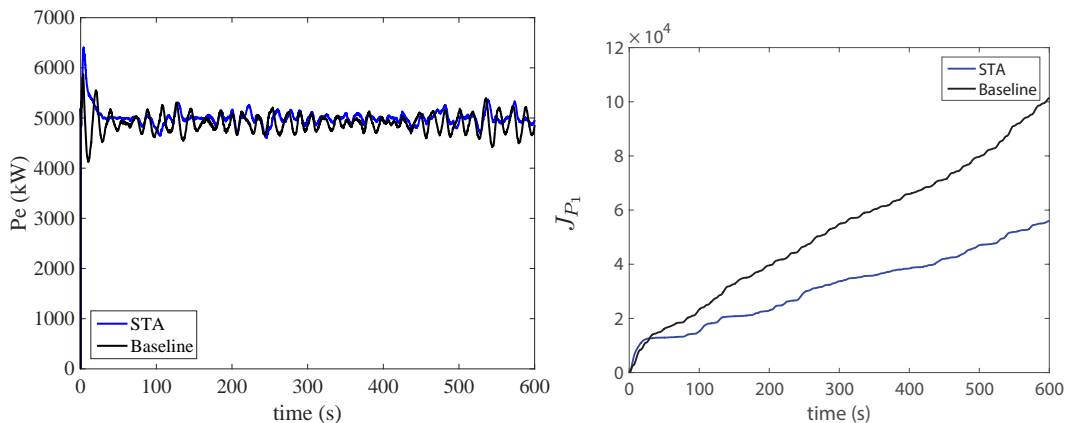


Figure 6.13. Electrical power (left) and $J_{P_1}$ index (right) under hydraulic leakage faulty condition.

82
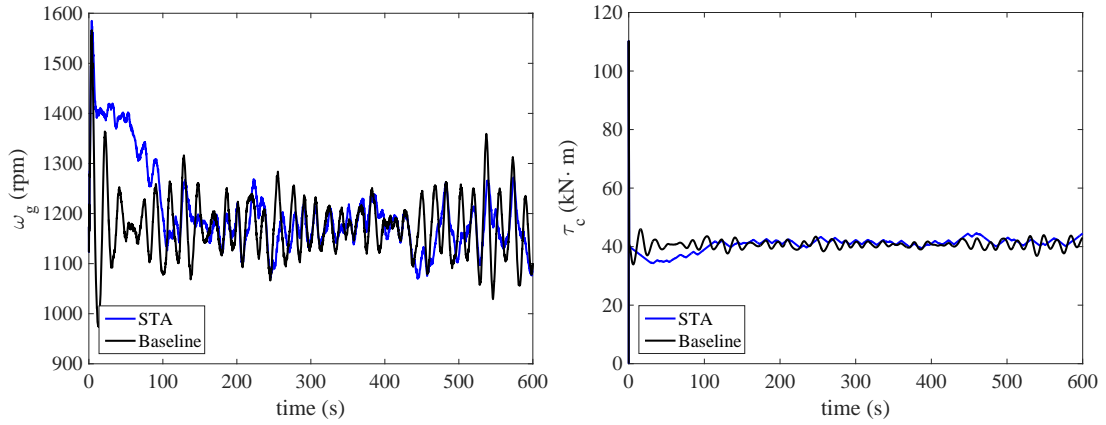
Figure 6.14. Generator speed (left) and torque control (right) under hydraulic leakage faulty condition.
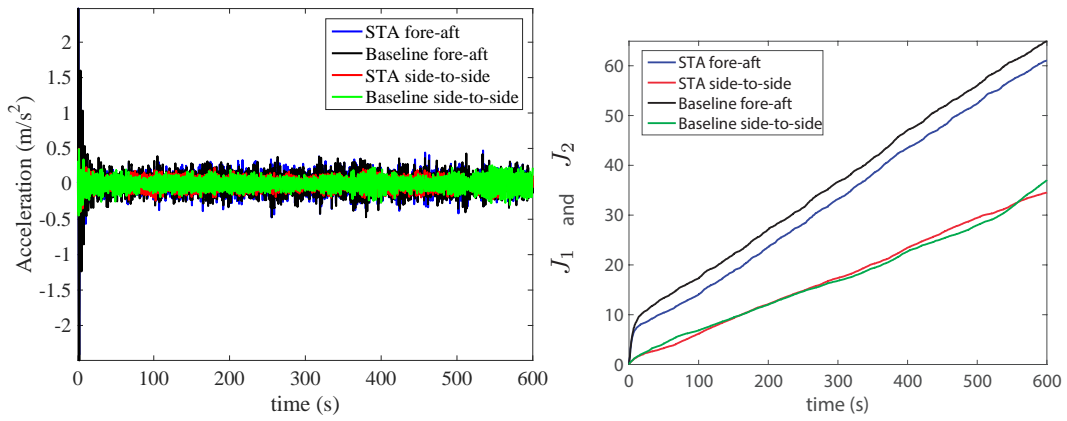


Figure 6.15. *Fore-aft* and *side-to-side* acceleration (left) and related indices (right) at the tower top under hydraulic leakage faulty condition.
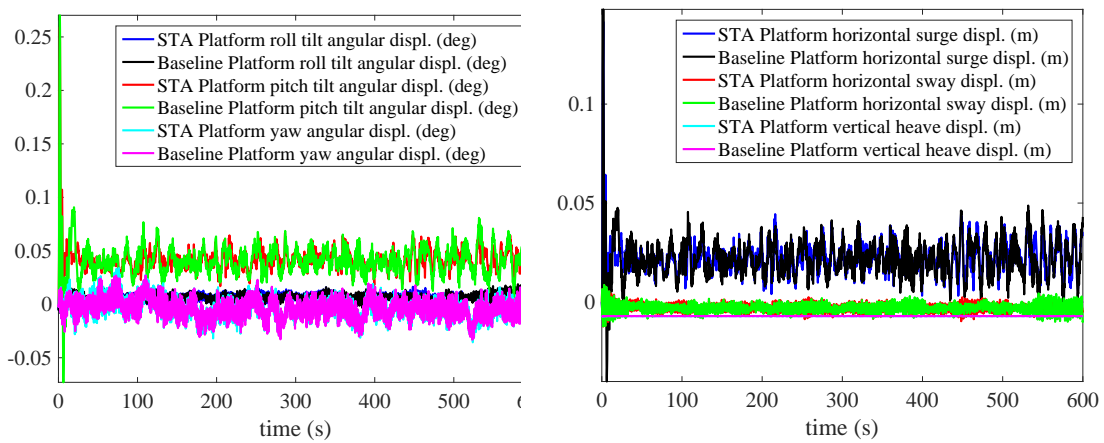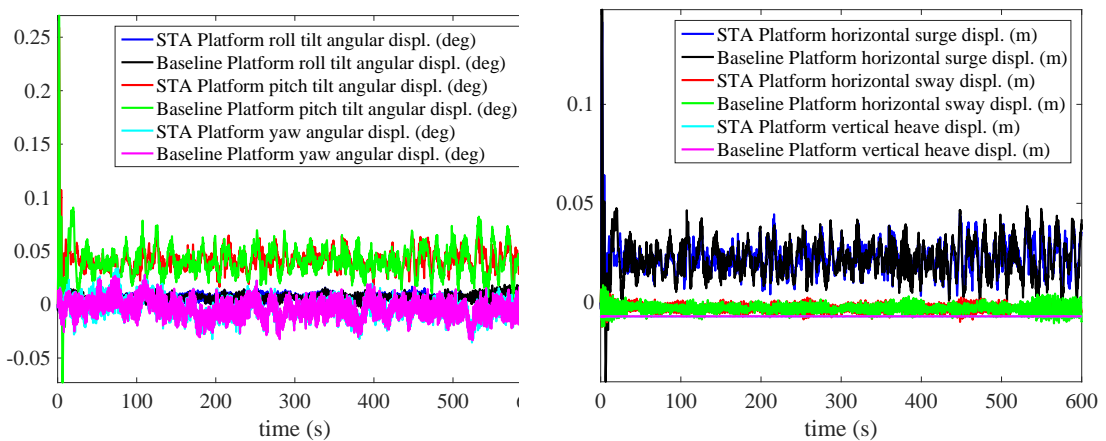


Figure 6.16. Platform rotational data (left) and platform translational data (right) under hydraulic leakage faulty condition.
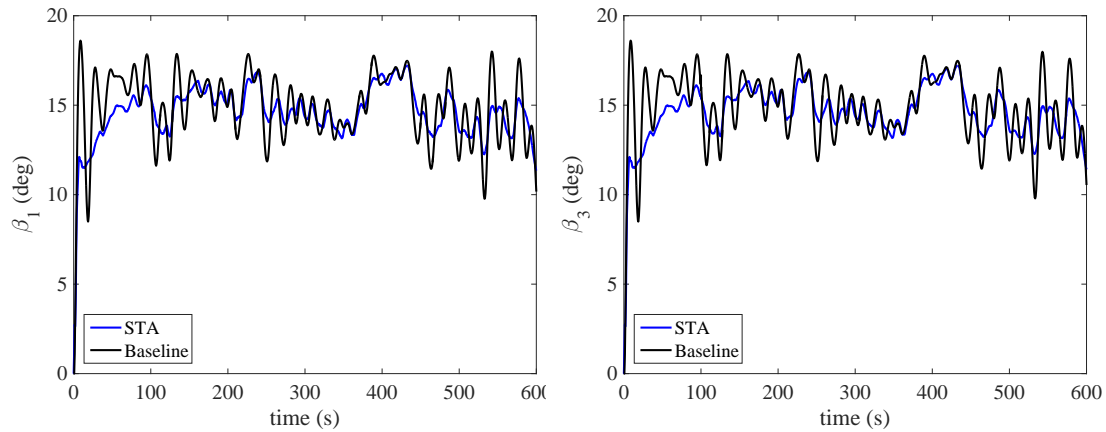
Figure 6.17. Pitch angle under hydraulic leakage faulty condition (only the third pitch actuator is faulty).

## 6.3 Conclusions

This chapter addressed the design of a robust STA for efficient and reliable control of a large offshore WT with jacket platform operating in the full load region, and in the presence of wind turbulence and different realistic fault scenarios. Compared to the baseline controllers, the developed STA-controllers have been able to improve the overall performance of the WT in healthy and faulty conditions, and to reduce the *fore-aft* and *side-to-side* acceleration with respect to the baseline control. In a nutshell, a STA design has been developed for control of WT with added vibration reduction properties.

CHAPTER 7

# HYSTERESIS-BASED DESIGN OF DYNAMIC REFERENCE TRAJECTORIES TO AVOID SATURATION IN CONTROLLED WIND TURBINES

The main objective of this chapter is to design a dynamic reference trajectory based on hysteresis to avoid saturation in controlled WTs. Basically, the torque controller and pitch controller set-points are hysteretically manipulated to avoid saturation and drive the system with smooth dynamic changes. Simulation results obtained from a 5MW WT benchmark model show that our proposed strategy has a clear added value with respect to the baseline controller (a well-known and accepted industrial WT controller). Moreover, the proposed strategy has been tested in healthy condition but also in presence of a realistic fault where the baseline controller caused saturation to finally conduct to instability.

## 7.1 Problem statement

In control systems, every actuator is prone to saturation due to its maximum and minimum physical limits. The analysis and design of a system that contains saturation nonlinearities, such as actuator saturation, is an important and challenging problem [63, 132, 162–164]. It is important that the control design takes into account the actuator limits to avoid undesirable

effects such as transient response, degradation of the closed-loop performance, and even closed-loop instability [63]. In WTs, saturation can create limit cycles inducing dangerous vibrations on the WT structure.

In the literature, there have been efforts in addressing actuator saturation. For example, reference [165] presents a synthesis of modern anti-windup techniques. A direct approach to deal with actuator saturation in WTs is used in [166] where an anti-windup controller to minimize the $H_\infty$ norm of the closed-loop system is designed. The design of a compensation method, which is based on variable structure systems to avoid both amplitude and rate input saturation by means of an auxiliary loop, is presented in [120]. In [167] the enlargement of the domain of stability of an actuator constrained state time-delay system with a novel dynamic two controller anti-windup design is proposed. It is also relevant the recent research on model predictive control in which constraint handling is given to cope with the actuator physical limitations, see [168–170]. Note that, in WT, some kind of faults can saturate the control action [171], and these saturation nonlinearities might lead to instability. Therefore, a robust system against saturation can better deal with faults.

### 7.1.1  Controllers

The torque controller used by the proposed strategy is the scalar Super-Twisting Algorithm (STA) based controller described in Equation (7.1.1) and [158]. The controller is recalled here to ease the reading:

$$\tau_c(t) = -\alpha_1\sqrt{|P_e(t) - P_n|}\text{sign}(P_e(t) - P_n) + y(t),$$

$$\dot{y}(t) = -\alpha_2\text{sign}(P_e(t) - P_n) + \alpha_3 a_{ss}(t),$$

Note that $\tau_c(t)$ is the torque control signal before the saturation and rate limiter actions (see Figure 7.6). On the other hand, the pitch control given in Equation (7.1.1) is used [158]. Is recalled the STA for the pitch controller loop:

$$\beta_c(t) = K_p(\gamma)(\hat{\omega}_g(t) - \omega_{g,n}) + K_i(\gamma)z(t),$$

$$\dot{z}(t) = \text{sign}(\hat{\omega}_g(t) - \omega_{g,n}) + \alpha_4 a_{fa}(t),$$

The STA-based torque and pitch controllers [158], compared to the baseline controllers, improve the overall performance of the WT in healthy and faulty conditions, and reduce the *fore-aft* and *side-to-side* acceleration, which is relevant in terms of vibration reduction. Under actuator saturation, the baseline and the STA-based controllers, both, may induce limit cycles. In this case, it leads to instability of the overall closed-loop system (a phenomenon also observed in controlled mechanical systems under saturation (see, for instance [160]).

The proposed saturation strategy can be used with any controller. In this work, it is used in conjunction with the baseline controllers and also with the STA-based controllers. Their respective performances are compared to the baseline controllers without any strategy to avoid saturation.

## 7.1.2 Design of the hysteresis-based avoid saturation strategy

Recall that WTs are basically controlled by manipulating the generator load torque (with the so-called torque control) and the blade pitch angles (with the so-called pitch control). These two controllers unitedly work to achieve the control objectives. Note that the main torque control objective is to regulate the electrical power and the main pitch control objective is to regulate the generator speed. This section describes the design of a strategy for saturation avoidance (SSA) based on a hysteresis law. Its main objective is to dynamically adapt $P_{\text{ref}}$ and $\omega_{g,r}$ to avoid saturation and the consequent undesired effects, guaranteeing the closed-loop operation of the control system.

The first step is to define a so-called safety band (narrower than the band given by the actuator saturation limits) such that when the torque control signal leaves this band the reference power and generator speed are readjusted to bring back the torque control signal into the safety band. The safety band is defined by an upper torque value ($\tau_u$) and a lower torque value ($\tau_l$) given as follows and illustrated in Figure 7.1:

$$\tau_u = \tau_n + h, \qquad \tau_l = \tau_n - h, \tag{7.1}$$

where $\tau_n$ is the nominal torque and $h$ is defined as

$$h = \frac{\tau_{\text{max}} - \tau_n}{f}, \tag{7.2}$$

where $f > 1$ is a parameter to be selected (the larger the value of $f$, the narrower will be

Table 7.1. Values used by the SSA in the numerical simulations.

| Values used by the SSA | |
|---|---|
| $\tau_{\max}$ | 47.40 KNm |
| $\tau_n$ | 40.68 KNm |
| $\tau_u$ | 41.80 KNm |
| $\tau_l$ | 39.55 KNm |
| $\Gamma$ | 0.5 |
| $f$ | 6 |
| $P_n$ | 5.00 MW |
| $P_u$ | 5.97 MW |
| $P_l$ | 4.07 MW |
| $\omega_{g,n}$ | 122.91 rad/s |
| $\omega_{g,u}$ | 142.91 rad/s |
| $\omega_{g,l}$ | 102.91 rad/s |

the safety band) and $\tau_{max}$ is the maximum allowable torque (saturation limit). Table 7.1 gives values of the above parameters, which will be used later on in the simulation results.

The second step is to introduce hysteresis loops relating the torque control signal, $\hat{\tau}_c$, with the desired reference power, $P_{\text{ref}}$, and the desired reference generator speed, $\omega_{g,r}$, respectively. With the purpose of introducing the idea in a qualitative manner, Figures 7.1 and 7.2 illustrate scenarios where the torque control leaves the safety band with either an increasing or decreasing tendency.

Point 1 in Figure 7.1 indicates a time instant in which the torque control signal, $\hat{\tau}_c$, surpasses the upper torque value $\tau_u$. Then, the hysteresis loop, as indicated by point 1 in Figure 7.2, readjusts the reference power, $P_{\text{ref}}$, to a slightly lower value (called $P_l$) with respect to the nominal one, $P_n$. A similar loop is considered for the reference generator speed, $\omega_{g,r}$, in Figure 7.2 with the corresponding lower value $\omega_{g,l}$. These lower values for the reference signals drive the torque control signal back to the safety band region (see point 2 in Figure 7.1 and Figure 7.2).

On the other hand, when the torque control signal, $\hat{\tau}_c$, falls below the lower torque value, $\tau_l$, (see point 3 in Figure 7.1) the reference power and the reference generator speed are adapted to slightly upper values with respect to the nominal ones, called $P_u$ and $\omega_{g,u}$ (see point 3 in Figure 7.2). These increased values for the reference signals drive the torque control signal back to the safety band region (see point 4 in Figure 7.1 and Figure 7.2).

The lower values $\omega_{g,l}$, $P_l$ and the upper values $\omega_{g,u}$, $P_u$ are parameters of the SSA. In the simulations we use the values shown in Table 7.1.
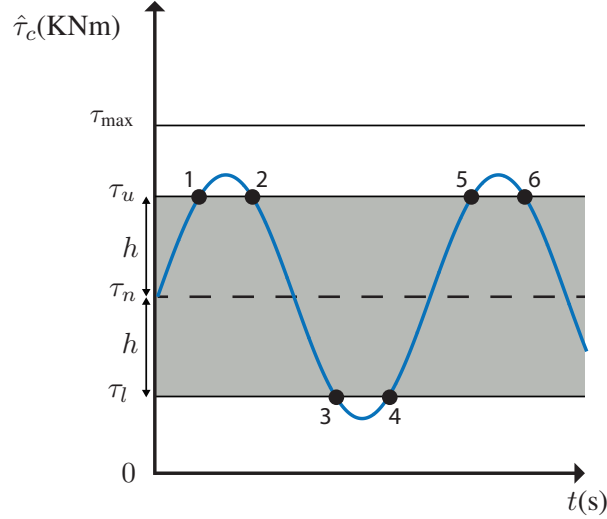


Figure 7.1. Safety band defined by the upper torque value ($\tau_u$) and the lower torque value ($\tau_l$).

Source:( [119])
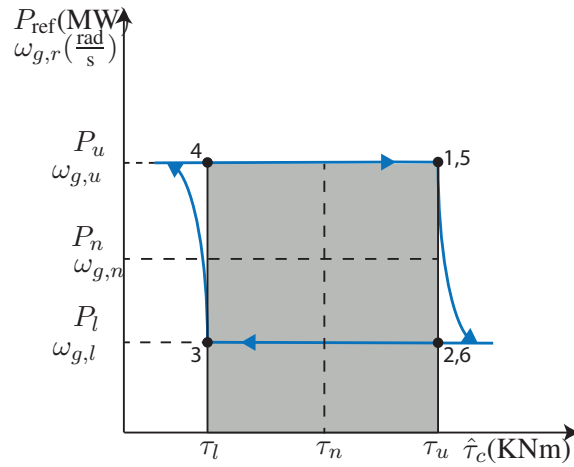


Figure 7.2. Hysteresis-based reference signals readjustment.

Source:( [119])

One way to construct a hysteresis loop is through a special dynamic system described by a nonlinear differential equation. In this work, the following system is used:

$$\dot{z}(t) = \Gamma[-z(t) + n\,\text{sign}(x(t) + m\,\text{sign}(z(t)))], \qquad \Gamma > 0, \tag{7.3}$$

89

where $m$ and $n$ are the hysteresis loop parameters shown in Figure 7.3. This is a BIBO-stable system previously proposed in [172]. The transition speed between $n$ and $-n$ is governed by the positive parameter $\Gamma$. With illustrative purposes, Figure 7.4 shows the hysteresis loop obtained for the input $x = 10\sin(t)$ with parameters $m = n = 1$, and $\Gamma = 10$. The vertical axis is $-z(t)$ instead of $z(t)$, in order to obtain an hysteresis loop with clock-wise orientation as proposed in Figure 7.2.
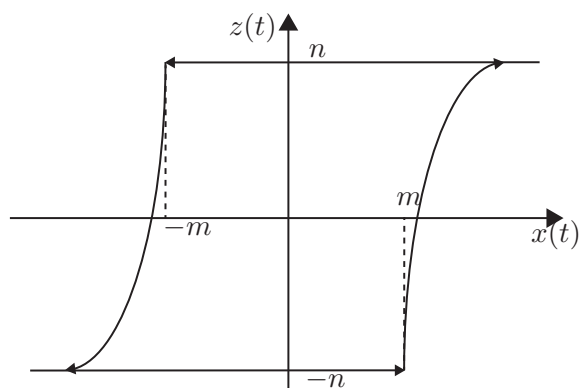


Figure 7.3. Hysteresis behavior of system 7.3.

Source:( [119])
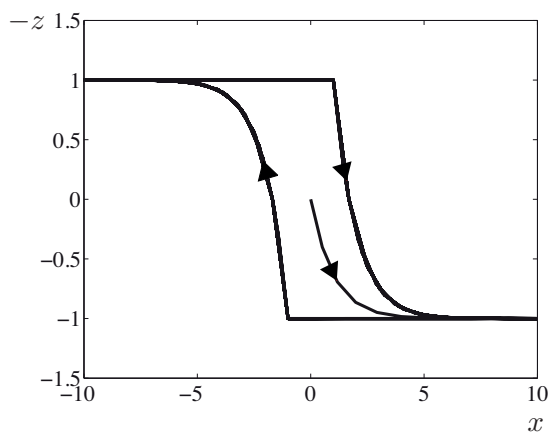


Figure 7.4. Simulation results: $-z$ versus $x$.

Source:( [119])

Note that the hysteresis-loop generated by (7.3) is centered in the origin. However, torque values are centered around $\tau_n$, and set-point values, $P_{\text{ref}}$ and $\omega_{g,r}$, are centered around $P_n$ and $\omega_{g,n}$ respectively, see Figure 7.2. Thus, in order to adapt this hysteresis system, a translation is

90

needed as shown in Figure 7.5. This translation is done by subtracting the nominal torque, $\tau_n$, before the hysteresis block and adding the corresponding nominal reference values (power, $P_n$, and generator speed, $\omega_{g,n}$, respectively) after this block. Figure 7.5 depicts the final SSA block, where the input is the torque control signal and the outputs are the reference generator speed and the reference power, respectively.
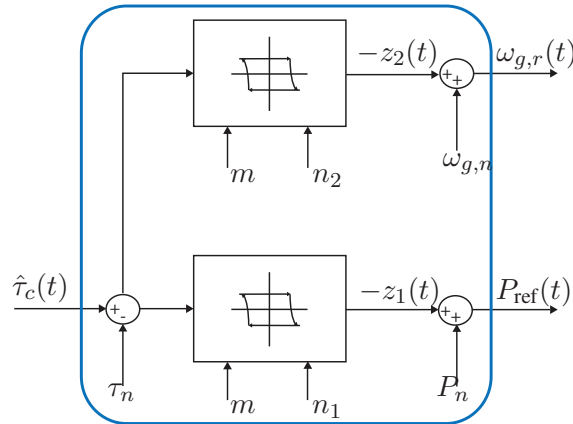


Figure 7.5. Avoid saturation strategy (SSA) block ($m = 1.12$KNm, $n_1 = 0.97$MW, $n_2 = 20.00\frac{\text{rad}}{\text{s}}$ and $\Gamma = 0.5$).

Source:( [119])

Finally, Figure 7.6 shows the closed-loop system for the 5MW benchmark WT, including the generator, pitch actuator, torque and pitch STA controllers and integrating the newly proposed SSA block.

## 7.2 Simulation results

The characteristics of the WT used in the simulations are described in Chapter 2, Table 2.3.

The study compares the performance of the contributed SSA added to the baseline and also to the STA controllers, with respect to the standard baseline controller under two scenarios: fixed pitch measurement fault and healthy case.
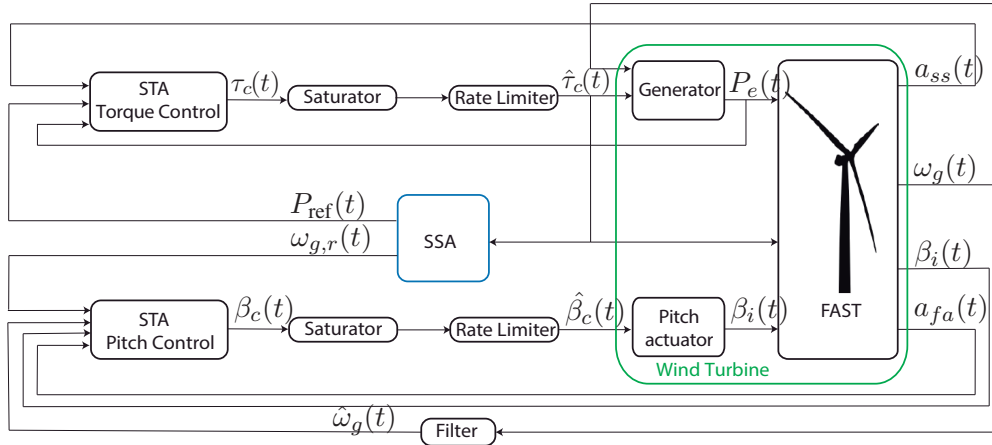
Figure 7.6. Block diagram of the STA controllers with the added avoid saturation strategy (STA+SSA).

Source:( [119])
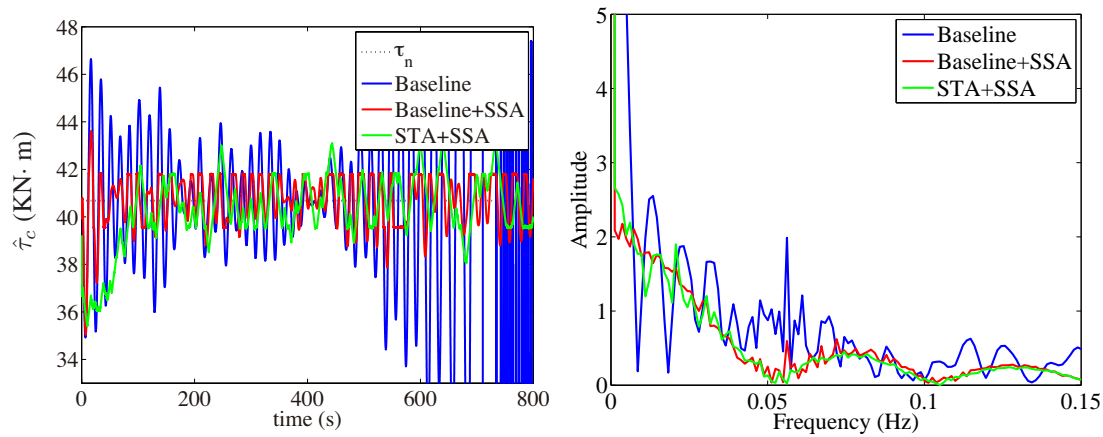


Figure 7.7. Torque control (left), and its fourier transform (right) with fixed pitch angle measurement.

### 7.2.1 Fixed pitch angle measurement fault

From Figures 7.7 (left) and 7.8 (right) we can observe that, with this fault, the standard baseline controllers (blue line) saturate and give rise to instability of the closed-loop system. On the other hand, the proposed SSA design, when used with the STA (green line) or the baseline controllers (red line), avoids saturation of $\tau_c(t)$, maintaining its values within the configured limits ($\tau_u$ and $\tau_l$). Note that both torque and pitch control signals are smooth with a low dynamic activity (with respect to the standard baseline controllers) thanks to the used hysteresis system. This decreased actuators usage is relevant since it helps to increase the lifetime of these mechanical components.

Moreover, according to Figure 7.7 (right), the frequency harmonic content of the torque signal is also reduced, leading to a vibration attenuation in the WT structure. And according to Figure 7.8, a similar performance is appreciated for the pitch angle control signal. On the other hand,
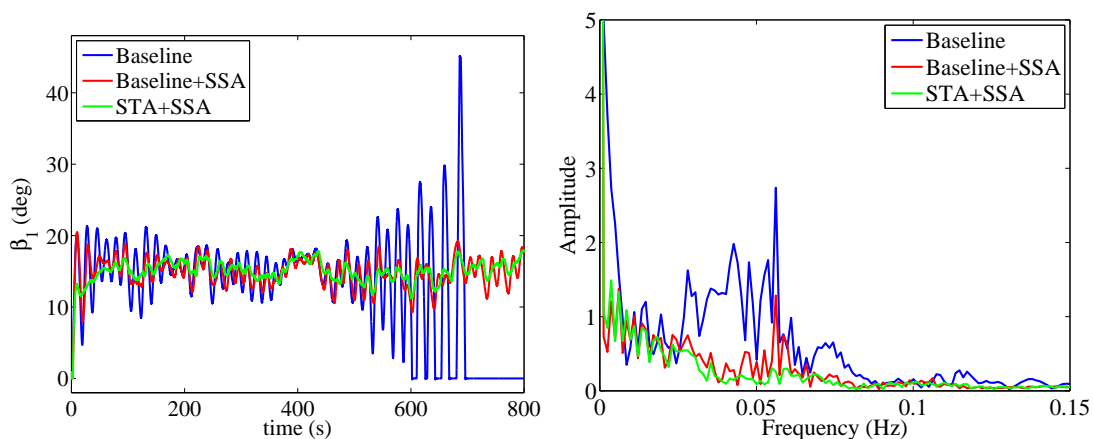


Figure 7.8. Pitch angle $\beta_1$(deg) (left), and its Fourier transform (right) with fixed pitch angle measurement fault.

Figures 7.9 and 7.10 show that, with the proposed SSA strategy (when added to the baseline or STA controllers), the electrical power and generator speed are controlled close to the nominal value, even when the fault is present. Clearly, the standard baseline controller becomes unstable (blue line) for this type of fault.
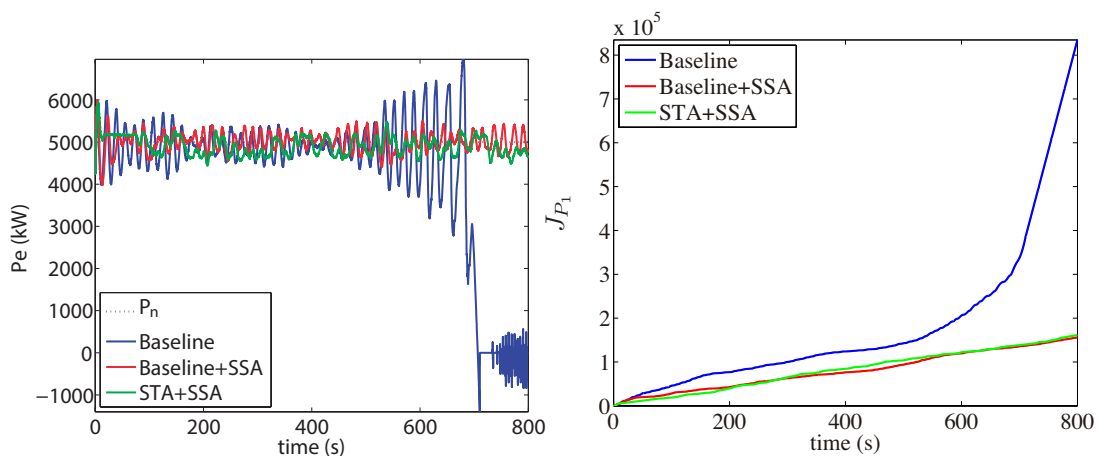


Figure 7.9. Electrical power with fixed pitch angle measurement fault and its associated performance index.
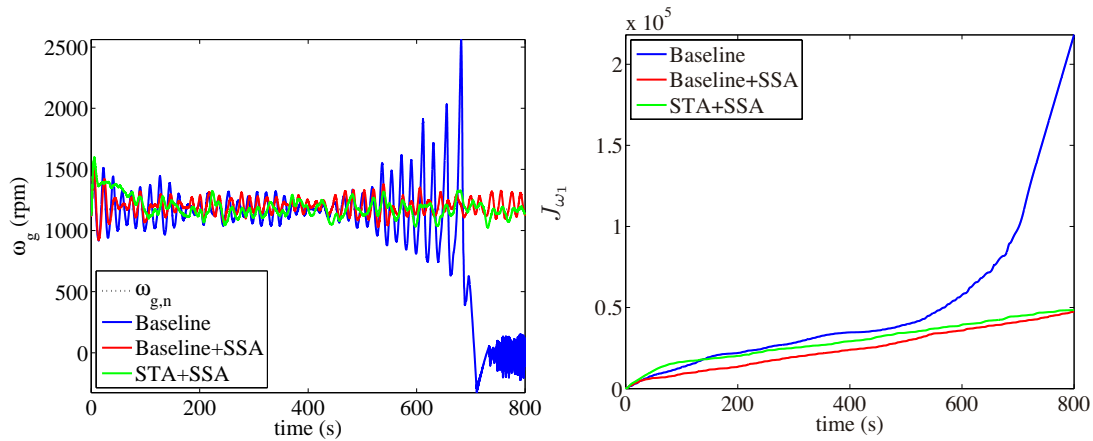
Figure 7.10. Generator speed with fixed pitch angle measurement fault and its associated performance index.
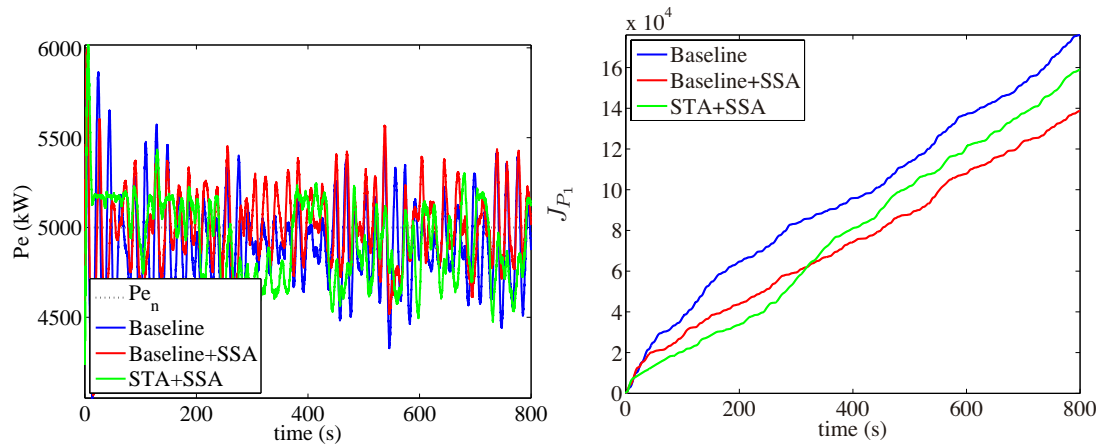


Figure 7.11. Electrical power (healthy case) an its associated performance index.

### 7.2.2 Healthy case

The simulation results, previously discussed, have been also reproduced in a healthy scenario. Figures 7.11 and 7.12 show that, the electrical power and generator speed are correctly regulated with a similar performance for the three tested controllers: baseline, baseline plus SSA, and STA plus SSA.

Similarly to the faulty case, the proposed strategy has a smoother torque control performance, with respect to the baseline, maintaining its values within the configured limits ($\tau_u$ and $\tau_l$), as can be observed in Figure 7.13.

Recall that, when designing the pitch angle control loop, it is of great importance to avoid a high activity of the actuator, since it could not only lead to damage but also give rise to unstable
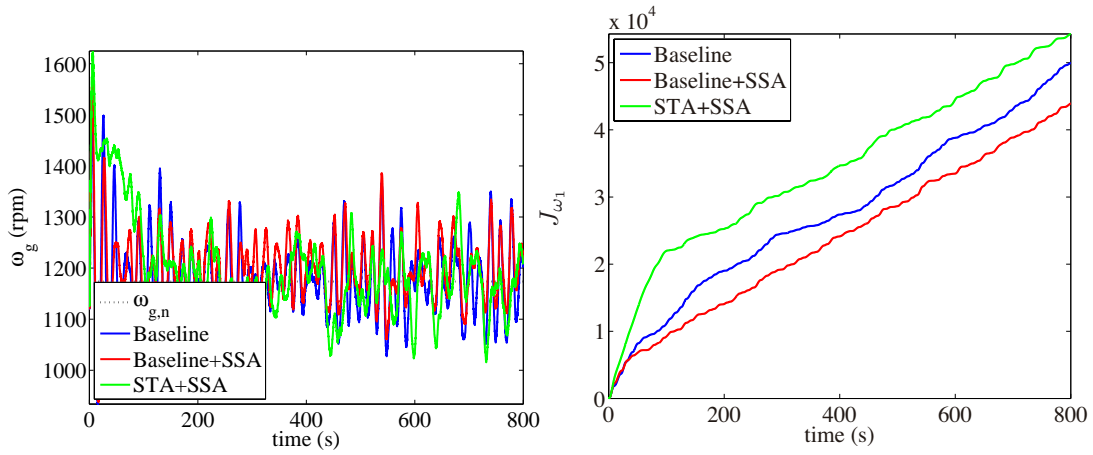
Figure 7.12. Generator speed (healthy case) and its associated performance index.
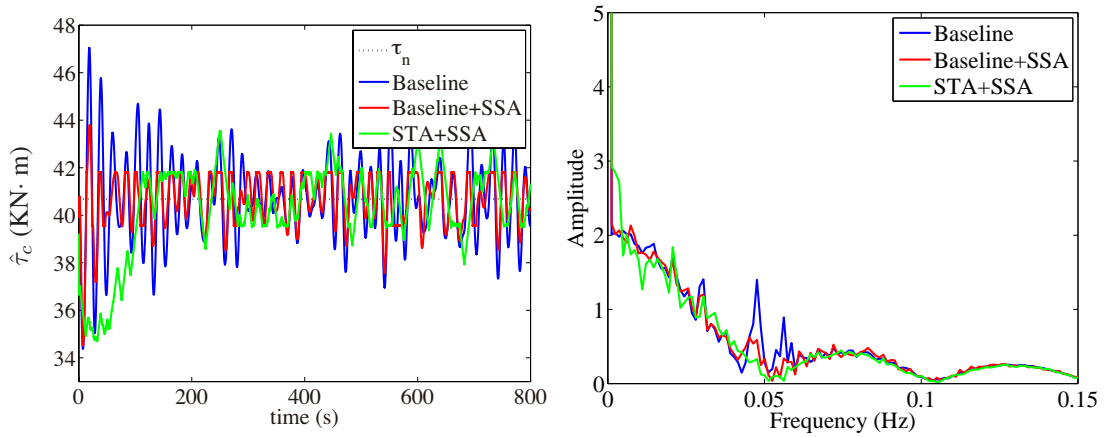


Figure 7.13. Torque control (left), and its Fourier transform (right) in healthy case.

modes of operation, see [135]. At this respect, the pitch control, shown in Figure 7.14, is smoothed with the proposed strategy with respect to the baseline controllers.

Lastly, due to the fact that the torque and pitch actions are softer, this strategy reduces the acceleration on the tower (see Figures 7.15 and 7.16). In particular $J_1(t)$ (related to *fore-aft* acceleration) and $J_2(t)$ (related to *side-to-side* acceleration) indices have been reduced with respect to the standard baseline controllers.

Tables 7.2 and 7.3 show the influence of narrowing the safety band on the operation and the performance of the WT. Comparison between the baseline controller and different values of $f$ used in the baseline plus SSA show that the standard deviation of electrical power, generator speed, torque control and pitch angle are dramatically reduced with the proposed strategy, while mean values remain similar (see Table 7.2). Table 7.3 shows that the proposed strategy improves

95
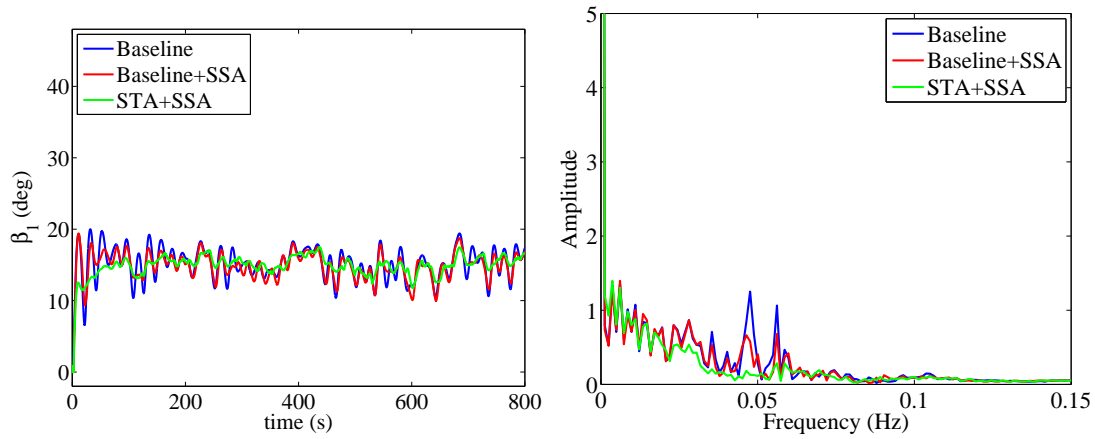
Figure 7.14. Pitch angle $\beta_1$(left), and its Fourier transform (right) in healthy case.
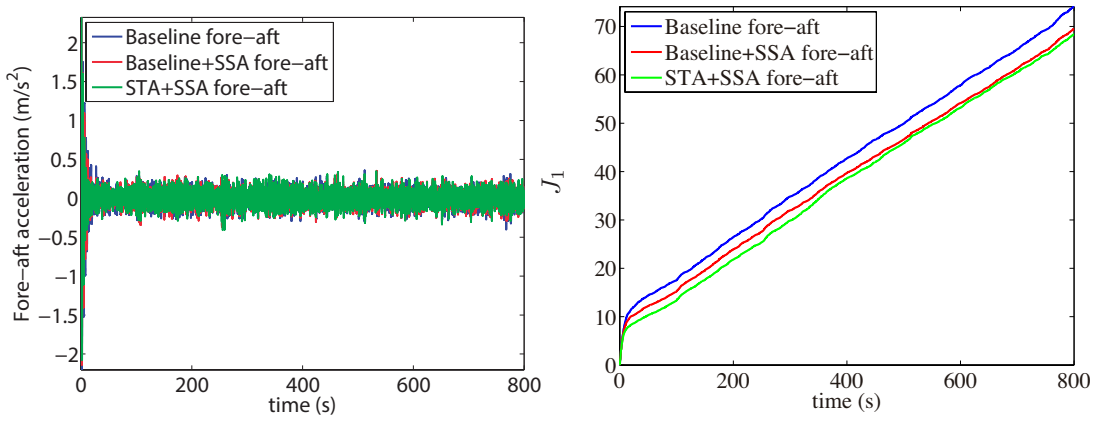


Figure 7.15. *Fore-aft* acceleration at top tower (healthy case) and its associated performance index.
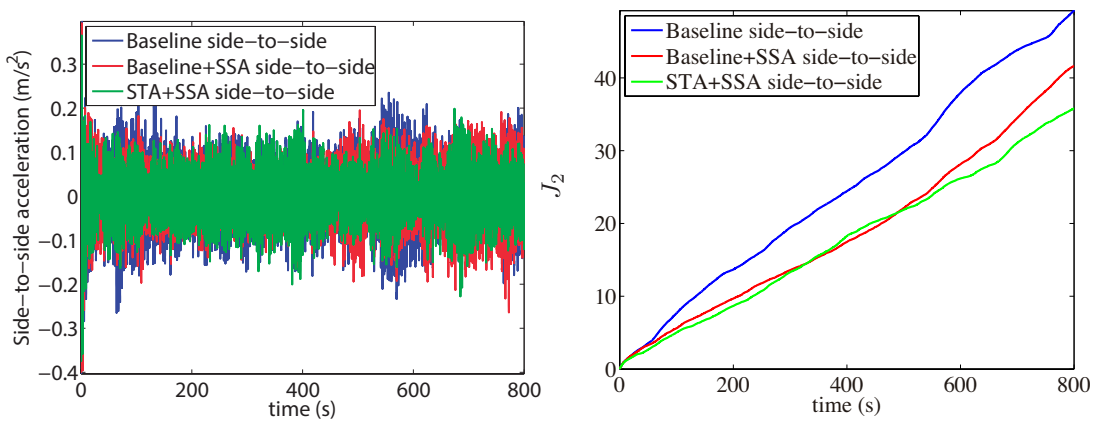


Figure 7.16. *Side-to-side* acceleration at top tower (healthy case) and its associated performance index.

96

Table 7.2. Influence of narrowing the safety band on the operation and the performance of the WT: mean and standard deviation.

| Controller | $f$ | mean | | | | std. deviation | | | |
|---|---|---|---|---|---|---|---|---|---|
| | | $Pe$ | $\omega_g$ | $\tau_c$ | $\beta$ | $Pe$ | $\omega_g$ | $\tau_c$ | $\beta$ |
| Baseline | - | 4900.7 | 1175.4 | 40.7 | 15.1 | 260.6 | 81.5 | 1.7 | 2.3 |
| Baseline+SSA | 1 | 6409.5 | 1356.0 | 0046.1 | 0012.5 | 445.4562 | 113.5582 | 1.4586 | 2.6511 |
| Baseline+SSA | 2 | 4261.3 | 1105.4 | 0037.6 | 0016.4 | 288.0413 | 73.6919 | 0.7904 | 2.1306 |
| Baseline+SSA | 4 | 5157.2 | 1217.8 | 0041.3 | 0014.5 | 236.8083 | 71.5444 | 1.1187 | 2.0614 |
| Baseline+SSA | 6 | 5004.9 | 1199.8 | 40.7 | 14.8 | 223.4 | 68.5 | 1.1 | 2.0 |
| Baseline+SSA | 8 | 4903.7 | 1187.7 | 0040.3 | 0015.0 | 208.2665 | 67.9753 | 1.1075 | 1.9947 |
| Baseline+SSA | 10 | 4903.7 | 1187.7 | 40.3 | 15.0 | 208.2 | 67.9 | 1.1 | 1.9 |

Source:( [119])

Table 7.3. Influence of narrowing the safety band on the operation and the performance of the WT: performance indices.

| Controller | $f$ | $J_{P_1}$ | $J_{\omega_1}$ | $J_1$ | $J_2$ |
|---|---|---|---|---|---|
| Baseline | - | 1.7e+05 | 4.9e+04 | 74.1 | 49.2 |
| Baseline+SSA | 1 | 1.1315e+06 | 1.5050e+05 | 74.0037 | 40.9140 |
| Baseline+SSA | 2 | 6.1183e+05 | 6.6716e+04 | 74.6037 | 35.0172 |
| Baseline+SSA | 4 | 1.8058e+05 | 5.2076e+04 | 71.0121 | 45.5007 |
| Baseline+SSA | 6 | 1.3e+05 | 4.3e+04 | 69.4 | 41.6 |
| Baseline+SSA | 8 | 1.4268e+05 | 4.3552e+04 | 71.0548 | 41.6218 |
| Baseline+SSA | 10 | 1.4e+05 | 4.2e+04 | 70.8 | 40.1 |
| STA+SSA | 1 | 1.1400e+06 | 1.4858e+05 | 69.3822 | 37.8612 |
| STA+SSA | 2 | 5.5016e+05 | 9.0547e+04 | 70.6486 | 45.5629 |
| STA+SSA | 4 | 2.3494e+05 | 5.9212e+04 | 70.1984 | 40.3959 |
| STA+SSA | 6 | 1.5904e+05 | 5.4283e+04 | 68.3795 | 35.8099 |
| STA+SSA | 8 | 1.2839e+05 | 5.2626e+04 | 69.7215 | 32.2515 |
| STA+SSA | 10 | 1.0920e+05 | 5.1322e+04 | 69.9899 | 39.4668 |

Source:( [119])

all the performance indices, however increasing $f$ (narrowing the safety band) does not lead always to a reduction in all the performance indices. Thus, to determine the optimal $f$ value an optimization problem should be solved predefining an objective functional to be minimized. This is beyond the scope of this work.

## 7.3 Conclusions

The main contribution of this chapter is a novel strategy to avoid control saturation. To the authors knowledge, hysteresis loops have not been previously considered in this context, which also reduces significantly the torque and pitch actuators activity as well as the *fore-aft* and *side-to-side* acceleration at the tower top (with respect to the baseline controllers). That is, lower

activity of the torque and pitch actuators is obtained, thus bringing on an extended lifetime of the actuators. Moreover, according to the numerical results, the overall closed-loop system is robust against the studied fault.

Although the avoid saturation strategy has been proposed within a control scheme and a control methodology for WTs, the concept can also be applied in other control problems and along with a variety of control methodologies where the design of dynamic reference trajectories with memory capabilities can be advisable.

# CHAPTER 8

# PASSIVE FTC FOR OFFSHORE FLOATING WIND TURBINES

Offshore floating WTs are one promising solution for the growth of wind energy. To tap the vast resource in deep water sites, new support structures, such as barge platform, are needed. WTs on barge platforms are subjected to completely different and soft foundation properties, than seen for onshore WTs and they must also withstand the offshore wind and wave environment. This leads to an increase in the platform motion and can also cause instability. The main contribution of this chapter is to reduce the platform pitch motion – a significant problem for floating structures. Also, it is crucial that the controllers are tolerant to possible faults in the WT system. Passive fault tolerant control comprises the design of robust controllers against disturbances and uncertainties. This enables the controller to counteract the effect of a fault without requiring reconfiguration or fault detection. In this regard, another contribution of this chapter is to provide fault tolerance capabilities to the WT and also improve the overall performance of the system in both fault free and faulty conditions. Coupled non-linear aero-hydro-servo-elastic simulations of an offshore WT with barge platforms are carried out for several pitch actuator faults. The barge platform motion and structure load caused by both, fault events and during normal operations with the proposed controllers are compared with respect to both, well-known baseline controllers and with a model predictive controller strategy. The proposed controllers are based on the super-twisting algorithm by using the feedback of the generator shaft speed, as well as the fore-aft and side-to-side acceleration signals of the WT tower, and making the reference generator speed a function of the platform pitch motion.

## 8.1  Super twisting algorithm

To make the control system design easier, most control strategies for WT uncouple the control problem into two different single input single output (SISO) control loops: the torque and the pitch controllers (see, for example, [38, 62, 134, 173]). Although the uncoupled assumption (used also in this work), these controllers work collaboratively in the WT overall closed loop system (see, for instance, [173]). In this chapter, the scalar STA torque controller proposed in in Chapter 6 and [158] is used and the PI-class pitch controller is modified in order to fulfill the new objective of reducing the platform pitch motion. A comprehensive analysis of the STA is conducted, for instance, in [137].

First, is recalled the super twisting algorithm (STA) for the generator torque control loop:

$$\tau_c(t) = -\alpha_1 \sqrt{|P_e(t) - P_n|} \text{sign}(P_e(t) - P_n) + y(t), \tag{8.1}$$

$$\dot{y}(t) = -\alpha_2 \text{sign}(P_e(t) - P_n) + \alpha_3 a_{ss}(t), \tag{8.2}$$

where $\alpha_1, \alpha_2, \alpha_3 > 0$ and $P_e(t)$ is the generator output power, $P_n$ is the generator rated power, and $a_{ss}(t)$ is the *side-to-side* acceleration measured at the tower top. The stability analysis for this controller is given in Chapter 6. Note that $\tau_c(t)$ is the torque control signal before the saturation and rate limiter actions (see Fig. 8.1).

On the other hand, we propose the following PI-class pitch controller:

$$\beta_c(t) = K_p(\hat{\omega}_g(t) - \omega_{g,r}(t)) + K_i z(t), \tag{8.3}$$

$$\dot{z}(t) = \text{sign}(\hat{\omega}_g(t) - \omega_{g,r}(t)) + \alpha_4 a_{fa}(t), \tag{8.4}$$

where $\alpha_4 > 0$, $a_{fa}(t)$ is the *fore-aft* acceleration measured at the tower top, $\beta_c(t)$ is the collective pitch control before the saturation and rate limiter actions (see Fig. 8.1), and $\omega_{g,r}(t)$ is the set point that the collective pitch control attempts to drive the actual generator speed towards and is no longer a constant value but instead is a variable that depends on the platform pitch velocity [57] (this in order to reduce the platform pitch motion of the OFWT, see Figure 2.12). Thus, when the platform is pitching upwind, the set point generator speed is greater than the nominal constant value, and vice versa. In practice, this controller is implemented by making the set point generator speed, $\omega_r$ a simple linear function of the platform pitch velocity, $\dot{\vartheta}$. As given by,

$$\omega_{g,r}(t) = 122.8 \frac{\text{rad}}{\text{s}} \cdot (1 + \kappa \cdot \dot{\vartheta}(t)). \tag{8.5}$$

Because a positive platform pitch velocity is defined as the platform pitching downwind, the slope $k$ in Equation (8.5) is negative. Three distinct values of $k$ are used by [57]: 0.0125, 0.025, and 0.0375, and the units of $k$ are 1/(deg/sec). By multiplying both sides of Equation (8.5) by the rated generator torque, 43093.55 Nm, it is clear that the rated power of the rotor also varies depending on the platform pitch velocity. These linear functions are shown graphically in Figure 8.2. Note that, the generator efficiency is taken into account in Figure 8.2, and so the electrical power is plotted (not the mechanical power), and the three lines all show values of 5000 kW for the rated generator power when the platform pitch velocity is 0 deg/sec. In Figure 8.2, VP1, VP2, and VP3 are the linear functions of the Equation (8.5) when $\kappa$ is equal to 0.0125, 0.025, and 0.0375, respectively. In the simulations we use $\kappa = -0.0125$.



Figure 8.1. Block diagram of the Super-Twisting-Algorithm (STA) closed loop system.

Source:(Author)

Finally the last modification is that the new STA pitch controller does not use the pitch position measurements, so this control is robust against pitch sensor faults.

## 8.2 Model predictive control

The model predictive controller (MPC) is implemented using the MPC toolbox from Matlab based in the Chaaban research [56] with four DOFs for the controller design. These DOFs are the generator inertia and the platform motions: yaw, roll, and pitch. The 4DOFs linear model is obtained by FAST in the above rated region at an operating wind speed (wind $^{OP}$ = 18ms),

Figure 8.2. Rated generator speed as a function of platform pitch velocity.

Source:( [57])

and at the rated rotor speed $\omega_r^{OP} = 12.1\text{rpm}$. FAST numerically linearizes the aeroelastic equations of motion by perturbing (see Fig. 8.3) each of the system variables about their respective operating point $(*^{OP})$ values. The linear model obtained from FAST has one input (the collective blade pitching command), one disturbance input (which is the hub height horizontal wind speed), and four measured outputs (which are the generator speed, the platform roll, pitch, and yaw angles). The control and prediction horizons are chosen to achieve better performance while keeping them as small as possible.

The MPC calculates the optimal control input trajectory to a system by minimizing a particular cost function J over a finite period of time into the future (horizon) to calculate the optimum control moves. The optimization problem to be solved online is read as follows:

$$\min_{\Delta u(k)} J(k) = \sum_{i=0}^{P-1} [||\hat{y}(k+i|k) - y^{ref}(k+i)||_Q^2 + ||\Delta\hat{u}(k+i|k)||_R^2] + \tag{8.6}$$

$$||\hat{y}(k+P|k) - y^{ref}(k+P)||_{Q_f}^2, \tag{8.7}$$

subject to the following constraints:

$$y_{min} \leq y \leq y_{max}$$
$$u_{min} \leq u \leq u_{max}$$
$$\dot{u}_{min} \leq \dot{u} \leq \dot{u}_{max}$$

where $P$ is the prediction horizon, $M$ is the control horizon, $Q$ and $R$ are the weighting matrices on the outputs and inputs, $Q_f$ is the terminal weight and the associated terminal cost used to

ensure closed loop stability, $y_{min} \leq y \leq y_{max}$ are the minimum and maximum output values, $u_{min} \leq u \leq u_{max}$ are the minimum and maximum input values, and $\dot{u}_{min} \leq \dot{u} \leq \dot{u}_{max}$ is the constraint for the rate of change of the pitching angle.

The target objectives are prioritized within the cost function using different weight ($Q$, $R$, and $Q_f$) for each objective. Regulating rotor speed to follow the set reference has the highest priority, reducing platform pitch velocity $\dot{\vartheta}(t)$ (see Figure 2.12), takes the second priority, while reducing the roll and yaw motions of the platform are given less priority.
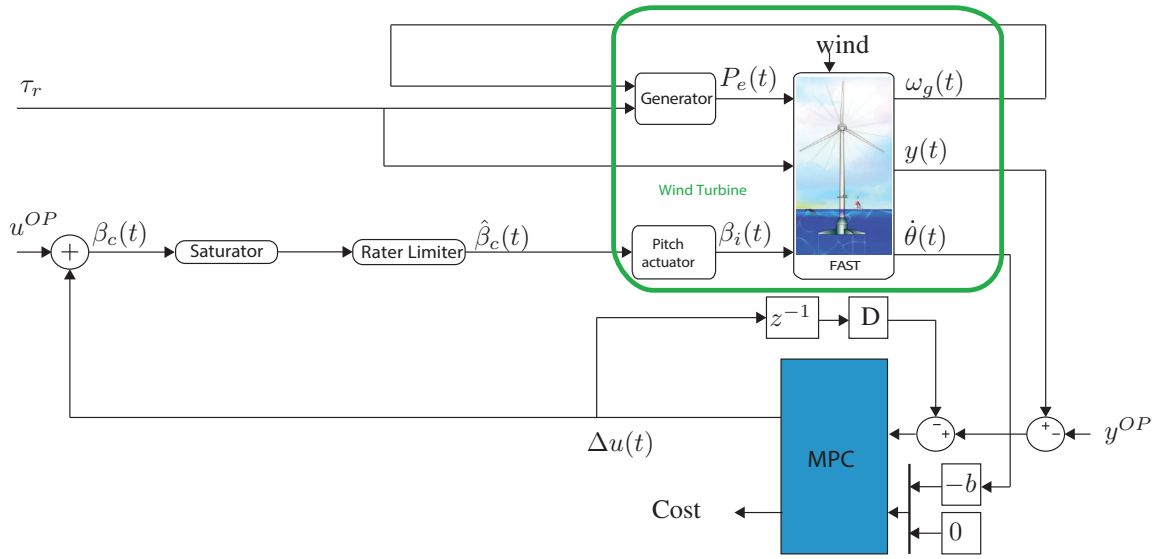


Figure 8.3. Block diagram of the Model Predictive Control (MPC) closed loop system.

Source:(Author)

As the main objective of the controller is to minimize platform motion, using zero reference values for the perturbed platform motion would be appropriate. The value for the perturbed generator speed is set as:

$$\Delta\omega_g = -b\dot{\vartheta}(t). \tag{8.8}$$

where

$$-b = (1173 \quad \text{rpm})\kappa. \tag{8.9}$$

## 8.3 Simulation results

The full nonlinear model of the NREL 5MW WT [36] mounted on a barge platform NREL model [15] is simulated. The main properties of this turbine are listed in Chapter 2, Table 2.4. In the simulations, new wind datasets are generated in order to capture a more realistic turbulent wind simulation and, thus, to test the turbine controllers in a more realistic scenario. Simulations are conducted for a realistic wind speed sequence with a mean speed of 18m/s, turbulence intensity of 15%, run time of over 1300s, and finally the reference height (the height where the mean wind speed is simulated.) is set to 90.25m. This wind speed sequence and the waves elevation are illustrated in Figure 8.4. The rated and cutout wind speeds are 11.4m/s and 25m/s, respectively. Thus, the wind profile lies in the above rated region of work. The water depth at the assumed installation site is 150m, the height of the waves is 3:673m, and the peak spectral period of the incident waves is set to 13:376s. These values correspond to the same location analyzed by Jonkman [15], located in the North Sea near Scotland. All simulations use the same wind and wave profiles.
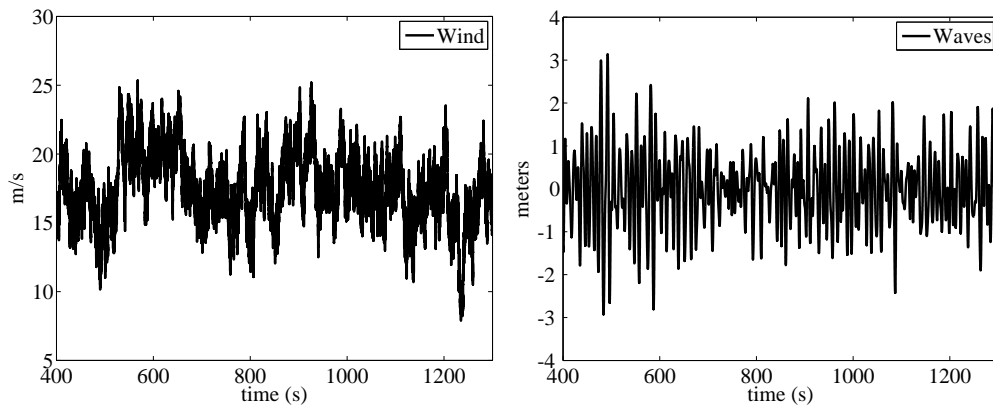


Figure 8.4. Wind speed (left) and wave elevation (right).

In order to compare the different control systems, the baseline control (Chapter 2) and the MPC controllers are used as frames of reference.

All degrees of freedom of the nonlinear model in FAST are enabled (except for the nacelle yaw and rotor teeter DOFs), in addition to the 6DOFs of the platform, namely, roll, pitch, yaw, surge, sway, and heave.

**Remark:** the controller gains used in the proposed strategy simulations are the same in healthy conditions as in faulty conditions, in particular, $\alpha_1 = 0.1$, $\alpha_2 = 200$, $\alpha_3 = 1$, and $\alpha_4 = 10$. Thus, in this work, the controller performance for the faulty or healthy case is shown

to be independent of these gains. Tuning of the controller gains may be rather time-consuming or may rely on sophisticated methods [174]. Thus, in this chapter, the gains are selected by experience and trial-and-error but are not finely tuned. The values are selected to reduce the platform pitch motion and the acceleration at the tower-top (*fore-aft* and *side-to-side*), and to improve the regulation of the power generation. However, other gain values could be used. In particular, only for the healthy case, an example is shown where the platform pitch motion and the electrical error can be reduced or increased by changing $\alpha_4$.

### 8.3.1 Healthy scenario

First, the high performance of the STA strategy is demonstrated in the fault-free operation of the WT.

The STA strategy improves the power generation quality as can be seen in Figure 8.5 (left) and the $J_{P_1}$ performance index (right) is improved, that is, the error in the regulation of the electrical power is reduced compared to the MPC and baseline strategies.
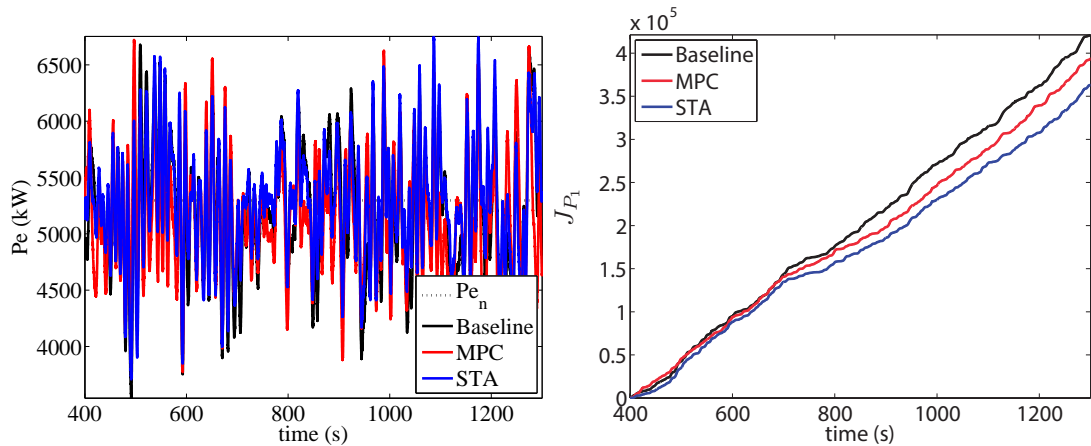


Figure 8.5. Electrical power (left) and $J_{P_1}$ index (right).

It can be seen from Figure 8.6 (left) that the system behavior of the STA has an acceptable variability increase of the generator speed compared to that obtained with the other strategies. While the increased variability on the generator speed may increase the noise production of the WT, in offshore applications this issue is again likely to be irrelevant. On the other hand, from Figure 8.6 (right), a constant value of torque control used by the MPC and baseline strategies can be observed. The STA torque control signal in some points is saturated, but this does not induce instability as the pitch control compensates it.
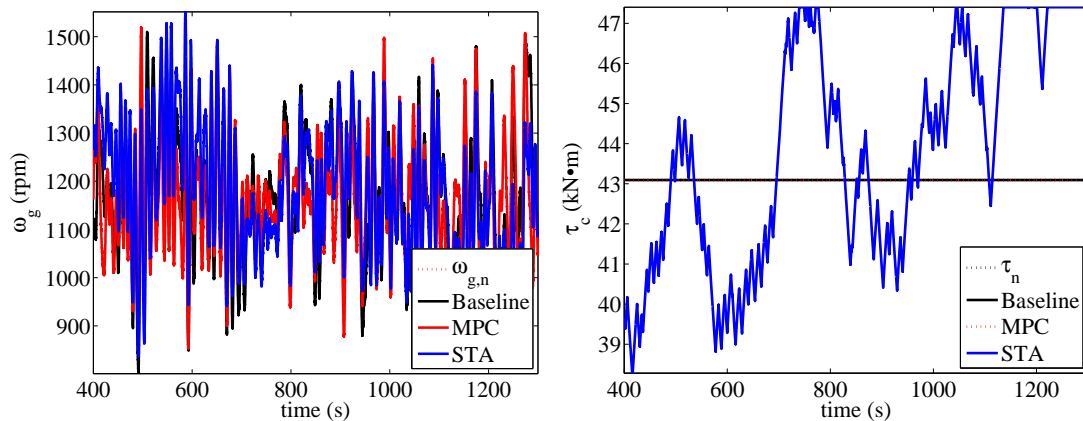
Figure 8.6. Generator speed (left) and torque control (right).

The pitch control, shown in Figure 8.7, is smoothed with the STA strategy with respect to the other controllers. Recall that, when designing the pitch angle control loop, it is of great importance to avoid a high activity of the pitch, since it could not only damage the pitch actuators but also give rise to unstable modes of operation, see, for instance, [173]. Indeed, and as expected, this leads to a reduction of the acceleration in the tower, as can be seen in Figure 8.8 and Figure 8.9. In particular, $J_1(t)$ (related to *fore-aft* acceleration) and $J_2(t)$ (related to *side-to-side* acceleration) indices have been reduced with respect to the MPC and baseline controllers.
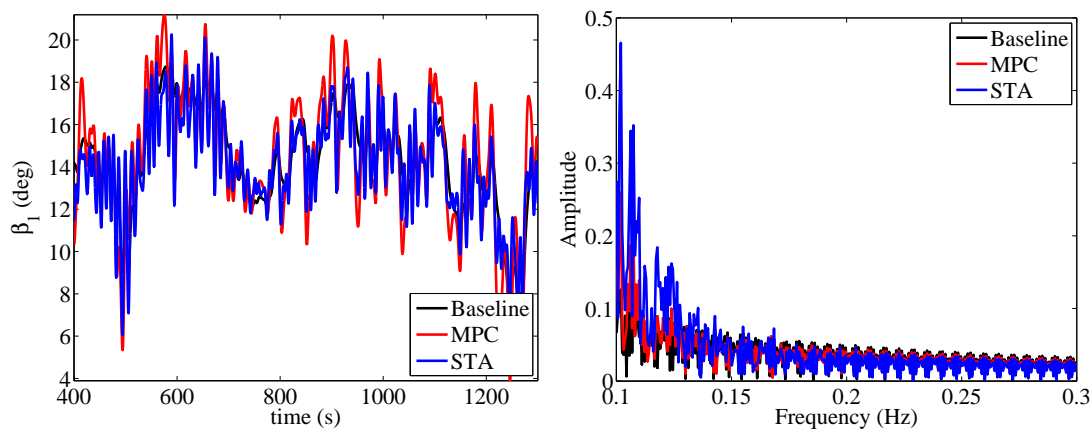


Figure 8.7. Pitch angle $\beta_3$ (left) and its Fourier transform (right).

The platform pitch angle and the related index are shown in Figure 8.10. A reduction is obtained in the platform pitch motion with the proposed STA, with respect to the baseline and MPC controllers. Also, it can be observed that the STA and MPC are the strategies with more platform pitch motion reductions, and this is because both pitch controllers use the set point ($W_{g,r}$) described in the Equation 8.5. This set point depends on the platform pitch velocity

Figure 8.8. *Fore-aft* acceleration (left) and related index (right) at tower top.
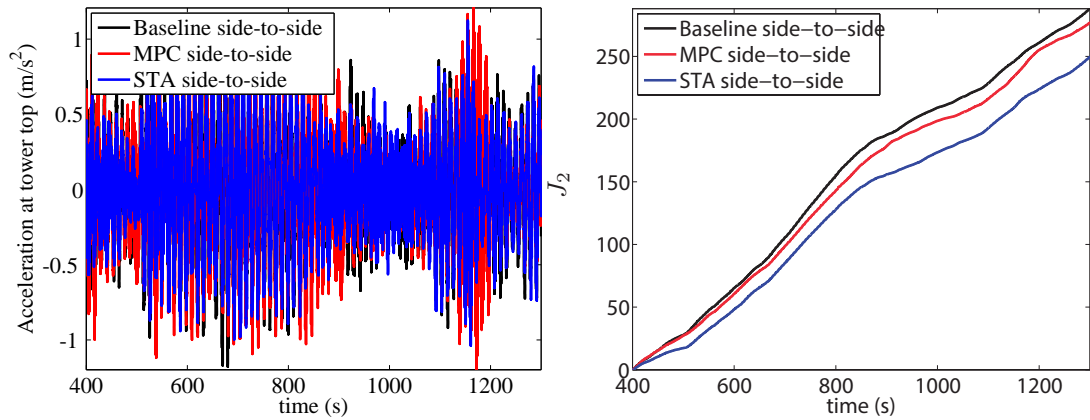


Figure 8.9. *Side-to-side* acceleration (left) and related index (right) at tower top.

and helps to reduce the platform pitch motion. In general, it appears that significant reduction in the platform pitch motion is achieved with an improvement in the generated power and an acceptable increase in the speed error.

**Remark**: when $\alpha_4$ increases, there exists a reduction of the platform pitch motion but at the same time there exists an increase in the electrical power error. The results are not shown because the goal of this research is not to develop an optimal controller, but instead to evaluate a new approach.

### 8.3.2 Change pitch actuator dynamics fault

Here faults, high air content in the oil (F1), pump wear (F2) and hydraulic leakage (F3) described in Chapter 2 and Table 2.2 are considered. The faults are introduced only in the third
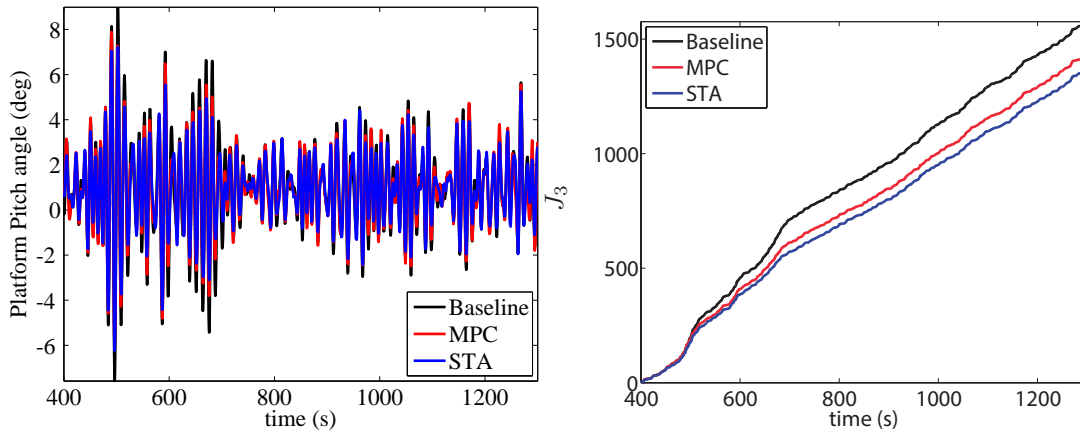
Figure 8.10. Platform pitch angle (left) and related indices (right).

pitch actuator (thus $\beta_1$ and $\beta_2$ are always fault free) in the following way. From 0s to 400s, it is fault free (FF). From 400s a 401s, a fault due to high air content in oil (F1) is linearly introduced. From 401s a 601s, F1 is fully active. From 601s a 602s, F1 is linearly eliminated. From 602s to 702s, it is fault free. From 702s a 722s, a fault due to pump wear (F2) is linearly introduced. From 722s a 922s, F2 is fully active. From 922s a 942s, F2 is linearly eliminated. From 942s to 1042s, it is fault free. From 1042s a 1062s, a fault due to hydraulic leakage (F3) is linearly introduced. From 1062s a 1262s, F3 is fully active. From 1262s a 1282s, F3 is linearly eliminated. From 1282s to 1300s, it is fault free. The changes of the pitch actuator dynamics for the simulations, can be observed in Figure 8.11.
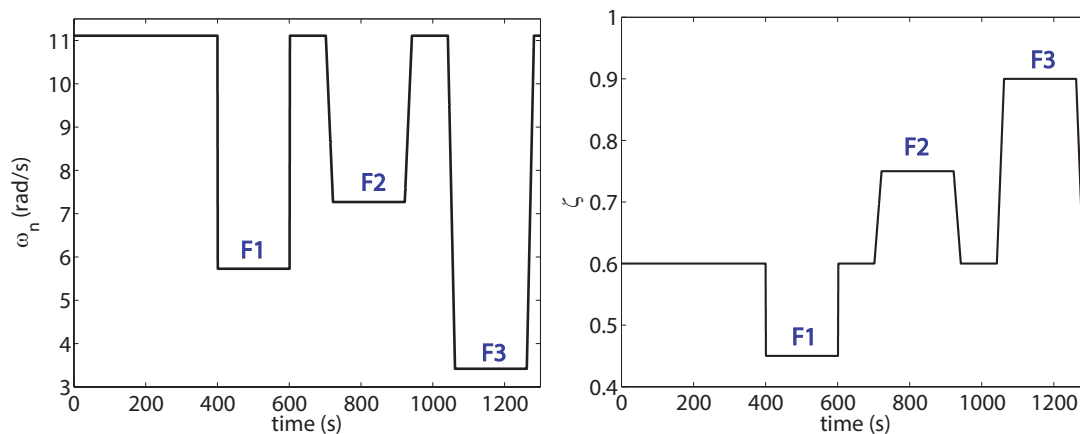


Figure 8.11. Variation of $\omega_n$ (left) and $\zeta$ (right) in the three faulty case.

The proposed controllers have a better performance of the electrical power compared to the baseline and MPC strategies, Figure 8.12 (left). The performance index $J_{P_1}$ corroborates this

108

statement, see Figure 8.12 (right).
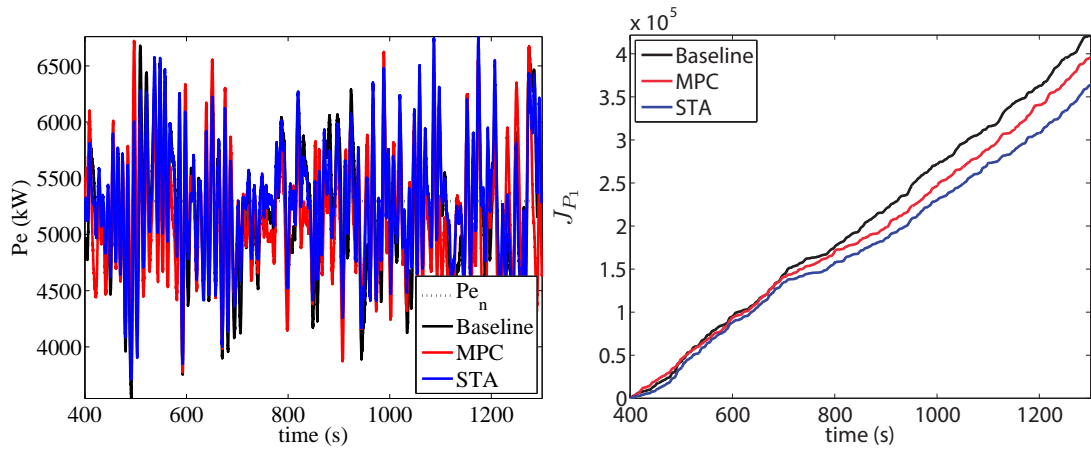


Figure 8.12. Electrical power (left) and $J_{P_1}$ index (right).

Figure 8.13 shows that the first pitch angle ($\beta_1$), which is always FF, has a slightly different behavior with respect to the third pitch angle ($\beta_3$) (when the fault 3 is fully active). This is due to the fact that the fault is introduced in the third pitch actuator ($\beta_3$).
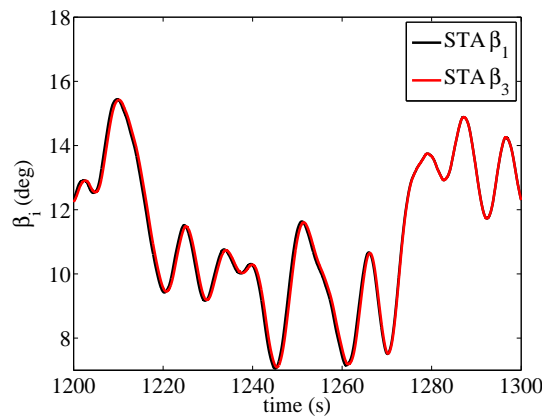


Figure 8.13. STA healthy pitch compared against STA faulty pitch.

There exists a reduction in the movement of the pitch actuator as can be observed in Figure 8.14.

The acceleration at the tower top is improved in the *fore-aft* direction and in the *side-to-side* direction, see Figure 8.15 and Figure 8.16.

Similar to the healthy case, a reduction is obtained in the pitch platform angle with the proposed controllers with respect to the others, see Figure 8.17.
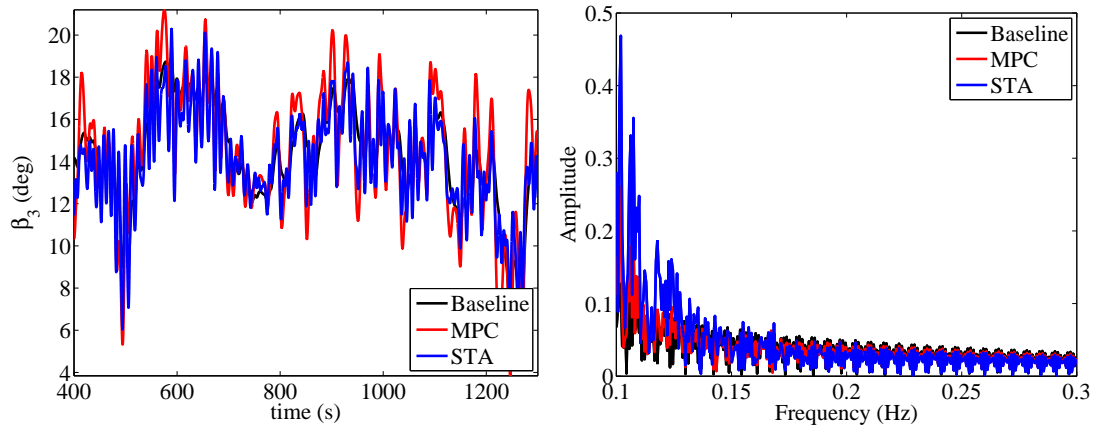
Figure 8.14. Pitch angle $\beta_3$ (left) and its Fourier transform (right).
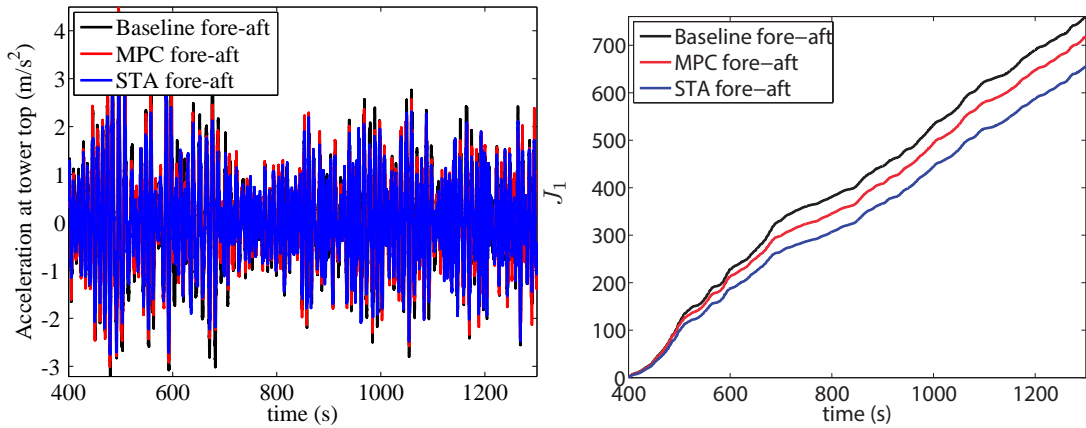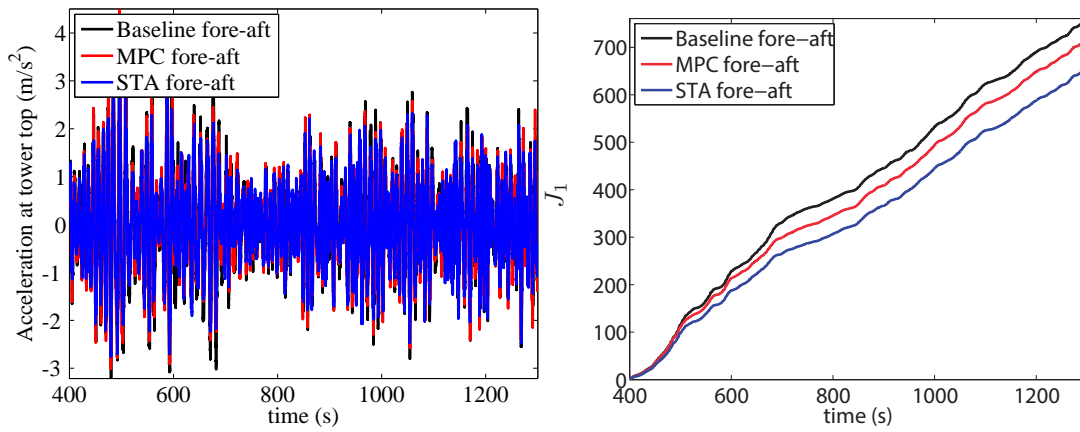


Figure 8.15. *Fore-aft* acceleration (left) and related index (right) at tower top.
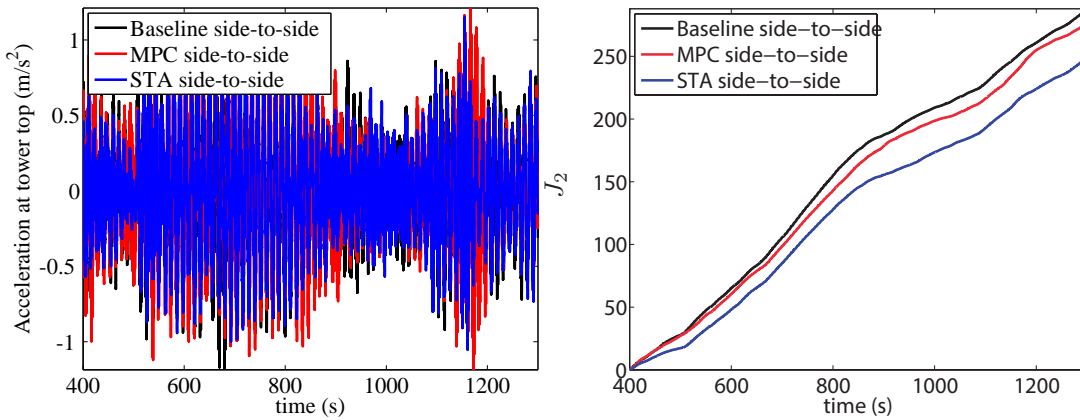


Figure 8.16. *Side-to-side* acceleration (left) and related index (right) at tower top.

### 8.3.3 Stuck/unstuck pitch actuator

Here a stuck/unstuck fault (F4) described in 2, Section 2.5.2 is considered and recalled here:
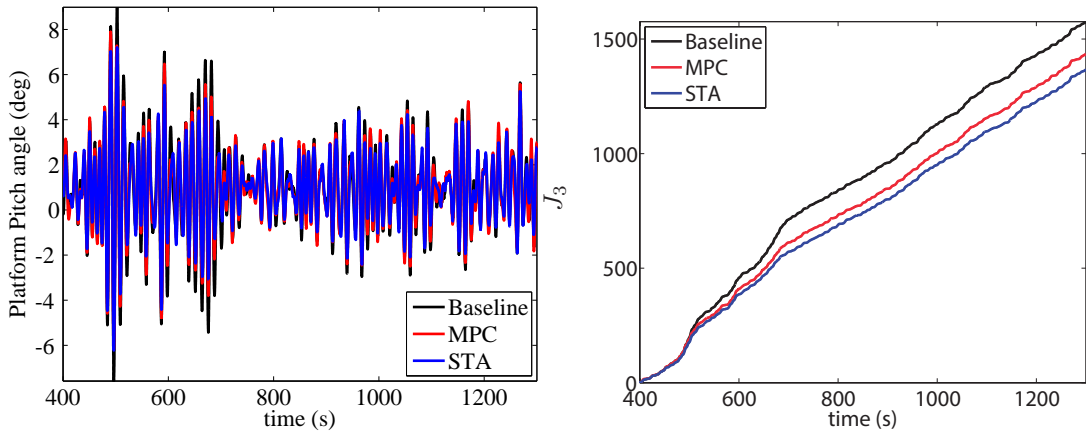
Figure 8.17. Platform pitch angle (left) and related indices (right).

$$\dot{\beta}_i = p(-\beta_3 - \beta_1),$$

Figure 8.18 (left) shows that the first blade pitch angle remains always within the authorized variation domain. The third blade switches between being stuck/unstuck as can be seen in Figure 8.18 (right). Only the MPC strategy saturates at around 1200s in both the first and the third blade pitch angle.
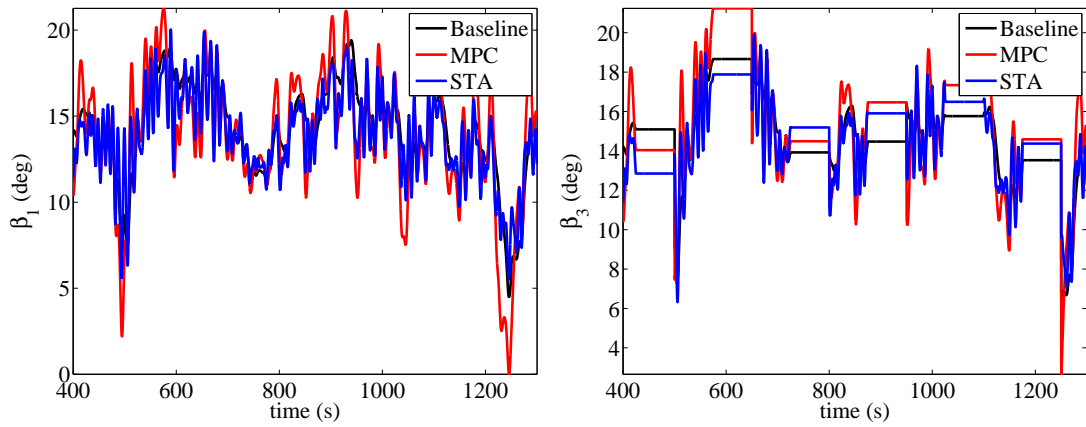


Figure 8.18. Pitch angle under stuck/unstuck faulty condition (only the third pitch actuator is faulty).

The transient response of the electrical power has a larger oscillation for the baseline and MPC controllers, as shown in Figure 8.19 (left) and the $J_{P_1}$ performance index (right) is improved.

The platform pitch angle and the related index are reduced with the proposed control with
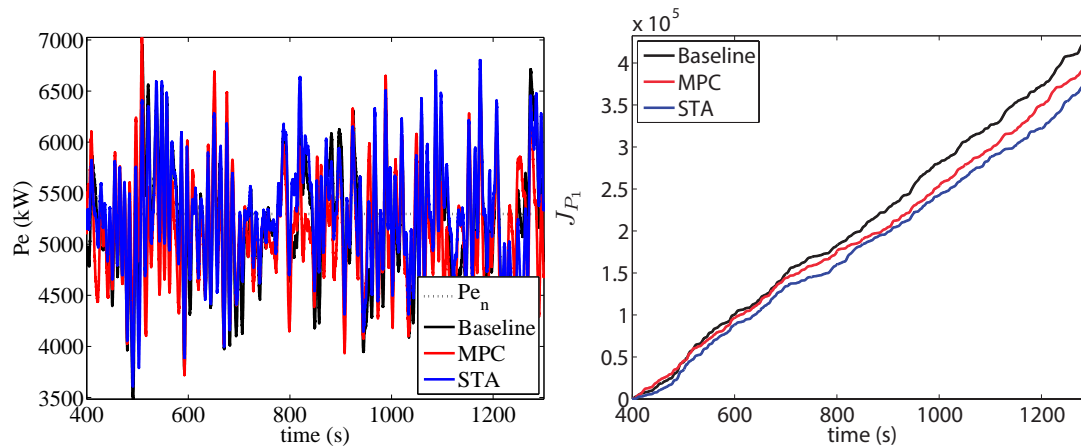
Figure 8.19. Electrical power (left) and $J_{P_1}$ index (right).

respect to the other controllers, as shown in Figure 8.20.
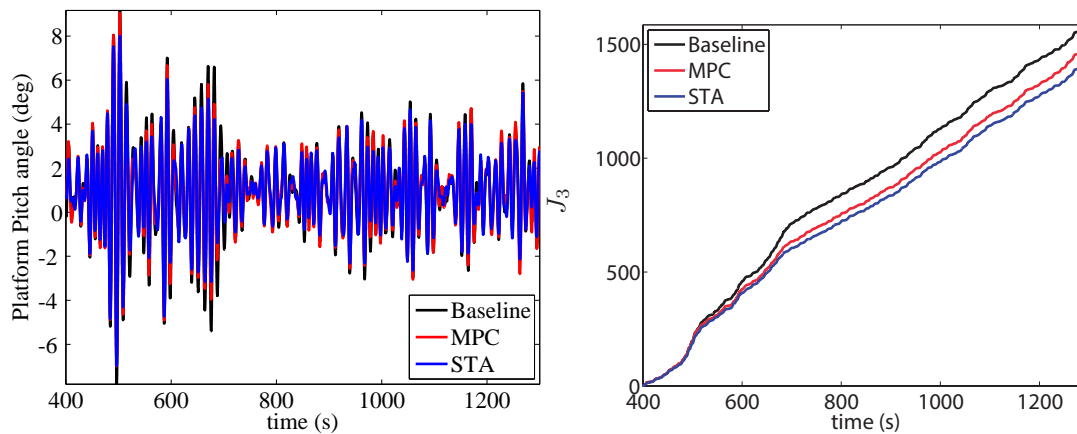


Figure 8.20. Platform pitch angle (left) and related indices (right).

Also, the acceleration at the tower top has been improved not only in the *fore-aft* but also in the *side-to-side* direction, see Figures 8.21 and 8.22. Both indices have been reduced with respect to the other controllers.

## 8.4 Conclusions

This chapter has presented a novel nonlinear robust control of a large offshore floating WT with barge platform operating in the full load region, and in the presence of wind turbulence, waves, and different realistic fault scenarios. Compared to the baseline and MPC strategies, the modified STA-controllers have been able to improve the overall performance of the WT in
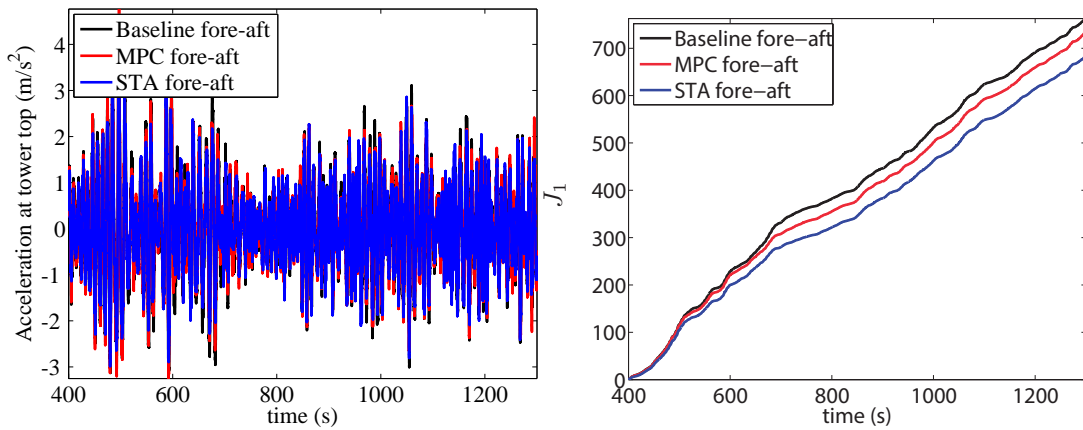
Figure 8.21. *Fore-aft* acceleration (left) and related index (right) at tower top.
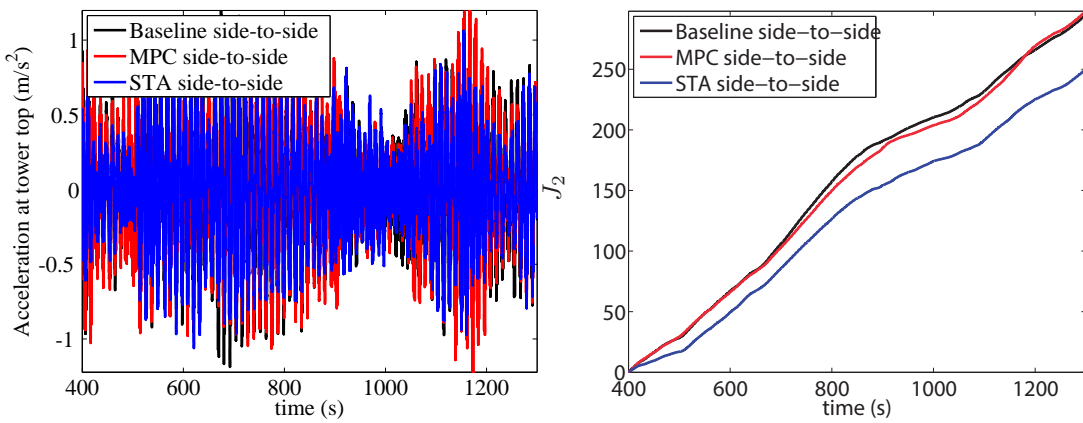


Figure 8.22. *Side-to-side* acceleration (left) and related index (right) at tower top.

healthy and faulty conditions, and reduce the platform pitch motion and the *fore-aft* and *side-to-side* acceleration with respect to the other controls. The proposed controllers allow a better regulation of the electrical power as they use a non-constant torque control. The cost of this performance improvement is an acceptable increase in the blade pitching actuation.

# CHAPTER 9

## CONCLUSIONS AND FUTURE WORK

The specific conclusions of each particular contribution of this thesis have been presented at the end of previous chapters. Here, an overall conclusion is drawn. Furthermore, some future work is outlined.

## 9.1 Conclusions

The power generation systems based on wind energy represent a technology with great potential to solve the environmental problem of reducing carbon emissions. Wind turbines are complex systems that depend, among other factors, on the cost associated with maintenance. Thus, it is necessary further research in techniques that allow WTs to continue operating in the presence of faults. This is crucial as they will extend operating periods, minimizing downtime and maximizing productivity of WTs. WTs have different placement classifications. Each WT type is subjected to completely different and soft foundation properties as well as different realistic scenarios (wind turbulence, waves). In this thesis, onshore, fixed offshore (jacket structure) and floating offshore (barge) versions of a large WT were used for the simulations and analyzed to take in account these properties in the design of FDI and FTC strategies.

This thesis proposes different design techniques to detect and isolate WTs faults, as well as the design of fault tolerant control systems for these faults. Various model-based FDI and FTC approaches are proposed and used for the design of the new techniques.

The first work was to detect any fault that implies changes in the dynamics of the WT pitch

actuator. Residual signals were proposed to detect faults in an onshore WT. The numerical simulations were tested using a hardware in the loop platform and demonstrated a good performance.

Second, using the same onshore WT, a fault diagnosis and fault tolerant control of WTs via a discrete time controller with a disturbance compensator was proposed. With this method, the appearance of the faults is detected in short time. Also, the behavior with faults is close to the behavior of the baseline controllers in the fault-free case. This strategy can be easily implemented in practice due to the required low data storage and the simple mathematical operations used (sums and products between scalars).

Third, a robust super-twisting algorithm control technique was designed, which not only provides fault tolerance capabilities to the WT system, but also improves the overall performance of the system and reduces the tower accelerations in both fault free and faulty conditions. In this case, a more complex WT (jacket offshore fixed) was considered.

Throughout the research in the previous third work, it was observed that saturation was a challenging control problem. Therefore, a hysteresis-based dynamic reference trajectories system was designed to avoid saturation in controlled WTs. This is a novel strategy because hysteresis loops have not been previously considered in this context. This work also reduces significantly the pitch and torque actuators activity as well as the *fore-aft* and *side-to-side* accelerations at the tower top (with respect the baseline controllers). This concept can also be applied in other control problems and along with a variety of control methodologies where the design of dynamic reference trajectories with memory capabilities can be advisable.

In the last work, a robust nonlinear control for barge offshore floating WT was proposed. There, the designed controllers were able to improve the overall performance of the WT in healthy and faulty conditions, as well as to reduce tower acceleration and the platform pitch motion, particularly important problem in barge offshore floating WTs.

With all the proposed FTC strategies, the system behaviors in FAST simulations in healthy and faulty conditions are better or close to the behavior of the baseline controllers. Meanwhile, the proposed FDI strategies detect in short time the appearance of the faults. This is in itself a benefit for the development of fault diagnosis schemes for WTs.

Finally, we remark that the resulting FDI and FTC strategies in this thesis can be easily implemented in practice.

## 9.2 Future work

During the development of this thesis, although the proposed objectives have been covered, some issues have been detected that could be further investigated to increase progress in the respective fields.

- In this thesis three different types of WTs structures were used. In future works, new types of floating WTs can be used to analyze the different problematics of each structure.

- Different types of faults were studied and used, but more types could be investigated. Among the future faults to study can be named, ice accumulation in the blades, train drive misalignment and blade root bending moment sensor fault.

- In chapter 4 measurement noise was not taken into account. As future work we will study the sensitivity of the method to this noise and we will design a filter to guarantee the quality of the estimate.

- In chapter 8, we will consider an MPC strategy incluiding both torque and pitch commands.

- As the main purpose of this thesis is fault detection and fault-tolerant control, in chapter 5 the design parameters were chosen heuristically but, as future work, optimization functions will be used to tune its values.

- Finally, the study of FDI and FTC in WTs could be extended to consider new techniques, as for instance, interval observers, machine learning algorithms, linear matrix inequalities and model predictive control. With the first two mentioned techniques, it has already been possible to detect and isolate different WTs fault types and also several works have been sent to different international congresses. Additionally, we are working on its journal versions.

# CHAPTER 10

# NOTATION

**Acronym**

| | |
|---|---|
| ANN | Artificial neural network |
| BIBO | Bounded-input bounded-output |
| CO2 | Carbon dioxide |
| DOF | Degree of freedom |
| EA | Eigenstructure assignment |
| FD | Fault detection |
| FDI | Fault detection and isolation |
| FFT | Fast fourier transformation |
| FTC | Fault tolerant control |
| F1 | Fault due to high air content in oil |
| FZ | Fuzzy logic |
| F2 | Fault due to pump wear |
| F3 | Fault due to hydraulic leakage |
| F4 | Stuck/unstuck pitch actuator fault |
| F5 | Fixed pitch angle measurement fault |
| GSPI | Gain scheduling proportional integral controller |
| HAWT | Horizontal axis wind turbine |
| HIL | Hardware in the loop |
| LMI | Linear matrix inequality |
| LPV | Linear parameter varying |
| LR | Linear regression |
| MIMO | Multi-input multi-output |

| | |
|---|---|
| MLR | Multiple linear regression |
| MPC | Model predictive controller |
| NREL | National Renewable Energy Laboratory |
| OFWT | Offshore floating wind turbine |
| R | Rotor radius |
| SISO | Single-input single-output |
| SMC | Sliding mode control |
| SSA | Strategy for saturation avoidance |
| STA | Super-twisting-algorithm |
| TLP | Tension leg platform |
| VAWT | Vertical axis wind turbine |
| WT | Wind turbine |

**Symbol**

| | |
|---|---|
| $A_b$ | Blades sweep area |
| $\Delta A$ | Accounts for a fault in the system |
| $\Delta A x[k]$ | Disturbance term that will be estimated |
| $a$ | Design parameter |
| $a_{fa}$ | *Fore-aft* acceleration measured at the tower top |
| $a_{ss}$ | *Side-to-side* acceleration measured at the tower top |
| $a_{xi}$ | *Fore-aft* tower acceleration |
| $a_{yi}$ | *Side-to-side* tower acceleration |
| $B$ | Bias value (constant) |
| $b$ | design perturbed parameter |
| $C$ | Constant value |
| $C_p$ | Aerodynamic efficiency |
| $c$ | Design parameter |
| $\hat{d}[k]$ | Disturbance estimator |
| $e$ | Error |
| $e[k]$ | Error vector |
| $e_x$ | State error |
| $f$ | Safety band parameter |
| $g$ | Design parameter |

| | |
|---|---|
| $h$ | Design hysteresis parameter |
| $J$ | Cost function |
| $J_{p_1}$ | Accumulated generated power error index |
| $J_{p_2}$ | Normalized integral absolute generated power error index |
| $J_{\omega_1}$ | Accumulated generator speed index |
| $J_{\omega_2}$ | Normalized integral absolute generator speed index |
| $J_t$ | Wind turbine total inertia |
| $J_{xi}$ | *Fore-aft* tower acceleration performance index |
| $J_{yi}$ | *Side-to-side* tower acceleration performance index |
| $J_1$ | *Fore-aft* tower acceleration performance index |
| $J_2$ | *Side-to-side* tower acceleration performance index |
| $J_3$ | Platform pitch performance index |
| $K_\alpha$ | Design parameter |
| $[k]$ | Discrete time signal |
| $k_i$ | Integral gain |
| $k_p$ | Proportional gain |
| $k_t$ | Wind turbine total external damping |
| $L$ | Observer matrix gain |
| $M$ | Model coefficient |
| $M_0$ | Normal model coefficient |
| $m$ | Hysteresis loop parameter |
| $n$ | Hysteresis loop parameter |
| $P$ | Prediction horizon |
| $P_\mathrm{e}$ | Electric power produced by the generator |
| $P_l$ | Lower Electric power |
| $P_m$ | Mechanical power |
| $P_n$ | Nominal Electric power |
| $P_u$ | Upper Electric power |
| $P_\mathrm{ref}$ | Reference power |
| $P_t$ | Captured power by the turbine |
| $P_{wind}$ | Wind power |
| $p$ | Generator pulse |
| $Q$ | Weighting matrix |
| $Q_f$ | Terminal weight |
| $q$ | Design parameter |

| | |
|---|---|
| $r$ | residual signal |
| $R$ | Weighting matrix |
| $R_{rot}$ | Rotor radius |
| $s[k]$ | Switching function |
| $T_s$ | Sampling time |
| $u$ | input |
| $u[k]$ | Discrete control law |
| $u_{max}$ | Maximum input |
| $u_{min}$ | Minimum input |
| $V_{wind}$ | Wind velocity |
| $x$ | state vector |
| $y$ | Output |
| $y_h$ | Healthy output |
| $y_{max}$ | Maximum output |
| $y_{min}$ | Minimum output |
| $\hat{y}$ | Output estimation |

**Greek letters**

| | |
|---|---|
| $\alpha_{g,c}$ | Generator and converter model parameter |
| $\alpha_1$ | Design STA parameter |
| $\alpha_2$ | Design STA parameter |
| $\alpha_3$ | Design STA parameter |
| $\beta_c$ | Reference pitch angle (given by the pitch controller) |
| $\hat{\beta}_c$ | Filtered reference pitch angle |
| $\dot{\beta}_c$ | Reference pitch velocity |
| $\beta_i$ | Actual pitch angle |
| $\dot{\beta}_i$ | Actual pitch velocity |
| $\Gamma$ | Hysteresis loop parameter |
| $\gamma$ | Scheduling parameter |
| $\Delta\omega_g$ | Perturbed generator speed |
| $\eta$ | Design parameter |
| $\eta_g$ | Generator efficiency |
| $\theta$ | Parameters vector |

| | |
|---|---|
| $\vartheta$ | Platform pitch position |
| $\kappa$ | Slope parameter |
| $\lambda$ | Tip speed |
| $\rho$ | Air density |
| $\varrho$ | Estimation gain |
| $\tau_a$ | Aerodynamic torque |
| $\tau_c$ | Reference torque (given by the torque controller) |
| $\hat{\tau}_c$ | Saturated and limited reference torque |
| $\dot{\tau}_c$ | Reference torque velocity |
| $\tau_g$ | Generator torque |
| $\tau_l$ | Lower torque |
| $\tau_n$ | Nominal torque |
| $\tau_{max}$ | Maximum allowable torque |
| $\tau_u$ | Upper torque |
| $\phi$ | Regression vector |
| $\zeta$ | Damping factor |
| $\omega_g$ | Generator speed measurement |
| $\dot{\omega}_g$ | Generator speed acceleration |
| $\hat{\omega}_g$ | Filtered generator speed |
| $\omega_{g,l}$ | Lower generator speed measurement |
| $\omega_{g,n}$ | Nominal generator speed measurement |
| $\omega_{g,r}$ | Rated generator speed measurement |
| $\omega_{g,u}$ | Upper generator speed speed measurement |
| $\omega_n$ | Natural frequency |
| $\omega_r$ | Rotor speed measurement |
| $\dot{\omega}_r$ | Rotor acceleration measurement |

# BIBLIOGRAPHY

[1] Francesc Vives. Viabilitat d'una plataforma de generació marina amb aerogeneradors i boies. B.S. thesis, Universitat Politècnica de Catalunya, 2013.

[2] Global Wind Energy Council. Global wind 2015 report: Annual market update, 2016.

[3] Johan Ribrant. Reliability performance and maintenance a survey of failures in wind power systems. Master's thesis, KTH School of Electrical Engineering, 2006.

[4] Pierre Tchakoua, René Wamkeue, Mohand Ouhrouche, Fouad Slaoui-Hasnaoui, Tommy Andy Tameghe, and Gabriel Ekemb. Wind turbine condition monitoring: State-of-the-art review, new trends, and future challenges. *Energies*, 7(4):2595–2630, 2014.

[5] Peter F. Odgaard and Kathryn E. Johnson. Wind turbine fault detection and fault tolerant control-an enhanced benchmark challenge. In *American Control Conference (ACC)*, pages 4447–4452, 2013.

[6] Rannam Chaaban, Daniel Ginsberg, and Claus-Peter Fritzen. Structural load analysis of floating wind turbines under blade pitch system faults. In Ningsu Luo, Yolanda Vidal, and Leonardo Acho, editors, *Wind Turbine Control and Monitoring*, pages 301–334. Springer, 2014.

[7] Yassine Amirat, Mohamed Benbouzid, Elie Al-Ahmar, Bachir Bensaker, and Sylvie Turri. A brief status on condition monitoring and fault diagnosis in wind energy conversion systems. *Renewable and Sustainable Energy Reviews*, 13(9):2629–2636, 2009.

[8] Zafar Hameed, Sung-Hoon Ahn, and Young Man Cho. Practical aspects of a condition monitoring system for a wind turbine with emphasis on its design, system architecture, testing and installation. *Renewable Energy*, 35(5):879–894, 2010.

[9] Erich Hau. Basic concepts of wind energy converters. In *Wind Turbines*, pages 65–78. Springer, 2013.

[10] Alstom. Wind power solutions, 2013.

[11] ABB. Wind power plants, 2011.

[12] Lucy Y. Pao and Kathryn E. Johnson. A tutorial on the dynamics and control of wind turbines and wind farms. In *American Control Conference (ACC)*, pages 2076–2089, 2009.

[13] David A. Spera. *Wind turbine technology: Fundamental concepts in wind turbine engineering*. ASME, 2009.

[14] Yolanda Vidal, Leonardo Acho, Ningsu Luo, Mauricio Zapateiro, and Francesc Pozo. Power control design for variable-speed wind turbines. *Energies*, 5(8):3033–3050, 2012.

[15] Jason M. Jonkman. *Dynamics modeling and loads analysis of an offshore floating wind turbine*. PhD thesis, University of Colorado at Boulder, 2007.

[16] Greg Watson, Barbara Hill, Fara Courtney, Peter Goldman, Stan Calvert, Robert Thresher, Eliot Assimakopoulos, James Lyons, and Benjamin Bell. A framework for offshore wind energy development in the united states. Technical report, Massachusetts Technology Collaborative, 2005.

[17] Spenser Anderson. Comparing offshore and onshore wind, 2013.

[18] Andrew R. Henderson, Colin Morgan, Bernie Smith, Hans C. Sørensen, Rebecca J. Barthelmie, and Bart Boesmans. Offshore wind energy in Europe-A review of the state-of-the-art. *Wind Energy*, 6(1):35–52, 2003.

[19] Walt Musial and Sandy Butterfield. Future for offshore wind energy in the united states. Technical report, National Renewable Energy Laboratory (NREL), 2004.

[20] Athanasia Arapogianni, Anne-Benedicte Genachte, Raul M. Ochagavia, Javier P. Vergara, Daniel Castell, Arturo R. Tsouroukdissian, Jaco Korbijn, Nico Bolleman, Francisco J. Huera-Huarte, Frieder Schuon, et al. Deep water: The next step for offshore wind energy. Technical report, European Wind Energy Association (EWEA), 2013.

[21] Antoine Peiffer and Dominique Roddier. Floating wind turbines: The new wave in offshore wind power. In Jay H. Lehr and Jack Keeley, editors, *Alternative Energy and Shale Gas Encyclopedia*, pages 69–79. John Wiley & Sons, Inc., 2016.

[22] Jason M. Jonkman. *Dynamics modeling and loads analysis of an offshore floating wind turbine*. National Renewable Energy Laboratory (NREL), 2007.

[23] Torben J. Larsen and Tor D. Hanson. A method to avoid negative damped low frequent tower vibrations for a floating, pitch controlled wind turbine. *Journal of Physics: Conference Series*, 75(1):1–11, 2007.

[24] Jason Jonkman and Paul Sclavounos. Development of fully coupled aeroelastic and hydrodynamic models for offshore wind turbines. Technical report, National Renewable Energy Laboratory (NREL), 2006.

[25] Albert Betz. Wind energy and its exploitation by windmills. *Gottingen: Van-denhoeck und Ruprccht*, 64, 1926.

[26] Howard Glauert. Windmills and fans. *Aerodynamic theory*, pages 324–340, 1963.

[27] Albert Betz. *Introduction to the theory of flow machines*. Pergamon Press, 2014.

[28] Mohit Singh and Surya Santoso. Dynamic models for wind turbines and wind power plants. Technical report, National Renewable Energy Laboratory (NREL), 2011.

[29] Ming Yin, Gengyin Li, Ming Zhou, and Chengyong Zhao. Modeling of the wind turbine with a permanent magnet synchronous generator for integration. In *Power Engineering Society General Meeting, 2007. IEEE*, pages 1–6. IEEE, 2007.

[30] Hernán De Battista, Pablo F. Puleston, Ricardo J. Mantz, and Carlos F. Christiansen. Sliding mode control of wind energy systems with DOIG-power efficiency and torsional dynamics optimization. *IEEE Transactions on Power Systems*, 15(2):728–734, 2000.

[31] JG Slootweg, Henk Polinder, and Wil L. Kling. Dynamic modelling of a wind turbine with doubly fed induction generator. In *Power Engineering Society Summer Meeting*, volume 1, pages 644–649. IEEE, 2001.

[32] Yongduan Song, B Dhinakaran, and Xiangyu Bao. Variable speed control of wind turbines using nonlinear and adaptive algorithms. *Journal of Wind Engineering and Industrial Aerodynamics*, 85(3):293–308, 2000.

[33] Leonardo Acho, Yolanda Vidal, and Francesc Pozo. Robust variable speed control of a wind turbine. *International Journal of Innovative (Computing, Information and Control)*, 6:1925–1933, 2010.

[34] Brice Beltran, Tarek Ahmed-Ali, and Mohamed El Hachemi Benbouzid. High-order sliding-mode control of variable-speed wind turbines. *IEEE Transactions on Industrial electronics*, 56(9):3314–3321, 2009.

[35] Nadhira Khezami, Naceur Benhadj Braiek, and Xavier Guillaud. Wind turbine power tracking using an improved multimodel quadratic approach. *ISA Transactions*, 49(3):326–334, 2010.

[36] Jason Jonkman, Sandy Butterfield, Walter Musial, and George Scott. Definition of a 5-MW reference wind turbine for offshore system development. Technical report, National Renewable Energy Laboratory (NREL), 2009.

[37] Peter F. Odgaard, Jakob Stoustrup, and Michel Kinnaert. Fault-tolerant control of wind turbines: A benchmark model. *IEEE Transactions on Control Systems Technology*, 21(4):1168–1182, 2013.

[38] Yolanda Vidal, Christian Tutivén, José Rodellar, and Leonardo Acho. Fault diagnosis and fault-tolerant control of wind turbines via a discrete time controller with a disturbance compensator. *Energies*, 8(5):4300–4316, 2015.

[39] Mogens Blanke, W. Christian Frei, Franta Kraus, Ron J. Patton, and Marcel Staroswiecki. What is fault-tolerant control? *IFAC Proceedings Volumes*, 33(11):41–52, 2000.

[40] Vicenç Puig, Joseba Quevedo, Teresa Escobet, Bernardo Morcego, and Carlos Ocampo. Control tolerante a fallos (parte I): Fundamentos y diagnóstico de fallos. *Revista Iberoamericana de Automática e Informática Industrial*, 1(1):15–31, 2004.

[41] Reliability focused research on optimizing wind energy systems design, operation and maintenance: tools, proof of concepts, guidelines & methodologies for a new generation. Technical report, Reliawind, 2011.

[42] Peter F. Odgaard, Jakob Stoustrup, and Michel Kinnaert. Fault tolerant control of wind turbines-a benchmark model. *IFAC Proceedings Volumes*, 42(8):155–160, 2009.

[43] Thomas Esbensen and Christoffer Sloth. Fault diagnosis and fault-tolerant control of wind turbines. Master's thesis, Aalborg University, 2009.

[44] Javad Mohammadpour and Carsten W. Scherer. *Control of linear parameter varying systems with applications*. Springer Science & Business Media, 2012.

[45] Yolanda Vidal, Leonardo Acho, Ningsu Luo, and Christian Tutivén. Hardware in the loop wind turbine simulator for control system testing. In Ningsu Luo, Yolanda Vidal, and Leonardo Acho, editors, *Wind Turbine Control and Monitoring*, pages 449–466. Springer, 2014.

[46] Jason M. Jonkman, Marshall L. Buhl Jr., et al. Fast user's guide. Technical report, National Renewable Energy Laboratory (NREL), 2005.

[47] Andreas Manjock. Design codes FAST and ADAMS for load calculations of onshore wind turbines, 2005. *National Renewable Energy Laboratory (NREL): Golden, Colorado, USA*, 2005.

[48] Peter Davidson. *Turbulence: an introduction for scientists and engineers*. Oxford University Press, 2015.

[49] Henk K. Versteeg and Weeratunge Malalasekera. *An introduction to computational fluid dynamics: the finite volume method*. Pearson Education, 2007.

[50] Jason Jonkman. NWTC computer-aided engineering tools (FAST), 2013.

[51] Bonnie J. Jonkman. *TurbSim user's guide: Version 1.50*. National Renewable Energy Laboratory (NREL), 2009.

[52] David J. Laino and A. Craig Hansen. *Users guide to the wind turbine dynamics aerodynamics computer software AeroDyn*. National Renewable Energy Laboratory, 2002.

[53] MSC Software. Adams, 2005.

[54] Fabian Vorpahl, Wojciech Popko, and Daniel Kaufer. Description of a basic model of the UpWind reference jacket for code comparison in the OC4 project under IEA Wind Annex XXX. *Fraunhofer Institute for Wind Energy and Energy System Technology (IWES), Germany*, 2011.

[55] Huimin Song, Rick Damiani, Amy Robertson, Jason Jonkman, et al. A new structural-dynamics module for offshore multimember substructures within the wind turbine computer-aided engineering tool FAST. In *International Society of Offshore and Polar Engineers*, volume 23. International Society of Offshore and Polar Engineers, 2013.

[56] Rannam Chaaban and Claus-Peter Fritzen. Reducing blade fatigue and damping platform motions of floating wind turbines using model predictive control. In *International Conference on Structural Dynamics (EURODYN)*, volume 9, pages 3581–3588, July 2014.

[57] Matthew A. Lackner. Controlling platform motions and reducing blade loads for floating wind turbines. *Wind Engineering*, 33(6):541–554, 2009.

[58] Bjørn Skaare, Tor David Hanson, Finn Gunnar Nielsen, Rune Yttervik, Anders Melchior Hansen, Kenneth Thomsen, and Torben J. Larsen. Integrated dynamic analysis of floating

offshore wind turbines. In *European Wind Energy Conference and Exhibition (EWEA)*, 2007.

[59] Hazim Namik, Karl Stol, and Jason M. Jonkman. State-space control of tower motion for deepwater floating offshore wind turbines. In *Aerospace Science Meeting and Exhibit*, number 46, pages 1–18, 2008.

[60] Hazim Namik and Karl Stol. Individual blade pitch control of floating offshore wind turbines. *Wind Energy*, 13(1):74–85, 2010.

[61] David S Ochs, Ruth Douglas Miller, and Warren N White. Simulation of electrome-chanical interactions of permanent-magnet direct-drive wind turbines using the FAST aeroelastic simulator. *IEEE Transactions on Sustainable Energy*, 5(1):2–9, 2014.

[62] Asier Díaz de Corcuera, Aron Pujana-Arrese, Jose M Ezquerra, Aitor Milo, and Joseba Landaluze. Design of robust controllers for load reduction in wind turbines. In *Wind Turbine Control and Monitoring*, pages 97–133. Springer, 2014.

[63] Vikram Kapila and Karolos Grigoriadis. *Actuator saturation control*. CRC Press, 2002.

[64] Steven W. Smith. *The scientist and engineer's guide to digital signal processing*. California Technical Pub. San Diego, 1997.

[65] Jason Mark Jonkman. Influence of control on the pitch damping of a floating wind turbine. Technical report, National Renewable Energy Laboratory (NREL), 2008.

[66] Jason Jonkman. Definition of the Floating System for Phase IV of OC3. Technical report, National Renewable Energy Laboratory (NREL), 2010.

[67] Jie Chen and Ron J. Patton. *Robust model-based fault diagnosis for dynamic systems*, volume 3. Springer Science & Business Media, 2012.

[68] Joaquim Blesa, Damiano Rotondo, Vicenç Puig, and Fatiha Nejjari. FDI and FTC of wind turbines using the interval observer approach and virtual actuators/sensors. *Control Engineering Practice*, 24:138–155, 2014.

[69] Baoping Tang, Tao Song, Feng Li, and Lei Deng. Fault diagnosis for a wind turbine transmission system based on manifold learning and shannon wavelet support vector machine. *Renewable Energy*, 62:1–9, 2014.

[70] Carl Svärd and Mattias Nyberg. Automated design of an FDI-system for the wind turbine benchmark. *IFAC Proceedings Volumes*, 44(1):8307–8315, 2011.

[71] Joaquim Blesa, Vicenç Puig, Juli Romera, and Jordi Saludes. Fault diagnosis of wind turbines using a set-membership approach. *IFAC Proceedings Volumes*, 44(1):8316–8321, 2011.

[72] Shen Yin, Guang Wang, and Hamid Reza Karimi. Data-driven design of robust fault detection system for wind turbines. *Mechatronics*, 24(4):298–306, 2014.

[73] Fariborz Kiasi, Jagadeesan Prakash, Sirish L. Shah, and Jong Min Lee. Fault detection and isolation of a benchmark wind turbine using the likelihood ratio test. *IFAC Proceedings Volumes*, 44(1):7079–7085, 2011.

[74] Vicenç Puig, Joseba Quevedo, Teresa Escobet, Bernardo Morcego, and Carlos Ocampo. Control tolerante a fallos (parte II): Mecanismos de tolerancia y sistema supervisor. *Revista Iberoamericana de automática e Informática industrial*, 1(2):5–21, 2004.

[75] Rolf Isermann. *Fault-diagnosis systems: an introduction from fault detection to fault tolerance*. Springer Science & Business Media, 2006.

[76] Luisa F Villa, Aníbal Reñones, Jose R Peran, and Luis J de Miguel. Statistical fault diagnosis based on vibration analysis for gear test-bench under non-stationary conditions of speed and load. *Mechanical Systems and Signal Processing*, 29:436–446, 2012.

[77] Jimeng Li, Xuefeng Chen, Zhaohui Du, Zuowei Fang, and Zhengjia He. A new noise-controlled second-order enhanced stochastic resonance method with its application in wind turbine drivetrain fault diagnosis. *Renewable Energy*, 60:7–19, 2013.

[78] Tomasz Barszcz and Robert B Randall. Application of spectral kurtosis for detection of a tooth crack in the planetary gear of a wind turbine. *Mechanical Systems and Signal Processing*, 23(4):1352–1365, 2009.

[79] Xiang Gong and Wei Qiao. Imbalance fault detection of direct-drive wind turbines using generator current signals. *IEEE Transactions on energy conversion*, 27(2):468–476, 2012.

[80] Srinivas Katipamula and Michael R Brambley. Methods for fault detection, diagnostics, and prognostics for building systems-A review, part I. *Hvac&R Research*, 11(1):3–25, 2005.

[81] Shulian Yang, Wenhai Li, and Canlin Wang. The intelligent fault diagnosis of wind turbine gearbox based on artificial neural network. In *Condition Monitoring and Diagnosis, 2008. CMD 2008. International Conference on*, pages 1327–1330. IEEE, 2008.

[82] ASAE Zaher, SDJ McArthur, DG Infield, and Y Patel. Online wind turbine fault detection through automated scada data analysis. *Wind Energy*, 12(6):574–593, 2009.

[83] Nassim Laouti, Nida Sheibat-Othman, and Sami Othman. Support vector machines for fault detection in wind turbines. *IFAC Proceedings Volumes*, 44(1):7067–7072, 2011.

[84] Silvio Simani. *Model-based fault diagnosis in dynamic systems using identification techniques*. PhD thesis, Universit degli Studi di Modena e Reggio Emilia, 2002.

[85] Silvio Simani, Cesare Fantuzzi, and Ron J. Patton. *Model-based Fault Diagnosis in Dynamic Systems Using Identification Techniques*, volume 1. Springer-Verlag London, 2003.

[86] Edward Chow and Alan Willsky. Issues in the development of a general design algorithm for reliable failure detection. In *1980 19th IEEE Conference on Decision and Control including the Symposium on Adaptive Processes*, number 19, pages 1006–1012, 1980.

[87] Yolanda Vidal, Leonardo Acho, and Francesc Pozo. Robust fault detection in hysteretic base-isolation systems. *Mechanical Systems and Signal Processing*, 29:447–456, 2012.

[88] Rolf Isermann. Supervision, fault-detection and fault-diagnosis methods-An introduction. *Control engineering practice*, 5(5):639–652, 1997.

[89] Alan S Willsky. A survey of design methods for failure detection in dynamic systems. *Automatica*, 12(6):601–611, 1976.

[90] Michèle Basseville, Albert Benveniste, et al. *Detection of abrupt changes in signals and dynamical systems*, volume 77. Springer, 1986.

[91] Ron J. Patton, Paul M. Frank, and Robert N. Clark. *Issues of fault diagnosis for dynamic systems*. Springer Science & Business Media, 2013.

[92] Ron J. Patton and Jie Chen. Observer-based fault detection and isolation: Robustness and applications. *Control Engineering Practice*, 5(5):671–682, 1997.

[93] Peter Fogh Odgaard, Jakob Stoustrup, Rasmus Nielsen, and Chris Damgaard. Observer based detection of sensor faults in wind turbines. In *Proceedings of European wind energy conference*, pages 4421–4430, 2009.

[94] Peter Fogh Odgaard and Jakob Stoustrup. Unknown input observer based scheme for detecting faults in a wind turbine converter. In *Proceedings of the 7th IFAC Symposium*

*on Fault Detection, Supervision and Safety of Technical processes*, volume 1, pages 161–166. IFAC–Elsevier Barcelona, Spain, 2009.

[95] Christopher Edwards and Sarah K. Spurgeon. On the development of discontinuous observers. *International Journal of control*, 59(5):1211–1229, 1994.

[96] Vadim I. Utkin. *Sliding modes in control and optimization*. Springer Science & Business Media, 2013.

[97] Bruce L. Walcott and Stanislaw H. Zak. State observation of nonlinear uncertain dynamical systems. *IEEE Transactions on automatic control*, 32(2):166–170, 1987.

[98] Ahmet Arda Ozdemir, Peter Seiler, and Gary J Balas. Wind turbine fault detection using counter-based residual thresholding. *IFAC Proceedings Volumes*, 44(1):8289–8294, 2011.

[99] Hector Sanchez, Teresa Escobet, Vicenc Puig, and Peter Fogh Odgaard. Fault diagnosis of an advanced wind turbine benchmark using interval-based ARRs and observers. *IEEE Transactions on Industrial Electronics*, 62(6):3783–3793, 2015.

[100] Aslan Mojallal and Saeed Lotfifard. Multi-physics graphical model based fault detection and isolation in wind turbines. *IEEE Transactions on Smart Grid*, 2017.

[101] Xiaoxu Liu, Zhiwei Gao, and Michael ZQ Chen. Takagi–sugeno fuzzy model based fault estimation and signal compensation with application to wind turbines. *IEEE Transactions on Industrial Electronics*, 64(7):5678–5689, 2017.

[102] Paul M Frank. Enhancement of robustness in observer-based fault detection. *IFAC Proceedings Volumes*, 24(6):99–111, 1991.

[103] Ron J. Patton and Jie Chen. Robust fault detection and isolation (FDI) systems. In Leondes Cornelious, editor, *Techniques in discrete and continuos robust systems*, volume 74, pages 171–224. Academic Press, 1996.

[104] Silvio Simani, Saverio Farsoni, and Paolo Castaldi. Fault diagnosis of a wind turbine benchmark via identified fuzzy models. *IEEE Transactions on Industrial Electronics*, 62(6):3775–3782, 2015.

[105] Shadi Asgari and Alireza Yazdizadeh. Robust model-based fault diagnosis of mechanical drive train in v47/660 kW wind turbine. *Energy Systems*, pages 1–32, 2017.

[106] Zhiwei Gao, Xiaoxu Liu, and Michael ZQ Chen. Unknown input observer-based robust fault estimation for systems corrupted by partially decoupled disturbances. *IEEE Transactions on Industrial Electronics*, 63(4):2537–2547, 2016.

[107] Christoffer Sloth, Thomas Esbensen, and Jakob Stoustrup. Robust and fault-tolerant linear parameter-varying control of wind turbines. *Mechatronics*, 21(4):645–659, 2011.

[108] Zhi-Feng Gao, Jin-Xing Lin, and Teng Cao. Robust fault tolerant tracking control design for a linearized hypersonic vehicle with sensor fault. *International Journal of Control, Automation and Systems*, 13(3):672–679, 2015.

[109] Ron J. Patton. Fault-tolerant control. *Encyclopedia of systems and control*, pages 422–428, 2015.

[110] Nazih Mechbal and Eurípedes G. Nóbrega. Spatial H∞ approach to damage-tolerant active control. *Structural Control and Health Monitoring*, 22(9):1148–1172, 2015.

[111] Lubomír Bakule, Fideliu Paulet-Crainiceanu, José Rodellar, and Josep M Rossell. Overlapping reliable control for a cable-stayed bridge benchmark. *IEEE Transactions on Control Systems Technology*, 13(4):663–669, 2005.

[112] Jin Jiang and Xiang Yu. Fault-tolerant control systems: A comparative study between active and passive approaches. *Annual Reviews in Control*, 36(1):60–72, 2012.

[113] Pedro Casau, Paulo Rosa, Seyed Mojtaba Tabatabaeipour, and Carlos Silvestre. Fault detection and isolation and fault tolerant control of wind turbines using set-valued observers. *IFAC Proceedings Volumes*, 45(20):120–125, 2012.

[114] Jiyeon Kim, Inseok Yang, and Dongik Lee. Control allocation based compensation for faulty blade actuator of wind turbine. *IFAC Proceedings Volumes*, 45(20):355–360, 2012.

[115] Damiano Rotondo, Fatiha Nejjari, Vicenc Puig, and Joaquim Blesa. Fault tolerant control of the wind turbine benchmark using virtual sensors/actuators. *IFAC Proceedings Volumes*, 45(20):114–119, 2012.

[116] Montadher Sami and Ron J. Patton. Global wind turbine FTC via TS fuzzy modelling and control. *IFAC Proceedings Volumes*, 45(20):325–330, 2012.

[117] Silvio Simani and P Castaldi. Active actuator fault-tolerant control of a wind turbine benchmark model. *International Journal of Robust and Nonlinear Control*, 24(8-9):1283–1303, 2014.

[118] Xiaoke Yang and Jan M. Maciejowski. Fault-tolerant model predictive control of a wind turbine benchmark. *IFAC Proceedings Volumes*, 45(20):337–342, 2012.

[119] Christian Tutivén, Yolanda Vidal, Leonardo Acho, and José Rodellar. Hysteresis-based design of dynamic reference trajectories to avoid saturation in controlled wind turbines. *Asian Journal of Control*, 19(2):438–449, 2016.

[120] Fabricio Garelli, Pablo Camocardi, and Ricardo J. Mantz. Variable structure strategy to avoid amplitude and rate saturation in pitch control of a wind turbine. *International Journal of Hydrogen Energy*, 35(11):5869–5875, 2010.

[121] Dan Ye and G-H Yang. Adaptive fault-tolerant tracking control against actuator faults with application to flight control. *IEEE Transactions on Control Systems Technology*, 14(6):1088–1096, 2006.

[122] Zhiwei Gao, Carlo Cecati, and Steven X. Ding. A survey of fault diagnosis and fault-tolerant techniques– part I: Fault diagnosis with model-based and signal-based approaches. *IEEE Transactions on Industrial Electronics*, 62(6):3757–3767, 2015.

[123] Sajjad Pourmohammad and Afef Fekih. Fault-tolerant control of wind turbine systems-a review. In *Green Technologies Conference (IEEE-Green)*, pages 1–6. IEEE, 2011.

[124] Gang Tao. *Adaptive control design and analysis*, volume 37. John Wiley & Sons, 2003.

[125] Mark G Frei, Ruslan L Davidchack, and Ivan Osorio. Least squares acceleration filtering for the estimation of signal derivatives and sharpness at extrema [and application to biological signals]. *IEEE transactions on biomedical engineering*, 46(8):971–977, 1999.

[126] Wei-zhong Wang, Yan-wei Guo, Bang-yu Huang, Guo-ru Zhao, Bo-qiang Liu, and Lei Wang. Analysis of filtering methods for 3d acceleration signals in body sensor network. In *Bioelectronics and Bioinformatics (ISBB), 2011 International Symposium on*, pages 263–266. IEEE, 2011.

[127] Christian Tutivén, Yolanda Vidal, Leonardo Acho, and José Rodellar. A fault detection method for pitch actuators faults in wind turbines. In *International Conference on Renewable Energies and Power Quality (ICREPQ)*, pages 1–6, 2015.

[128] Fernando Ornelas-Tellez, Edgar N. Sanchez, and Alexander G. Loukianov. Inverse optimal control for discrete-time nonlinear systems via passivation. *Optimal Control Applications and Methods*, 35(1):110–126, 2014.

[129] Yongsoon Eun, Jung-Ho Kim, Kwangsoo Kim, and Dong-Il Cho. Discrete-time variable structure controller with a decoupled disturbance compensator and its application to a CNC servomechanism. *IEEE Transactions on Control Systems Technology*, 7(4):414–423, 1999.

[130] Boubekeur Boukhezzar, L Lupu, Houria Siguerdidjane, and Maureen Hand. Multivariable control strategy for variable speed, variable pitch wind turbines. *Renewable Energy*, 32(8):1273–1287, 2007.

[131] Weibing Gao, Yufu Wang, and Abdollah Homaifa. Discrete-time variable structure control systems. *IEEE transactions on Industrial Electronics*, 42(2):117–122, 1995.

[132] Tingshu Hu and Zongli Lin. *Control systems with actuator saturation: analysis and design*. Springer Science & Business Media, 2001.

[133] Sergio Galeani, Sophie Tarbouriech, Matthew Turner, and Luca Zaccarian. A tutorial on modern anti-windup design. *European Journal of Control*, 15(3-4):418–440, 2009.

[134] WE Leithead and Sergio Dominguez. Controller design for the cancellation of the tower fore-aft mode in a wind turbine. In *Conference on Decision and Control and European Control Conference*, volume 44, pages 1276–1281. IEEE, 2005.

[135] Fernando D. Bianchi, Hernán de Battista, and Ricardo J. Mantz. *Wind Turbine Control Systems: Principles, Modelling and Gain Scheduling Design*. Springer Science & Business Media, 2006.

[136] Arie Levant. Robust exact differentiation via sliding mode technique. *Automatica*, 34(3):379–384, 1998.

[137] Vadim Utkin. On convergence time and disturbance rejection of super-twisting control. *IEEE Transactions on Automatic Control*, 58(8), 2013.

[138] Oscar Barambones. Sliding mode control strategy for wind turbine power maximization. *Energies*, 5(7):2310–2330, 2012.

[139] Brice Beltran, Tarek Ahmed-Ali, and Hachemi Benbouzid. Sliding mode power control of variable-speed wind energy conversion systems. *Energy Conversion, IEEE Transactions on*, 23(2):551–558, 2008.

[140] Vadim Utkin, Jürgen Guldner, and Jingxin Shi. *Sliding mode control in electromechanical systems*, volume 34. CRC press, 2009.

[141] Sachin Janardhanan, Mashuq Nabi, and Pyare M. Tiwari. Attitude control of magnetic actuated spacecraft using super-twisting algorithm with nonlinear sliding surface. In *International Workshop on Variable Structure Systems (VSS)*, volume 12, pages 46–51. IEEE, 2012.

[142] Michel Lopez-Franco, Angel Salome-Baylon, Alma Y. Alanis, and Nancy Arana-Daniel. Discrete super twisting control algorithm for the nonholonomic mobile robots tracking problem. In *International Conference on Electrical Engineering Computing Science and Automatic Control (CCE)*, volume 8, pages 1–5. IEEE, 2011.

[143] L Derafa, Leonid Fridman, Abdelaziz Benallegue, and Abdelaziz Ouldali. Super twisting control algorithm for the four rotors helicopter attitude tracking problem. In *International Workshop on Variable Structure Systems (VSS)*, volume 11, pages 62–67. IEEE, 2010.

[144] Suwat Kuntanapreeda. Super-twisting sliding-mode traction control of vehicles with tractive force observer. *Control Engineering Practice*, 38:26–36, 2015.

[145] Carolina Evangelista, Paul Puleston, Fernando Valenciaga, and Alejandro Dávila. Variable gains super-twisting control for wind energy conversion optimization. In *International Workshop on Variable Structure Systems (VSS)*, volume 11, pages 50–55. IEEE, 2010.

[146] Vadim Utkin. About second order sliding mode control, relative degree, finite-time convergence and disturbance rejection. In *International Workshop on Variable Structure Systems (VSS)*, volume 11, pages 528–533. IEEE, 2010.

[147] Michael Basin and Pablo Rodriguez-Ramirez. A super-twisting control algorithm for systems of relative degree more than one. In *Asian Control Conference (ASCC)*, volume 9, pages 1–6. IEEE, 2013.

[148] Jaime A. Moreno. On strict lyapunov functions for some non-homogeneous super-twisting algorithms. *Journal of the Franklin Institute*, 351(4):1902–1919, 2014.

[149] Wei Qiao and Dingguo Lu. A survey on wind turbine condition monitoring and fault diagnosis part II: Signals and signal processing methods. *IEEE Transactions on Industrial Electronics*, 62(10):6546–6557, 2015.

[150] Mariana Iorgulescu and Robert Beloiu. Vibration and current monitoring for faults diagnosis of induction motors. *Annals of the University of Craiova, electrical engineering series*, 57(32):102–107, 2008.

[151] Van T. Do and Ui-Pil Chong. Signal model-based fault detection and diagnosis for induction motors using features of vibration signal in two-dimension domain. *Strojniški vestnik-Journal of Mechanical Engineering*, 57(9):655–666, 2011.

[152] Van-Nguyen Dinh and Biswajit Basu. Passive control of floating offshore wind turbine nacelle and spar vibrations by multiple tuned mass dampers. *Structural Control and Health Monitoring*, 22(1):152–176, 2015.

[153] Zili Zhang, Biswajit Basu, and Søren RK Nielsen. Tuned liquid column dampers for mitigation of edgewise vibrations in rotating wind turbine blades. *Structural Control and Health Monitoring*, (3):500–517, 2015.

[154] Breiffni Fitzgerald, Biswajit Basu, and Søren RK Nielsen. Active tuned mass dampers for control of in-plane vibrations of wind turbine blades. *Structural Control and Health Monitoring*, 20(12):1377–1396, 2013.

[155] Seyed A. Mousavi, Khosrow Bargi, and Seyed M. Zahrai. Optimum parameters of tuned liquid column–gas damper for mitigation of seismic-induced vibrations of offshore jacket platforms. *Structural Control and Health Monitoring*, 20(3):422–444, 2013.

[156] John Arrigan, Vikram Pakrashi, Biswajit Basu, and Satish Nagarajaiah. Control of flapwise vibrations in wind turbine blades using semi-active tuned mass dampers. *Structural Control and Health Monitoring*, 18(8):840–851, 2011.

[157] Eetan Sonmez, Satish Nagarajaiah, Chao Sun, and Biswajit Basu. A study on semi-active tuned liquid column dampers (sTLCDs) for structural response reduction under random excitations. *Journal of Sound and Vibration*, 362:1–15, 2016.

[158] Christian Tutivén, Yolanda Vidal, José Rodellar, and Leonardo Acho. Acceleration-based fault-tolerant control design of offshore fixed wind turbines. *Structural Control and Health Monitoring*, 24(5), 2016.

[159] Jason Jonkman and Bonnie Jonkman. NWTC information portal (fast v8), 2016.

[160] Thomas L. Vincent and Walter J. Grantham. *Nonlinear and optimal control systems*. John Wiley & Sons, 1997.

[161] Zhiyu Jiang, Madjid Karimirad, and Torgeir Moan. Dynamic response analysis of wind turbines under blade pitch system fault, grid loss, and shutdown events. *Wind Energy*, 17(9):1385–1409, 2014.

[162] Yong-Yan Cao and Zongli Lin. Robust stability analysis and fuzzy-scheduling control for nonlinear systems subject to actuator saturation. *Fuzzy Systems, IEEE Transactions on*, 11(1):57–67, 2003.

[163] Yeng-Fang Li. Design of $H_\infty$ static output feedback control for discrete-time systems with limited actuator. *Asian Journal of Control*, 17(1):284–296, 2015.

[164] Jinming Luo and Jun Zhao. Robust control for a class of uncertain switched fuzzy systems with saturating actuators. *Asian Journal of Control*, 17(4):1462–1469, 2015.

[165] Luca Zaccarian and Andrew R. Teel. *Modern anti-windup synthesis: control augmentation for actuator saturation*. Princeton University Press, 2011.

[166] Mona Meisami-Azad and Karolos M. Grigoriadis. Anti-windup linear parameter-varying control of pitch actuators in wind turbines. *Wind Energy*, 18(2):187–200, 2015.

[167] Abrar Ahmed, M. Umer Khan, Muhammad Rehan, and Naeem Iqbal. Two-controller anti-windup design for enlarging domain of stability of actuator constrained state-delay systems. *Asian Journal of Control*, 15(6):1821–1832, 2013.

[168] Peter F. Odgaard, Lars Larsen, Rafael Wisniewski, and Tobias Gybel Hovgaard. On using pareto optimality to tune a linear model predictive controller for wind turbines. *Renewable Energy*, 87:884–891, 2016.

[169] Lars Christian Henriksen, Morten H. Hansen, and Niels Kjolstad Poulsen. Wind turbine control with constraint handling: a model predictive control approach. *Control Theory & Applications, IET*, 6(11):1722–1734, 2012.

[170] David Q. Mayne. Model predictive control: Recent developments and future promise. *Automatica*, 50(12):2967–2986, 2014.

[171] Christopher Edwards, Thomas Lombaerts, and Hafid Smaili. *Fault tolerant flight control*. Springer, 2010.

[172] Leonardo Acho Zuppa and Yolanda Vidal Seguí. Hysteresis modeling of a class of RC-OTA hysteretic-chaotic generators. In *International Conference on Physics and Control*, volume 5, 2010.

[173] Fernando D. Bianchi, Hernán De Battista, and Ricardo J. Mantz. *Wind turbine control systems principles, modelling and gain scheduling design*. SpringerSpringer Science & Business Media, 2011.

[174] Alexander Barth, Markus Reichhartinger, Johann Reger, Martin Horn, and Kai Wulff. Lyapunov-design for a super-twisting sliding-mode controller using the certainty-equivalence principle. In *IFAC Proceedings Volumes*, volume 48, pages 860–865, 2015.